Distribution Agreement

In presenting this thesis or dissertation as a partial fulfillment of the requirements for an advanced degree from Emory University, I hereby grant to Emory University and its agents the non-exclusive license to archive, make accessible, and display my thesis or dissertation in whole or in part in all forms of media, now or hereafter known, including display on the world wide web. I understand that I may select some access restrictions as part of the online submission of this thesis or dissertation. I retain all ownership rights to the copyright of the thesis or dissertation. I also retain the right to use in future works (such as articles or books) all or part of this thesis or dissertation.

Signature:

_____ _____

Roman Romanovich Baglay Date

Local Glass Transition Gradients near Dissimilar Polymer-Polymer Interfaces in Nanostructured Polymeric Materials

By

Roman Romanovich Baglay
Doctor of Philosophy

Physics

Connie B. Roth
Advisor

Justin C. Burton
Committee Member

Stefan Boettcher
Committee Member

Meisha L. Shofner
Committee Member

Eric R. Weeks
Committee Member

Accepted:

Lisa A. Tedesco, Ph.D.
Dean of the James T. Laney School of Graduate Studies

Date

Local Glass Transition Gradients near Dissimilar Polymer-Polymer Interfaces in Nanostructured Polymeric Materials

By

Roman Romanovich Baglay
B.A., New York University, 2011

Advisor: Connie B. Roth, Ph.D.

An abstract of
A dissertation submitted to the Faculty of the
James T. Laney School of Graduate Studies of Emory University
in partial fulfillment of the requirements for the degree of
Doctor of Philosophy
in Physics
2017

Abstract

Local Glass Transition Gradients near Dissimilar Polymer-Polymer Interfaces in Nanostructured Polymeric Materials
By Roman Romanovich Baglay

In this dissertation, I show how perturbations arising from dissimilar polymer-polymer interfaces locally affect the glass transition temperature (T_g) within nanostructured polymeric materials, an issue of critical importance to understanding polymeric blends with sub 100 nm domain sizes. Using a 10-15 nm polymer layer chemically labeled with trace amounts of a fluorescent T_g sensitive pyrene dye inserted at positions z away from dissimilar polymer-polymer interfaces in semi-infinite polymer bilayer films, I measured local $T_g(z)$ profiles for a variety of polymer pairs. I demonstrate that the local $T_g(z)$ profile across a polystyrene (PS) / poly(n-butyl methacrylate) (PnBMA) interface in a PS/PnBMA semi-infinite bilayer with a T_g difference of 80 K between the high T_g glassy-PS ($T_g^{\text{bulk, PS}}$ = 101 ^{o}C) side and low T_g rubbery-PnBMA ($T_g^{\text{bulk, PnBMA}}$ = 21 ^{o}C) side of the bilayer is highly asymmetric towards the high T_g PS component. The $T_g(z)$ profile surprisingly extends 350-400 nm across the PS/PnBMA interface before bulk T_gs of each component are recovered. I then extend the semi-infinite bilayer geometry to a variety of dissimilar polymer pairs, and show that the local $T_g(z)$ length scales seem to be universally grouped by if the measured polymer component is the high T_g or low T_g component of the semi-infinite bilayer, so called hard vs. soft confinement. I find that the $T_g(z)$ profiles are not strongly affected by the bulk T_g difference between the polymer pairs, chemical structure, interaction parameter (equilibrium interfacial width of the interface) or fragility.

I then further show how local T_g profiles are affected by the presence of two PS/PnBMA interfaces and the effect of increased cooling rates in a fixed 300 nm thick PS domain sandwiched between two thick PnBMA domains, mimicking the periodic boundary condition geometry and extended cooling rates (faster timescales) commonly employed by computer simulations. Finally, I introduce a PS polymer chemically labeled with a photomechanical dye capable of generating stresses within polymer films.

The results presented in my dissertation challenge the theoretical textbook understanding of polymer blends, specifically how material properties are affected in nanostructured materials that are dominated by polymer-polymer interfaces with domain sizes reaching below 100 nm.

Local Glass Transition Gradients near Dissimilar Polymer-Polymer Interfaces in Nanostructured Polymeric Materials

By

Roman Romanovich Baglay
B.A., New York University, 2011

Advisor: Connie B. Roth, Ph.D.

A dissertation submitted to the Faculty of the
James T. Laney School of Graduate Studies of Emory University
in partial fulfillment of the requirements for the degree of
Doctor of Philosophy
in Physics
2017

Acknowledgments

First and foremost, I would like to thank my advisor Connie B. Roth for all of the support and guidance she has given me throughout all of these years at Emory University. Connie is a wonderful advisor that loves nothing more than sharing her experience and wisdom with the people fortunate enough to meet her. A great big thank you also goes out to my former lab mate Justin Pye for all of the great discussions we have had about the ins and outs of life over beer, which with great disappointment and annoyance to most, quickly turned into discussions about science. I would also like to thank all of the current and past group members of the Roth lab, especially my former lab mate Laura Gray, and current lab members Michael Thees and Xinru Huang who never disappoint to bring in engaging discussions and laughs into and outside of the lab.

To my committee, Justin C. Burton, Stefan Boettcher, Meisha L. Shofner, and Eric R. Weeks, a big thank you for working with me during the dissertation process and taking your time to help me make this document up to your highest standard. All of your feedback has been greatly appreciated.

I would like to thank Cody Anderson and Horace Dale from our neighbor, the machine shop. Cody and Horace were always there to help anyway they could during my time building preliminary experiments, or as Connie would call them my "arts and crafts" time. Additional thanks go out to Josh Savory who resurrected the dynamic light scattering system. Also, I must thank the physics department staff, Calvin Jackson, Barbara Conner, Susan Cook, Connie Copeland and Paulette Evans that kept the department running, and Jason Boss and Art Kleyman that kept our computers operating smoothly.

Finally, I would like to say a thank you to my wife, Cevon, who has stuck with me through the thick and thin of this whole process. To everyone else that I have had the pleasure of meeting along the way, thank you for all of the laughs and discussions.

Table of Contents

List of Figures

List of Tables

Chapter 1

Introduction to the Glass Transition, Physical Aging, and Modulus in Polymer Thin Films

1.1 SYNOPSIS

As an introduction to my dissertation, here I will provide a general description of glassy behavior universal across many systems and later will focus on polymeric glasses. The glass transition temperature, or the temperature at which a glass forming liquid falls into a non-equilibrium amorphous solid phase is one of the most ill understood phenomenon in condensed matter physics. Here the glass transition, may it be kinetic or thermodynamic in nature, will be discussed alongside a general introduction to structural relaxation (physical aging) in polymeric systems. In the later sections I will discuss how perturbations due to various interfaces such as polymer-air and polymer-substrate interfaces alter glassy behavior in polymer thin films confined to geometries where the surface to volume ratio dominates the material.

In the last section prior to a general outline of the dissertation I will cover different modulus curves as a function of time or temperature for a number of different glass forming materials and will explain how polymers possess a unique rubbery plateau due to entanglements in the high molecular weight regime. Exploiting the rubbery plateau is a key ingredient in the experimental goals for the Chapters following this brief introduction to glasses and general glassy behavior.

1.2 INTRODUCTION TO POLYMERIC GLASSES

1.2.1 General Glassy Behavior

Many small molecules, polymers, colloidal suspensions, and granular materials share a common trait; they are all able to form a state of matter where the material avoids crystallization and forms what is known, as a glass. In the glassy state, these systems are nonergodic[1] because the relaxation process slows down to infinitum at any reasonable laboratory time scale, and do not possess translational symmetry. Microscopically, the lack of translational symmetry is a property reminiscent of a liquid, but at first glance the glass former macroscopically behaves like a solid. Unlike colloids, granular systems, and many small molecules, polymers do not easily crystalize due to their stereo irregularity and slow relaxation dynamics. Even at temperatures well above the glass transition temperature (T_g), many high molecular weight polymers behave like solids with a relatively high rubbery plateau modulus.[2] This mechanical property, which is due to entanglements of polymer chains, will be discussed further in later sections of this Chapter and will be exploited to make local measurements of dynamics in glass forming polymer systems.

It has been debated that the transition from a liquid to amorphous solid state is not a true first or second order phase transition,[3] rather the onset of the glassy state is postulated to be a kinetic event with possibly a true second order transition underlying the kinetic transition,[1] generally characterized by a 12 order of magnitude rapid increase in viscosity upon reaching T_g. Figure 1.1a plots the specific volume or entropy as a function of temperature for a polymeric or small molecule glass forming material. Ellipsometry T_g measurements track film thickness as a function of temperature upon cooling the material,

which then can be linked to changes in specific volume under certain assumptions.[4,5] Above the melting temperature T_m, the system resides in an equilibrium liquid state and therefore is able to sample all of coordinate space, or consequently the system is ergodic. Upon cooling, if the glass former is successfully able to avoid crystallization, the system enters into a supercooled regime. The supercooled regime reveals rich dynamics where glassy systems evolve heterogeneously, both spatially and temporally.[3,6-9] Avoiding crystallization in polymeric glasses is usually trivial since most canonical polymers such as polystyrene (PS) contain bulky side groups and are typically atactic. Small molecules are able to avoid crystallization by simply increasing the cooling rate and not allowing the system enough time to adequately sample coordinate space upon reaching T_m. Past the supercooled regime "glass 1" is formed, which is manifested by a slower heat flow rate or a smaller thermal expansion coefficient. Cooling the same sample at a slower cooling rate will allow the glassy material more time to sample a more entropically favorable state,[10] or a state deeper along the liquid line as shown by "glass 2".

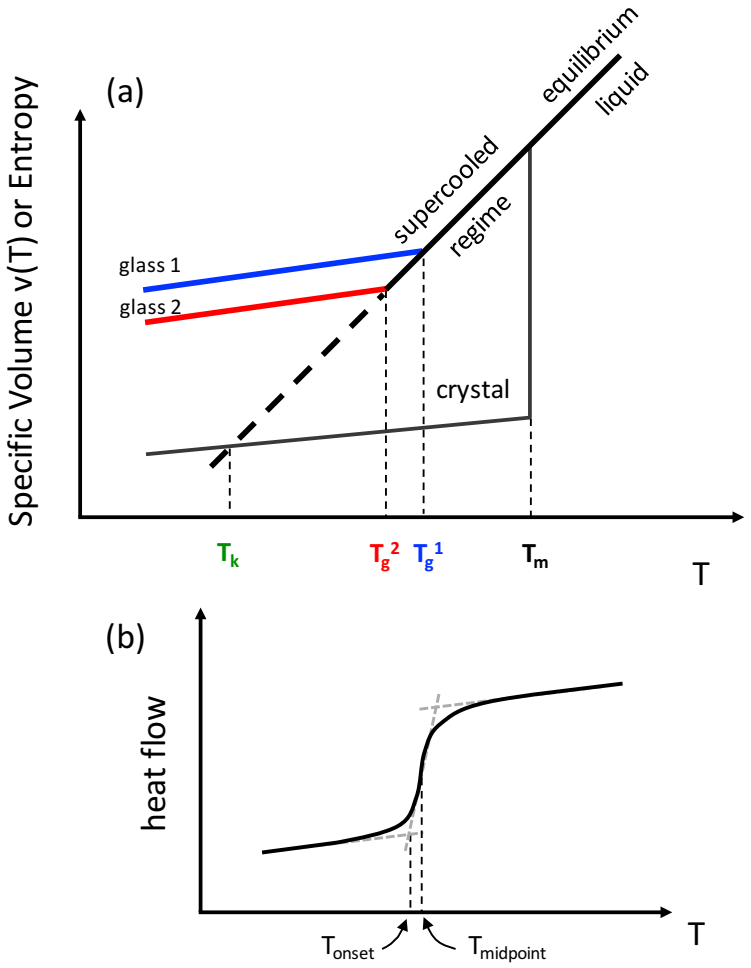

Figure 1.1: (a) A schematic of the specific volume or entropy of a polymer glass as a function of temperature. Above the crystallization temperature T_m, the material is in an equilibrium state. If the liquid is able to avoid crystallization at T_m upon cooling (such as cooling at much faster cooling rates so the liquid does not have time to adequately sample coordinate space) the material falls into a dynamically heterogeneous supercooled liquid.[3,6-9] Upon vitrification of "glass 1," the material falls off of the equilibrium line and forms an amorphous solid. Cooling the system at a slower cooling rate provides the glass former more time to sample space and find an entropically more favorable glassy state,[10] shown by "glass 2." At increasingly slow cooling rates the glass forming material can theoretically continue down the equilibrium line and hit the entropy of a crystalline material at T_k,[1] known as the Kauzmann temperature. (b) A typical heat flow curve collected by differential scanning calorimetry experiments where the glass transition is defined as the T_{onset} or $T_{midpoint}$ between the two specific heat regimes.

The cooling rate dependence of glass formers points to an inherent kinetic event upon vitrification where a true thermodynamic transition could be hiding deeper along the equilibrium line.[1,10-14] For example, cooling "glass 1" an order of magnitude slower accesses "glass 2," though the glass transition temperature is reduced by 3 K. The typical rule of thumb for reaching deeper glassy states is to cool the glass at increasingly slower cooling rates, with the glass typically falling 3 K deeper along the equilibrium line with every order of magnitude step in decreasing cooling rate.[15] Hence, reaching a true thermodynamic transition, if the transition even exists somewhere deep along the liquid line, is an experimentally challenging endeavor. Now, if we consider an exceptionally slow cooling rate, Figure 1.1a suggests that the glassy system can reach an ideal glass state where the entropy of the ideal glass is equal to the entropy of the crystal at the Kauzmann temperature T_k. The existence of a Kauzmann temperature is generally referred to as the Kauzmann paradox or the entropic breakdown.[1] Figure 1.1b plots a heat flow curve as measured by differential scanning calorimetry (DSC) as a function of temperature taken on heating. Typical convention in DSC measurements is to define T_g as the T_{onset} or $T_{midpoint}$ by linear fitting the three regions of the heat flow curve. A more accurate method to identify T_g is by defining T_g as the temperature at which the area between the heat flow and the extrapolated liquid line is equal to the area between the heat flow curve and the extrapolated glassy line.

It has been suggested that accessing a glassy state can be accomplished through a variety of different paths.[13,16-19] Figure 1.2 plots a generic jamming phase diagram depicting how a jammed state (colored regions) can be accessed through a combination of

temperature, stress, and specific volume (inverse density). It is important to note that the jamming point J of a jamming phase diagram is defined as the glassy phase at zero temperature where the volume fraction and stress are varied. In general, granular systems operate in the zero temperature plane since Brownian motion ceases to drive the particle motion, therefore granular systems typically have access to the jamming point J in finite-ranged potentials. In the case of polymeric glass formers and colloidal suspensions, Brownian motion, or thermally activated motion, is still highly present.

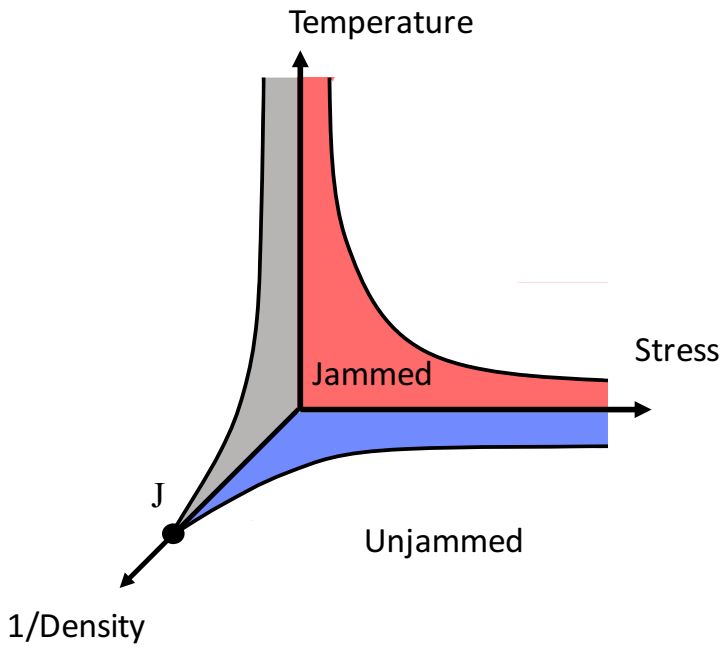

Figure 1.2: A typical jamming phase diagram[13] of a glass forming material where vitrification or jamming of the material can be controlled by temperature, stress, and volume fraction (density). The zero temperature jamming point J is accessible to granular systems since thermally activated motion or Brownian motion is effectively zero.

Another important signature of glass forming materials in the non-equilibrium state phenomenon known as structural relaxation or densification as a function of time below T_g.[20,21] This densification of glassy materials is commonly referred to as physical aging

when the physical properties of the glass start to change as the glass densifies.[21] Once the glass is formed, there is a thermodynamic drive towards the equilibrium line that is hindered by microscopic packing frustration as the glass approaches equilibrium.[22] The processes that control dynamics in the supercooled regime and the evolution of physical aging in the glassy state are so called α and β-relaxations. A simple illustration of β and α-relaxation modes in a liquid composed of hard spheres is illustrated in Figure 1.3a. Such simple systems are common in the glassy community since the dynamics are somewhat successfully treated mathematically with mode coupling theory[23-25] (MCT) and experimentally accessible with colloidal suspensions.[6,26] β-relaxations are typically referred to as the so called "cage rattling", or a ballistic type of motion within a "cage" of surrounding particles for a low temperature or high density liquid. As the volume fraction is decreased or the temperature is increased above the jamming transition, the middle red particle in Fig 1.3 is able to hop out of the neighboring cage via an α-relaxation process, where two or more particles experience a "cage breaking" event. It is important to note that α and β-relaxation modes defined by and used by MCT to describe cage breaking and ballistic motion in hard sphere systems are strictly not the same and should not be confused with the Johari-Goldstein (JG) α and β-relaxation modes most commonly referred to in structural relaxation or physical aging experiments of molecular glasses which can lack intramolecular motion.[27,28]

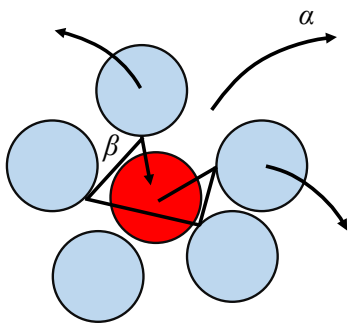

Figure 1.3: A simple schematic of MCT α and β-relaxation modes in a hard sphere system. The β-relaxations represent the ballistic motion or "cage rattling" motion of a particle locked in by a surrounding cage of neighbors. A cage breaking event or the α-relaxation mode allows the system to rearrange its neighbors by over one particle diameter.

In experimental systems below the glass transition, the slow or α-relaxation process essentially freeze out and becomes incredibly slow compared to any reasonable experimental timescales. The physical aging rate can then be measured from the thermodynamic drive towards the equilibrium line, or more specifically, the decreasing specific volume rate as a function of a given aging time. A sketch of an isothermal volumetric departure from equilibrium as a function of log time is shown in Figure 1.4a. The linear region is fit to a straight line defined in the figure,[20] and the experimental physical aging rate β is thereby defined as the slope of the line. It is important to note that reaching equilibrium at temperatures lower than a couple of degrees below T_g is experimentally inhibited by the large time scales associated with glassy dynamics well below the glass transition.[29] Figure 1.4b plots the *physical aging rate* β of PS collected at different aging temperatures, or equivalently, a plot of each individual β measured on isothermal plots in Figure 1.4a collected at different aging temperatures. The competition between the drive to equilibrium and kinetics is sketched in Figure 1.4b, with the roughly

parabolic shape of the graph reflecting the competition between the entropic drive towards equilibrium and the available thermal energy to facilitate the relaxation.[4,22]

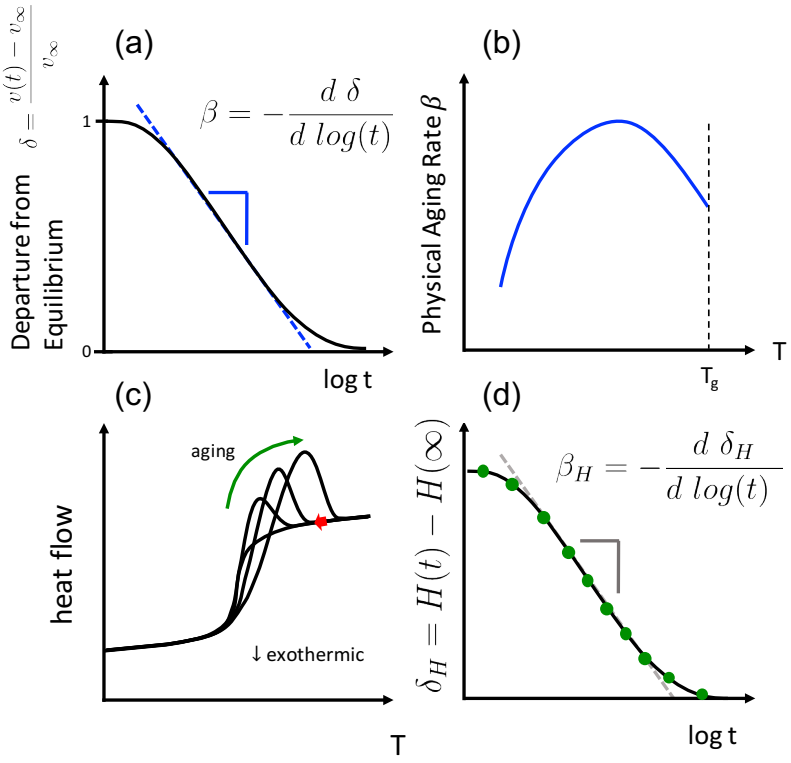

Figure 1.4 (a) Departure from equilibrium as a function of log time for a glassy system at a fixed temperature below T_g. The structural relaxation or physical aging rate is defined by the linear fit (given by the equation in the figure) to the linear region of the curve.[20] (b) Experimental aging rate β, not to be confused with the α and β-relaxation modes defined by MCT, as a function of aging temperature. The peak in the curve provides the optimal aging rate between the competition of the drive to equilibrium and available kinetic energy in the system.[4,22] (c) DSC heat flow curves collected on heating after different aging times for a given aging temperature. The amount of physical aging, enthalpic departure from equilibrium δ_H, is characterized by the excess area under the enthalpy overshoot peak.[21] (d) Many individual measurements of δ_H are required to map out the aging curve, where an enthalpic physical aging rate β_H can be defined.

Additionally, heat flow can be used to measure the physical aging rate of glassy materials upon heating.[30-32] A sketch of DSC heat flow curves as a function of aging time for a given aging temperature collected upon heating are shown in Figure 1.4c. In this case aging is determined from the growth of the enthalpy overshoot of the heat flow curve compared to the smooth curves in Fig. 1.4a. The area under the enthalpy overshoot increases with increasing aging time, which is used to determine the enthalpic departure from equilibrium for a given aging time. A full aging curve such as the one in 1.4a is constructed by measuring the full time dependence of the enthalpy overshoot with aging time in Fig. 1.4d. The physical aging rate β_H is thus similarly defined as the linear region of the enthalpy overshoot as a function of time.[21] Note that such a measurement of aging rate is much more involved when compared to a volumetric measurement of β shown in 1.4a.

1.2.2 Polymer T_g upon Confinement

One of the most ubiquitous technological goals is to create devices with shrinking components. For example, nano-lithography techniques can create sub 100 nm channels in polymers such as poly(methyl methacrylate) (PMMA) for masks in modern nano-electronics.[33,34] Unfortunately, once the polymer bridges become thin enough (approximately < 100 nm), the material loses its mechanical integrity compared to bulk material properties, and starts to buckle. Upon confinement of the material, or when the surface to volume ratio starts to become increasingly large, material properties such as modulus,[35,36] physical aging,[22] and T_g start to become altered.[15,37] For the purposes of this dissertation, I will focus on how the glass transition temperature starts to become perturbed

relative to its bulk value in the presence of various interfaces such as the polymer-air, polymer-substrate, and dissimilar polymer-polymer interfaces.

Over 20 years ago Keddie, Jones, and Cory were the first to measure T_g reductions in single layer PS films that were confined to very thin geometries and supported on a SiOx substrate, using ellipsometry.[38] Upon decreasing PS film thickness below 60 nm, the T_g of the PS films was observed to dramatically decrease. For example, the T_g of a 12 nm thick PS film was shown to be reduced by over 30 K and, surprisingly, the supported PS films showed no molecular weight (MW) dependence corresponding to the observed average T_g reductions,[39] even for films where the total film thickness was much smaller than the radius of gyration of the PS chains.[38-40] The apparent absence of correlations between MW and the reported T_g reductions in supported PS films suggests that the confinement effect is not simply due to chain confinement or the distortion of chain conformations within the film. There is strong evidence from numerous studies that the confinement effect is due to the presence of perturbative interfaces, such as the polymer-air interface in the original Keddie, Jones, and Cory experiments.

The observed T_g reductions do not seem to follow any yet understood intrinsic length scales observed in glass forming materials. For example, one length scale originally proposed by the Adam and Gibbs hypothesis suggests that there exists a minimum number of constituents, or minimum volume, within a material necessary for a relaxation process to occur.[41] In polymers, the Adam and Gibbs length scale of the so called cooperatively rearranging region (CRR) is typically 1-3 nm,[3,42,43] which is already bigger than the intrinsic flexibility (Kuhn length) of typical polymer chains, and additionally an order of magnitude smaller than the confinement length scale observed experimentally in supported

PS films. Although the Adam and Gibbs picture approximates the material by a mean field approach, with multiple CRRs inherently decoupled, recent theories such as Random First Order Transition (RFOT) theory[44] and a theory proposed by Schwiezer[45-47] contain additional long range mechanisms other than simple CRRs to model glassy dynamics.

Confined systems have recently been subjected to various perturbations from interfaces including polymer-air,[15,37,48] polymer-substrate,[49] and dissimilar polymer-polymer interfaces.[50-54] In the case of the polymer-air interface, a barrage of different experimental techniques all show very similar T_g reductions in the canonical PS film supported on a SiOx substrate system.[37] Generally, confinement studies of polymers are done in thin film geometries due to the ease of fabricating thin films via spin coating, but other studies have explored nano-rod[55,56] and spherical geometries,[57] both showing similar perturbations to T_g upon confinement. An example of the rich T_g behavior observed in polymer films containing various perturbative interfaces is plotted in Figure 1.5, where the average T_g of poly(2-vinyl pyridine) (P2VP), PMMA, and PS supported on SiOx is plotted as a function of polymer film thickness. It is clear from Fig. 1.5 that the confinement effect in polymers is material specific, but we can still use confinement to probe polymer thin film dynamics at the nano-scale. For example, P2VP can hydrogen bond to the substrate, reducing its mobility and increasing the T_g locally.[50] Such a system has been interpreted as a spin system with a pinned layer of spins that reduces local mobility, where the lack of mobility then trickles into the system over many spin sites.[58,59] Recent ellipsometry studies on P2VP supported thin films reveal a significant T_g broadening upon confinement and a surprising cooling rate effect.[60] At cooling rates below 10 K/min, the free surface effect seems to decouple from substrate pinning effects where the average T_g of P2VP decreases

with decreasing film thickness, but at cooling rates above 60 K/min, the substrate effect dominates the overall confinement of P2VP and the average T_g of the films increase. Changes in PMMA T_g upon confinement are particularly well understood, with comparable contributions from the free surface and the substrate interactions nearly canceling out deviations in the average T_g of the film.[40,61] In contrast to PMMA and P2VP, PS seems to not interact with SiOx, providing the best example of a purely free surface perturbation.[39,48] Furthermore, the PMMA T_g data shows how competing perturbative interfaces can convolute the confinement problem. In Chapter 2, I will demonstrate how dissimilar polymer-polymer interfaces coupled with a polymer-air interface further exacerbate the issue between competing interfaces, and in Chapter 3 I will then finally show how to experimentally deconvolve the free surface and polymer-substrate interfaces from a polymer-polymer interface in a polymer-polymer bilayer film.

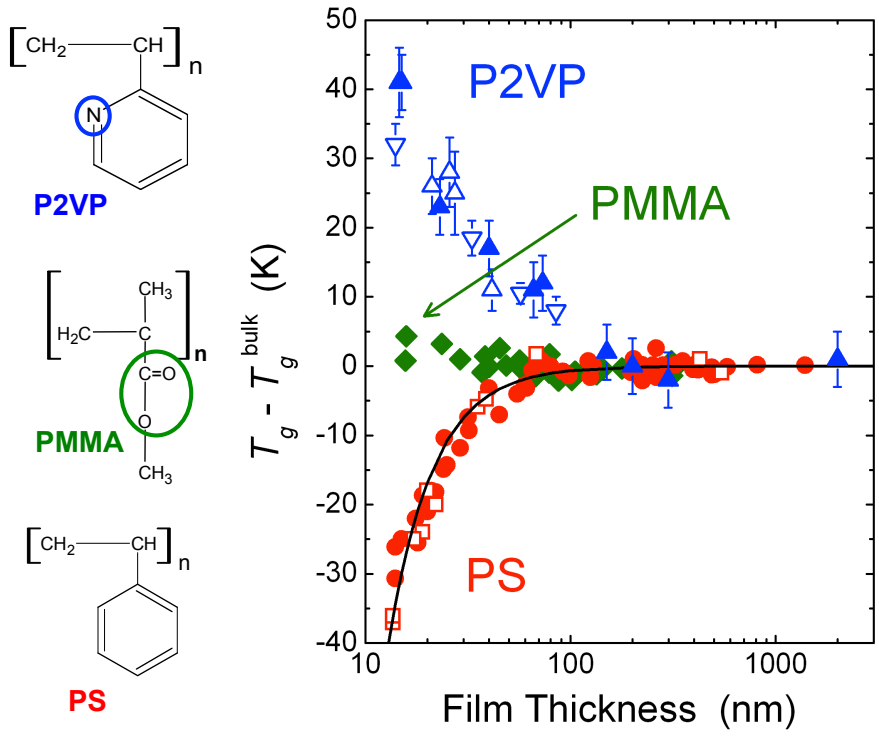

Figure 1.5: Average glass transition temperature as a function of film thickness plotted for PS, PMMA, and P2VP thin films supported on SiOx substrates. P2VP contains a side group (shown on the left) that can hydrogen bond to the SiOx substrate. The chemical interaction hinders mobility close to the substrate as seen by the dramatic average T_g increase with decreasing film thickness. PMMA weakly interacts with the SiOx substrate thus the T_g confinement effect is a competition between the polymer-air and polymer-substrate interactions. These two perturbative interfaces effectively cancel each other out and no significant change to T_g with decreasing PMMA film thickness is observed. PS on the other hand does not interact with the SiOx substrate[48] and provides the best example of a solely free surface perturbation. The chemical structure of the P2VP, PMMA, and PS monomer is shown on the left with circles isolating the components in the side groups of P2VP and PMMA responsible for hydrogen bonding to the SiOx substrate. P2VP data from Refs.,[62,63] PMMA data from Ref.,[40] PS data from Refs.[39,48] Figure adapted from Ref.[50]

Apart from a small number of groups, the perturbations to T_g from dissimilar polymer-polymer interfaces have been little studied experimentally.[50-54,64-69] With the advent of new synthesis and processing techniques, new block co-polymer materials with domain sizes reaching 100 nm or less are possible for macroscopic fabrication.[70-74] The macroscopic properties of these materials can then be possibly dominated by interactions from the dissimilar polymer-polymer interfaces. Understanding how the dissimilar polymer-polymer interfaces at the nanoscale alter mesoscopic or even microscopic properties is a fundamental goal for both polymer physics and materials engineering.

1.3 POLYMER GLASSY AND RUBBERY MODULUS BEHAVIOR

Unlike colloidal and granular systems, the modulus of entangled polymeric systems exhibits three regimes which depend on temperature, shear frequency, and number of entanglements in the polymer melt. Modulus curves as a function of temperature or logarithmic time for small molecule and polymer systems are plotted in Figure 1.6. Polymers with progressively higher molecular weights (MWs) (low MW left to high MW right) are shown as solid curves. The first solid curve on the left traces an unentangled polymer's rheological response where the rubbery plateau is completely avoided. Unentangled polymers have qualitatively similar modulus curves compared to small molecules (first dashed curve on the left). Upon entanglement, polymers undergo a transition from the glassy GPa region to the rubbery MPa plateau, where the rubbery plateau is reached by crossing the dynamic 100 s "transition zone" or by thermally crossing T_g. Terminal flow, or diffusive flow, is reached at much longer time scales or higher

temperatures, which in turn scales with the polymer's MW depicted by the middle and far right solid curves for a polymer with increasing MW. Additionally, the terminal flow region can be avoided by physically crosslinking the polymer either at the entanglement density, which does not change the magnitude of the rubbery plateau, or by more highly crosslinking the polymer. At high crosslink densities, the rubbery modulus curve lifts significantly in the rubbery region becoming stiffer.

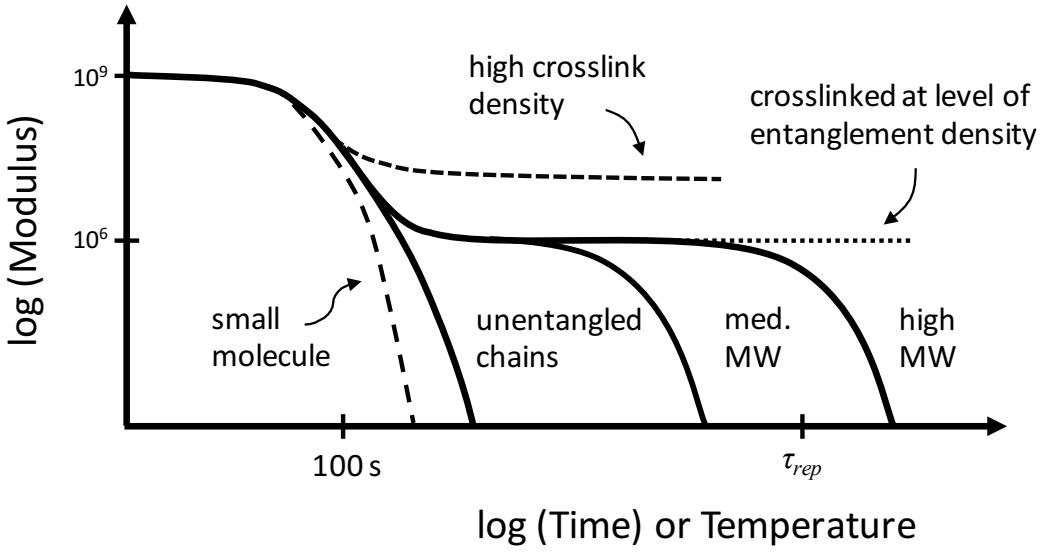

Figure 1.6: Log modulus as a function of temperature or log time for a variety of systems. The dashed small molecule curve shows the modulus behavior when the material falls out of a glassy state, around the 100 second mark in experimental time scales for the transition zone. Solid curves depict modulus as a function of increasing molecular weight for polymers where the modulus curves advance from left to right for unentangled polymers and entangled polymers with increasingly higher MW. For polymers above the entanglement density, the modulus curve forms a rubbery plateau that is extended further by increasing the MW. High MW polymer systems can thereby decouple α-relaxation modes associated with the glass transition and reptation at high temperatures above T_g or long times.

Experimentally, the modulus curves shown in Figure 1.6 are obtained by dynamic

mechanical analysis (DMA) via torsion or rheological experiments. Dynamic measurements extract storage (G′) and loss (G″) modulus terms, the real and imaginary components of the complex dynamic shear modulus (G*). The storage term represents the springiness of the material, or the restorable component in a viscoelastic material, while the loss term is an energy loss material property. The loss term peaks at the glass transition but then drastically falls as the polymer transitions into an amorphous solid. The phase angle between the storage and loss term, typically represented as δ, has the following relation to the loss to storage ratio.[2]

$$\tan\delta = \frac{\mathrm{G}''}{\mathrm{G}'}$$

These techniques collect raw dynamical response curves of the material as a function of temperature and frequency that are later converted into a master temperature or time dependent modulus curve. The master curves are created by first somewhat arbitrarily choosing a reference temperature (T_{ref}), which is then used to define the shift factor, a_T.[75] The amount required to shift each isotherm curve along the frequency axis defines the shift factor. Alternatively, the shift factor is defined as the ratio of temperature dependent relaxation times to an experimental reference relaxation time,

$$a_T = \frac{\tau(T)}{\tau(T_{ref})} = \exp\left(-\frac{C_1\left(T - T_{ref}\right)}{C_2 + T - T_{ref}}\right).$$

The functional form is the Williams-Landel-Ferry (WLF) empirical fitting equation, where the constants C_1 and C_2 are tabulated fitting parameters for a given viscoelastic material and reference temperature. The WLF equation is more frequently used with polymers, and is mathematically equivalent to the more familiar Vogel-Fulcher-Tammann (VFT) equation used in other glass studies.

1.4 EXPERIMENTAL GOALS AND OVERVIEW OF DISSERTATION

1.4.1 Experimental Summary

For over two decades, most of the experimental effort in the confinement literature has investigated the *average* T_g of glass forming materials under confinement, typically focusing on the effects of material-air or material-substrate interfaces on glassy dynamics. One of the most outstanding puzzles in the polymer physics literature is to understand the mechanisms by which interfaces such as polymer-air, polymer-substrate, polymer-liquid and polymer-polymer interfaces affect dynamics. In this dissertation, we explore how local dynamics (in our case T_g) are perturbed across a dissimilar polymer-polymer interface. By further developing an existing experimental technique,[48] I measured T_g *locally* in polymer semi-infinite bilayer films by inserting a 10 – 15 nm thick layer of high MW polymer chemically labeled with a fluorescent T_g sensitive molecule at distances z away from dissimilar polymer-polymer interfaces. Here we will explore how universal are $T_g(z)$ gradients that emanate from dissimilar polymer-polymer interfaces, what factors are required to obtain such extraordinary coupling of cooperative segmental dynamics across an immiscible polymer-polymer interface, and what properties of the interface such as the degree of immiscibility influence the behavior.

As discussed in section 1.3, α-relaxation modes can be decoupled from reptation or chain diffusion in high MW polymers well above bulk T_g. Decoupling diffusion from α-relaxations is a distinct and important characteristic of polymers that allows thin polymer layers to be localized in a polymer matrix and still remain in their designate position within

the film even at temperatures 20 K or more above bulk T_g. In polymer solution theory, χ represents the enthalpic component of the Flory-Huggins free energy equation of state, where the entropic term falls off to zero for high MW polymers. For most polymer pairs, χ does not favor mixing, but the interfacial width between two dissimilar polymer pairs evolves to an equilibrium thickness. Further discussion of equilibrating dissimilar polymer-polymer interfaces and the impact of not annealing the interfaces to equilibrium will be discussed in Chapter 4. The interfacial width *w* between two dissimilar polymer pairs is determined by both the interaction parameter χ and the statistical segmental length *a* (characteristic local length scale of a polymer segment due to local constraints on the chain dimension) by the following relation, $w = \frac{a}{\sqrt{6\chi}}$.[76] Experimentally, the interfacial width *w* for polymer pairs can be directly measured via neutron reflectivity,[77-79] or otherwise calculated from the cohesive energy density associated with each polymer. The square of the difference between two polymer specific cohesive energy densities is directly proportional to the interaction parameter χ, with which the interfacial width *w* can be determined using the relationship between χ and *w*.[67,80,81] Fortunately, most values of χ for canonical polymer pairs such as PS/PMMA and PS/poly(n butyl methacrylate) (PnBMA) are readily available and tabulated in polymer handbooks.[82] For the polymer pairs studied in this dissertation, the interfacial widths vary between 5 nm for weakly immiscible to 7 nm for very weakly immiscible polymer pairs. A schematic showing the dissimilar polymer-polymer bilayer geometry studied in Chapters 2, 3 and 4 of this dissertation is pictured in Figure 1.7, where the T_g difference across the polymer-polymer interface varies from 20 to 85 K depending on the particular polymer pair.

Prior to my work discussed in Chapters 3 and 4 that is published as a 2015 Communication in the *Journal of Chemical Physics*[83] and a follow-up article in 2017 *Journal of Chemical Physics*,[84] literature on phase separated polymer blends[2,42] and theory on miscible polymer blends[85] would have predicted that the local $T_g(z)$ profiles across a polymer-polymer interface would sharply transition from bulk T_g of one component to bulk T_g of the other component, closely following the $\phi(z) \approx \tanh(2z/w)$ composition profiles between the polymer pairs. As we have seen earlier in this Chapter, studies on confined polymers would not have necessarily predicted such abrupt transitions as expected by literature on phase separated polymer blends or theory on miscible polymer blends, given that it is generally well accepted in the confinement literature that interfaces can perturb local dynamics much more than a couple of nanometers deep into the material. Confinement literature would have rather predicted a $T_g(z)$ profile that penetrates approximately 50 nm into each component of the bilayer before bulk T_g is recovered on either side of the polymer-polymer interface.

Contrary to both of these predictions, I find that the local $T_g(z)$ profile across a PS/PnBMA interface is not only *highly asymmetric* towards the glassy high T_g PS component of the bilayer but that the local $T_g(z)$ profile extends 350 to 400 nm across the PS/PnBMA interface before both bulk T_gs are recovered. The length scales emanating from dissimilar polymer-polymer interfaces observed in this dissertation are approximately an order of magnitude larger than would have been predicted by confinement literature. An asymmetric mobility profile that extends deeper into the low mobility component across a low/high mobility interface was predicted in 2013 by a kinetically facilitated Limited Mobility model developed by the Lipson and Milner groups.[69,86] My work from

Chapters 3 and 4 experimentally supports these theoretical predictions by the Lipson and Milner groups, where I find that the glassy high T_g components show significantly larger length scales before bulk T_g is recovered[83,84] compared to the rubbery low T_g component of the semi-infinite bilayer.

Further expanding the semi-infinite bilayer geometry to a variety of dissimilar polymer pairs, I find that the $T_g(z)$ penetration length scale, or the length scale from which one side of the polymer-polymer interface recovers bulk T_g, on either side of the polymer-polymer interface appears to be universally grouped by the nature of the confinement; the $T_g(z)$ profile on the high T_g glassy side of the bilayer (so called soft confinement) penetrates 225-250 nm before bulk T_g is recovered, while the $T_g(z)$ profile on the low T_g rubbery side of the bilayer (so called hard confinement) penetrates 100-125 nm before bulk T_g is recovered. I find that the observed local $T_g(z)$ perturbation length scales are independent of bulk T_g differences across the polymer-polymer interfaces, the interaction parameter χ and consequently the equilibrium interfacial width w, chemical structure, and fragility. Instead, I find that extent to which the two dissimilar polymers are allowed to interdiffuse at the polymer-polymer interface affects the dynamical coupling across the interface. I show that if the dissimilar polymer-polymer interface is not allowed to form to equilibrium, the magnitude of the $Tg(z)$ profile is dramatically reduced.

My work suggests that perhaps the uniqueness of dissimilar polymer-polymer interfaces and their associated length scales may be attributed to the 5 to 7 nm interfacial width of the interface in contrast to the ~0.5 nm[87] breadth of polymer-air interfaces. A glass transition theory proposed by Mirigian and Schweizer[45-47] has recently predicted that by increasing the interfacial width of the free-surface layer, T_g reductions due to the

presence of an air interface are much longer and greater,[88] which supports our ideas in Chapter 4. The published results of Chapters 3 and 4 challenge the theoretical textbook understanding of polymer blends, specifically how material properties are affected in nanostructured materials that are dominated by polymer-polymer interfaces with domain sizes reaching below 100 nm.

Simulations by the David Simmons group[89] investigated how the interface between high T_g and low T_g simulated polymers affects the local dynamics. David Simmons has proposed that perhaps the Debye-Waller factor, or the high frequency shear modulus, is a key ingredient to understanding how a simulated high-T_g/low-T_g interface affects dynamics,[89] and that possibly the Debye-Waller factor, or the modulus of each component of my experimental semi-infinite bilayers, might be an important element for the astonishing dynamic coupling across dissimilar polymer-polymer interfaces. The role of modulus in systems with such large $T_g(z)$ profile length scales as demonstrated in this dissertation is currently being investigated in the Roth Lab. The results of Chapter 5 recently published in *ACS Macro Letters*[90] were directly influenced by simulations of a high-T_g/low-T_g interface from the Simmons group,[89] where I have experimentally limited the domain size of the high T_g PS component that was sandwiched between two bulk low T_g PnBMA components (mimicking periodic boundary conditions), and then by increasing the cooling rate (faster timescales) in my experiments, I was aiming to explore how faster timescales affect the $T_g(z)$ profile.

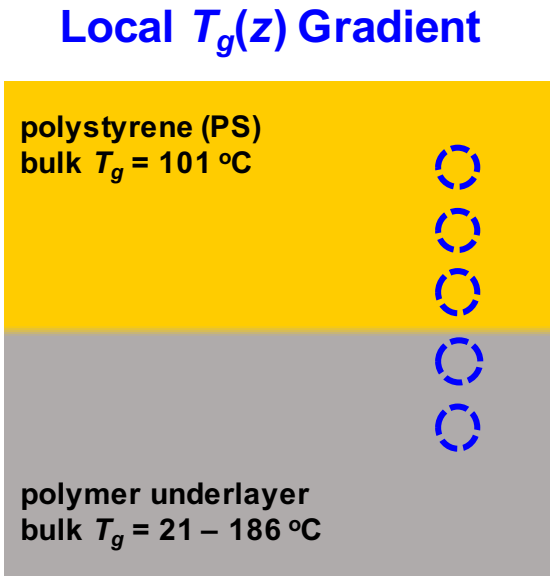

Figure 1.7: Polymer-polymer bilayer sample geometry composed of two dissimilar polymer pairs. The bilayers form an equilibrated polymer-polymer interfacial width w ranging from 5 nm for weakly immiscible to 7 nm for very weakly immiscible polymer pairs. The T_g difference across the polymer-polymer interface is varied from 20 to 85 K depending on the polymer pair. Average T_g of a PS layer atop a PnBMA film in PS/PnBMA bilayers is studied in Chapters 2. Chapters 3 and 4 measure local $T_g(z)$ profiles emanated from various dissimilar polymer-polymer interfaces in the semi-infinite bilayer geometry. Dashed circles indicate that T_g is investigated locally from dissimilar polymer-polymer interfaces. See Figure 3.1 for the sample geometry containing the 10 – 15 nm T_g reporting PS-pyrene layer.

1.4.2 Dissertation Outline

In Chapter 2, the fluorescence measurement technique utilized to measure local T_g profiles in systems containing dissimilar polymer-polymer interfaces is discussed, describing how it was modified from the original fluorescence methods established by the Torkelson group.[48] The local fluorescence technique measures T_g by localizing a 10 – 15 nm polymer layer chemically labeled with a florescent pyrene molecule sensitive to T_g at

a specific distance z from an interface. Pyrene is particularly sensitive to the local polarity and rigidity of its surrounding medium, and coupled with pyrene's high quantum yield, makes pyrene an excellent local measure of dynamics.[91] Chapter 2 then introduces how two interfaces, a combination of a free surface and a PS/PnBMA interface, perturb the average T_g of a PS layer atop a bulk PnBMA film as a function of PS layer thickness, and includes complimentary physical aging rate measurements done by Phillip Rauscher[92] on the PS layer atop PnBMA in the PS/PnBMA bilayer.

Chapters 3 and 4 explore how the presence of only one interface, specifically a dissimilar polymer-polymer interface in semi-infinite polymer-polymer bilayer systems, perturbs the local T_g as a function of depth z from the polymer-polymer interface, mapping the local $T_g(z)$ profile for a variety of immiscible polymer pairs. In Chapter 5, I then demonstrate how finite size and increasing cooling rates further affect the local $T_g(z,y)$ profile of a finite 300 nm PS domain sandwiched between two PnBMA layers, where the pyrene labeled PS layer is located at distance z from the first and distance y from the second PS/PnBMA interface. Due to the current lack of computational power, computer simulation studies are limited to employing periodic boundary conditions to generate enough "material" for their systems. The multilayer PnBMA/PS/PnBMA geometry experimentally mimics those periodic boundary conditions by repeating the PS/PnBMA interface in the semi-infinite bilayers discussed in Chapter 3. By then fixing the PS domain size, repeating the PS/PnBMA interfacial boundaries, and increasing cooling rate, I am trying to experimentally imitate computer simulation environments and identify how local T_g gradients are affected under common simulation conditions. Lastly, in Chapter 6 I will discuss the development of a new experimental fluorescence technique that can measure

modulus locally within a polymer film using a photomechanical dye chemically labeled to a polymer backbone.

1.5 REFERENCES

[1] A. Cavagna, Physics Reports **476**, 51 (2009).

[2] P.C. Hiemenz and T.P. Lodge, *Polymer Chemistry*, 2nd ed. (CRC Press, Boca Raton, 2007).

[3] M.D. Ediger, Annu Rev Phys Chem **51**, 99 (2000).

[4] E.A. Baker, P. Rittigstein, J.M. Torkelson, and C.B. Roth, J Polym Sci, Part B: Polym Phys **47**, 2509 (2009).

[5] X. Huang and C.B. Roth, J Chem Phys **144**, 234903 (2016).

[6] E.R. Weeks, J.C. Crocker, A.C. Levitt, A. Schofield, and D.A. Weitz, Science **287**, 627 (2000).

[7] L. Cipelletti, H. Bissig, V. Trappe, P. Ballesta, and S. Mazoyer, J Phys: Condens Matter **15**, S257 (2003).

[8] E. Wandersman, E. Dubois, V. Dupuis, A. Duri, A. Robert, and R. Perzynski, J Phys: Condens Matter **20**, 204124 (2008).

[9] S. Buzzaccaro, M.D. Alaimo, E. Secchi, and R. Piazza, J Phys: Condens Matter **27**, 194120 (2015).

[10] P.G. Debenedetti and F.H. Stillinger, Nature **410**, 259 (2001).

[11] F.H. Stillinger, Science **267**, 1935 (1995).

[12] J.C. Dyre, Rev. Mod. Phys. **78**, 953 (2006).

[13] A.J. Liu and S.R. Nagel, Annu. Rev. Condens. Matter Phys. **1**, 347 (2010).

[14] G. Biroli and J.P. Garrahan, J Chem Phys **138**, 12A301 (2013).

[15] M.D. Ediger and J.A. Forrest, Macromolecules **47**, 471 (2014).

[16] A.J. Liu and S.R. Nagel, Nature **396**, 21 (1998).

[17] C.S. O'Hern, L.E. Silbert, A.J. Liu, and S.R. Nagel, Phys. Rev. E **68**, 011306 (2003).

[18] C.S. O'Hern, A.J. Liu, and S.R. Nagel, Phys. Rev. Lett. **93**, 165702 (2004).

[19] M.E. Cates, J.P. Wittmer, J.P. Bouchaud, and P. Claudin, Phys. Rev. Lett. **81**, 1841 (1998).

[20] L.C.E. Struik, *Physical Aging in Amorphous Polymers and Other Materials* (Elsevier Scientific Publishing Company, Amsterdam, 1978).

[21] J.M. Hutchinson, Prog in Polym Sci **20**, 703 (1995).

[22] J.E. Pye, K.A. Rohald, E.A. Baker, and C.B. Roth, Macromolecules **43**, 8296 (2010).

[23] W. Gotze, *Complex Dynamics of Glass-Forming Liquids: a Mode-Coupling Theory* (Oxford University Press, Oxford, UK, 2009).

[24] W. Gotze and L. Sjogren, Rep. Prog. Phys. **55**, 241 (1992).

[25] S.P. Das, Rev. Mod. Phys. **76**, 786 (2004).

[26] G.L. Hunter and E.R. Weeks, Rep. Prog. Phys. **75**, 066501 (2012).

[27] U. Schneider, R. Brand, P. Lunkenheimer, and A. Loidl, Phys. Rev. Lett. **84**, 5560 (2000).

[28] M. Paluch, C.M. Roland, S. Pawlus, J. Zioło, and K.L. Ngai, Phys. Rev. Lett. **91**, 2372 (2003).

[29] C.B. Roth and R.R. Baglay, in *Polymer Glasses*, edited by C.B. Roth (CRC Press, Boca Raton, 2016), pp. 3–22.

[30] Y.P. Koh and S.L. Simon, Macromolecules **46**, 5815 (2013).

[31] Y.P. Koh and S.L. Simon, J Polym Sci, Part B: Polym Phys **46**, 2741 (2008).

[32] I.M. Hodge, J. Non-Cryst. Solids **169**, 211 (1994).

[33] S.Y. Chou, P.R. Krauss, and P.J. Renstrom, Appl. Phys. Lett. **67**, 3114 (1995).

[34] S.Y. Chou, P.R. Krauss, W. Zhang, L. Guo, and L. Zhuang, Journal of Vacuum Science Technology B Microelectronics and Nanometer Structures Processing, Measurement, and Phenomena **15**, 2897 (1997).

[35] P.A. O'Connell and G.B. McKenna, Science **307**, 1760 (2005).

[36] C.M. Stafford, C. Harrison, K.L. Beers, A. Karim, E.J. Amis, M.R. VanLandingham, H.-C. Kim, W. Volksen, R.D. Miller, and E.E. Simonyi, Nat Mater **3**, 545 (2004).

[37] C.B. Roth and J.R. Dutcher, Journal of Electroanalytical Chemistry **584**, 13 (2005).

[38] J.L. Keddie, R.A.L. Jones, and R.A. Cory, Europhys. Lett. **27**, 59 (1994).

[39] C.J. Ellison, M.K. Mundra, and J.M. Torkelson, Macromolecules **38**, 1767 (2005).

[40] J.L. Keddie, R.A.L. Jones, and R.A. Cory, Faraday Disc. **98**, 219 (1994).

[41] G. Adam and J.H. Gibbs, J Chem Phys **43**, 139 (1965).

[42] E. Hempel, G. Hempel, A. Hensel, C. Schick, and E. Donth, J. Phys. Chem. B **104**, 2460 (2000).

[43] U. Tracht, M. Wilhelm, A. Heuer, K. Schmidt-Rohr, and H.W. Spiess, Phys. Rev. Lett. **81**, 2727 (1998).

[44] J.D. Stevenson and P.G. Wolynes, J Chem Phys **129**, 234514 (2008).

[45] S. Mirigian and K.S. Schweizer, J Chem Phys **141**, 161103 (2014).

[46] S. Mirigian and K.S. Schweizer, J Chem Phys **140**, 194507 (2014).

[47] S. Mirigian and K.S. Schweizer, J. Phys. Chem. Lett. **4**, 3648 (2013).

[48] C.J. Ellison and J.M. Torkelson, Nat Mater **2**, 695 (2003).

[49] P. Rittigstein, R.D. Priestley, L.J. Broadbelt, and J.M. Torkelson, Nat Mater **6**, 278 (2007).

[50] C.B. Roth, K.L. McNerny, W.F. Jager, and J.M. Torkelson, Macromolecules **40**, 2568 (2007).

[51] C.B. Roth and J.M. Torkelson, Macromolecules **40**, 3328 (2007).

[52] C.M. Evans, S. Narayanan, Z. Jiang, and J.M. Torkelson, Phys. Rev. Lett. **109**, 038302 (2012).

[53] C.M. Evans, S. Kim, C.B. Roth, R.D. Priestley, L.J. Broadbelt, and J.M. Torkelson, Polymer **80**, 180 (2015).

[54] H. Yoon and G.B. McKenna, Macromolecules **47**, 8808 (2014).

[55] S. Askar, T. Wei, A.W. Tan, and J.M. Torkelson, J Chem Phys **146**, 203323 (2017).

[56] A.W. Tan and J.M. Torkelson, Polymer **82**, 327 (2016).

[57] D. Christie, C. Zhang, J. Fu, B. Koel, and R.D. Priestley, J Polym Sci, Part B: Polym Phys **54**, 1776 (2016).

[58] S. Butler and P. Harrowell, J Chem Phys **95**, 4454 (1991).

[59] S. Butler and P. Harrowell, J Chem Phys **95**, 4466 (1991).

[60] E.C. Glor, G.V. Angrand, and Z. Fakhraai, J Chem Phys **146**, 203330 (2017).

[61] R.D. Priestley, M.K. Mundra, N.J. Barnett, L.J. Broadbelt, and J.M. Torkelson, Aust. J. Chem. **60**, 765 (2007).

[62] C.H. Park, J.H. Kim, M. Ree, B.-H. Sohn, J.C. Jung, and W.-C. Zin, Polymer **45**, 4507 (2004).

[63] J.H. van Zanten, W.E. Wallace, and W.-L. Wu, Phys. Rev. E **53**, R2053 (1996).

[64] T.M. Murphy, D.S. Langhe, M. Ponting, E. Baer, B.D. Freeman, and D.R. Paul, Polymer **53**, 4002 (2012).

[65] T.M. Murphy, D.S. Langhe, M. Ponting, E. Baer, B.D. Freeman, and D.R. Paul, Polymer **52**, 6117 (2011).

[66] R. Casalini, L. Zhu, E. Baer, and C.M. Roland, Polymer **88**, 133 (2016).

[67] R.Y.F. Liu, T.E. Bernal-Lara, A. Hiltner, and E. Baer, Macromolecules **38**, 4819 (2005).

[68] R.J. Lang, W.L. Merling, and D.S. Simmons, ACS Macro Lett. **3**, 758 (2014).

[69] N.B. Tito, J.E.G. Lipson, and S.T. Milner, Soft Matter **9**, 9403 (2013).

[70] D.A. Bernards and T.A. Desai, Soft Matter **6**, 1621 (2010).

[71] E.A. Jackson, Y. Lee, and M.A. Hillmyer, Macromolecules **46**, 1484 (2013).

[72] V. Sethuraman and V. Ganesan, Soft Matter **12**, 7818 (2016).

[73] R.A. Segalman, B. McCulloch, S. Kirmayer, and J.J. Urban, Macromolecules **42**, 9205 (2009).

[74] H. Sai, K.W. Tan, K. Hur, E. Asenath-Smith, R. Hovden, Y. Jiang, M. Riccio, D.A. Muller, V. Elser, L.A. Estroff, S.M. Gruner, and U. Wiesner, Science **341**, 530 (2013).

[75] G.R. Strobl, *The Physics of Polymers*, 3rd ed. (Springer, Verlag Berlin Heidelberg, 2007).

[76] R.A.L. Jones and R.W. Richards, *Polymers at Surfaces and Interfaces* (Cambridge University Press, 1999).

[77] M. Stamm, S. Huttenback, G. Reiter, and T. Springer, Europhys. Lett. **14**, 451 (1991).

[78] D.F. Siqueira, D.W. Schubert, V. Erb, M. Stamm, and J.P. Amato, Colloid Polym Sci **273**, 1041 (1995).

[79] D.W. Schubert, V. Abetz, M. Stamm, T. Hack, and W. Siol, Macromolecules **28**, 2519 (1995).

[80] Y. Du, Y. Xue, and H.L. Frisch, *Physical Properties of Polymers* (AIP Press, New York,

1996), pp. 227–239.

[81] T. Matsuura, P. Blais, and S. Sourirajan, J. Appl. Polym. Sci. **20**, 1515 (1976).

[82] J.E. Mark, editor, *Physical Properties of Polymers* (AIP Press, New York, 1996).

[83] R.R. Baglay and C.B. Roth, J Chem Phys **143**, 111101 (2015).

[84] R.R. Baglay and C.B. Roth, J Chem Phys **146**, 203307 (2017).

[85] T.P. Lodge and T.C.B. McLeish, Macromolecules **33**, 5278 (2000).

[86] N.B. Tito, J.E.G. Lipson, and S.T. Milner, Soft Matter **9**, 3173 (2013).

[87] H.J. Butt, K. Graf, and M. Kappl, *Physics and Chemistry of Interfaces*, 3rd ed. (Wiley-VCH Verlag GmbH, Weinheim, Germany, 2013).

[88] S. Mirigian and K.S. Schweizer, J Chem Phys **146**, 203301 (2017).

[89] R.J. Lang and D.S. Simmons, Macromolecules **46**, 9818 (2013).

[90] R.R. Baglay and C.B. Roth, ACS Macro Lett. 887 (2017).

[91] B. Valeur, *Molecular Fluorescence: Principles and Applications* (Wiley-VCH, Weinheim, 2001).

[92] P.M. Rauscher, Honors Thesis: Effect of Adjacent Rubbery Layers on the Physical Aging of Polymer Glasses, 2013.

Chapter 2

Effect of Adjacent Rubbery poly(*n*-butyl methacrylate) Layer on the Glass Transition and Physical Aging of Glassy Polystyrene

A version of this chapter was published as Phillip M. Rauscher, Justin E. Pye, Roman R. Baglay and Connie B. Roth, *Macromolecules*, 46, 9806-9817, 2013.

2.1 SYNOPSIS

In this Chapter I will demonstrate that the modifications to the fluorescence method used in this dissertation reproduces the original data for single layer polystyrene (PS) films obtained by the fluorescence technique developed by the Torkelson group.[1-4] Torkelson and coworkers have previously demonstrated that the change in temperature-dependent fluorescence intensity of pyrene dye covalently attached to the PS backbone can be used to measure the local T_g in PS thin films. Pyrene dye is particularly sensitive to the local rigidity and polarity of the surrounding polymer matrix.[1] By utilizing a single wavelength measurement technique while ramping the temperature at 1 ^oC/min upon cooling, rather than the original full integration of emission spectra with 5 ^oC temperature jumps upon cooling, my modifications increase the number of data points collected, while minimizing photobleaching. Originally photobleaching would limit the operational temperature range of the experiments (generally more photobleaching at higher temperatures) and collection

frequency if the protocol required full integration scans of the pyrene emission spectrum. Photobleaching results from a non-trivial photochemical reaction composed of oxygen, heat, and UV radiation, working together to break down the fluorophores and degrading the measurement signal. The reaction is non-linear in temperature and cannot be simply removed by renormalization. Photobleaching seems have a greater effect on thinner films compared to bulk material, possibly because thinner films have more surface area per material, thereby having a greater influence of oxygen.

In addition to verifying that the modifications to the fluorescence method reproduce results in the literature, here I present how a dissimilar polymer-polymer interface, coupled with a polymer-air interface perturbs the glass transition of PS. Measurements of PS/PnBMA bilayer films, where the PS layer is labeled with a fluorescent dye pyrene that is sensitive to local T_g, are preformed via the modified fluorescence technique described further in section 2.4. The PS layer in the PS/PnBMA bilayer shows a much stronger decrease in T_g relative to a single layer PS film suggesting that the perturbative effects emanating from a dissimilar polymer-polymer interface play a significant role in thin film dynamics. Unlike the nonlinear average T_g decrease as a function of film thickness relative to bulk T_g found in single layer PS films, which follow a general Keddie, Jones, and Cory empirical equation,[5] the average PS layer T_g suggesting the mobility gradient from the PS/PnBMA interface observed in PS/PnBMA bilayers is almost linear on a semi-log scale, and penetrates more readily into PS. Pye et al.[6] have recently linked the local T_g gradient near a free surface in single layer PS films to reduced physical aging rate of single layer PS films, where the onset of the decrease in the aging rate tracks the onset of the T_g decrease. I include complementary measurements of the aging rate of glassy-PS layers by

Phillip Rauscher[7] (via ellipsometry) in PS/PnBMA bilayers (PS atop a bulk neat PnBMA underlayer), which found that the aging rate of PS as a function of PS layer thickness does not track the decrease in average T_g of the PS layer atop PnBMA in PS/PnBMA bilayers as measured by fluorescence.[8]

2.2 T_g BY FLUORESCENCE: ORIGINAL METHOD DEVELOPED BY THE TORKELSON GROUP

Over a decade ago, the Torkelson group proposed a fluorescence technique employing fluorescent small molecule dyes as probes within a polymer matrix.[1,3,9] The majority of the initial efforts were targeted to find fluorescent molecules that are sensitive to some property of the material such as the glass transition and physical aging in polymer thin films. Though the initial papers were first performed by exciting the doped chromophores in polymer films and monitoring the emission signal at a single wavelength (374, 384 and 395 nm corresponding to the first, third and fourth peaks of the emission intensity of pyrene dopant)[3,9] as the temperature was dropped 5 ^{o}C in successive steps upon cooling, the later work focused on integrating the full emission spectrum to alleviate scatter due to noise. In the early work by Ellison et al.,[3] they found that doping PS films with pyrene, a particularly good candidate for fluorescence measurements because pyrene possesses an incredibly high quantum yield,[10] reproduces the T_g reductions of single layer PS films upon decreasing the film thickness as first observed by Keddie, Jones, and Cory using ellipsometry.[5] In addition to doping films with chromophore, Ellison et al. were able to chemically attach a 1-pyrenyl butyl methacrylate monomer to the backbone of PS during polymerization of styrene with the pyrene monomer.[1]

Figure 2.1a plots the temperature dependence of fluorescence intensity for 545 nm (squares) and 17 nm (diamonds) thick single layer PS films labeled (chemically attached) with pyrene. The intersection of the two linear fit lines in the liquid to glassy regimes is taken to be the average T_g of the PS film. For film thicknesses larger than 100 nm, the chromophore reports bulk T_g, and for confined films such as the 17 nm thick PS sample, T_g is reduced by 26 K relative to bulk T_g consistent with T_g reductions as measured by ellipsometry in PS.[5] Figure 2.1b plots the average T_g as a function of PS film thickness where the measured T_g values are plotted as the difference relative to bulk PS T_g. Two different types of samples are plotted in Figure 2.1b, T_g as a function of film thickness for PS doped with pyrene (circles) and T_g as a function of film thickness for PS labeled with pyrene (triangles). The thin solid line is the empirical fit originally proposed by Keddie, Jones, and Cory to their ellipsometry data,[5] and the solid line is the same empirical equation fit to the Ellison et al.[1] pyrene labeled and doped single layer PS data from fluorescence.

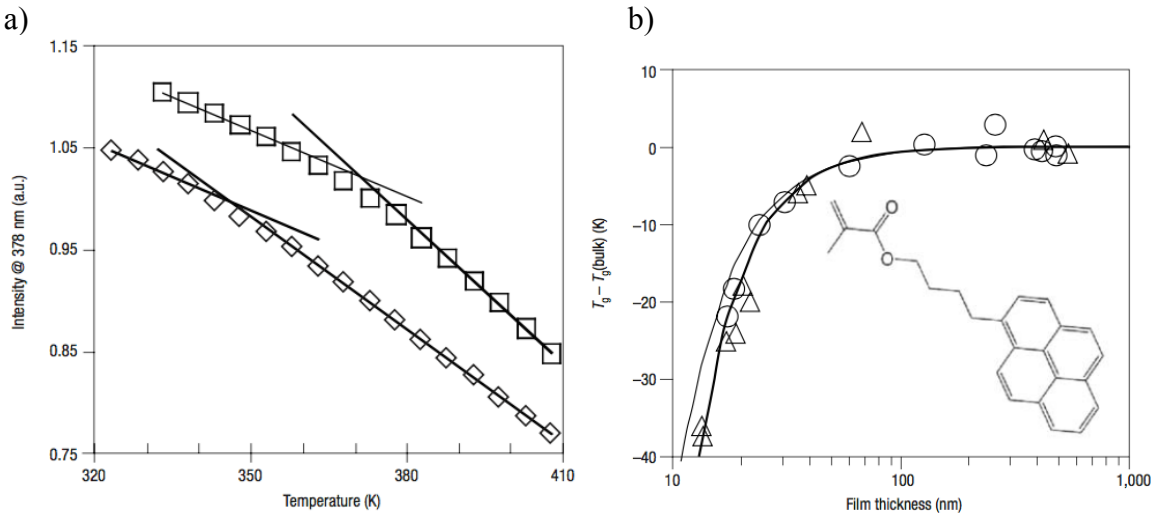

Figure 2.1. (a) Representative fluorescence intensity data as a function of temperature for bulk 545 nm (squares) and confined 17 nm (diamonds) thick PS films labeled with a pyrene fluorophore. The T_gs, as measured by the intersection of the glassy and liquid lines match both the bulk and confined T_g values found in the literature as measured by ellipsometry.[5] (b) T_g as a function of film thickness for PS doped with pyrene (circles) and T_g as a function of film thickness for PS labeled with pyrene (triangles). The thin line is the original Keddie, Jones, and Cory empirical fit to PS thin film T_g reductions as measured by ellipsometry.[5] The thick line is the same empirical function fit to PS thin film T_g reductions collected using the fluorescence technique. Insert is the chemical structure of the pyrene monomer chemically labeled to the PS backbone. Figures reproduced from ref.[1] with permission from the Nature Publishing Group.

Following their initial efforts and the ability to show that a PS film labeled with pyrene reproduces T_g reductions found in the literature, Ellison and Torkelson[1] introduced that by labeling PS with pyrene, it is possible to measure T_g *locally* in PS films, in contrast to techniques such as ellipsometry and differential scanning calorimetery (DSC), which measure the *average* T_g of the entire sample. In high molecular weight polymers, α-relaxations associated with T_g are effectively decoupled from diffusion of the chains, and

in polymers in particular it is possible to localize a layer within a matrix even above bulk T_g (decoupling of segmental motion and diffusion will be further discussed in Chapter 3).

Ellison and Torkelson[1] constructed PS bilayer samples of neat bulk (approximately 270 nm) PS capped with a pyrene labeled PS T_g sensitive layer, thermally annealed together to create a consolidated sample, and demonstrated by varying the PS-pyrene layer thickness that the free surface is the source of T_g reductions reported in the literature for supported PS films. By then using a thin 14 nm thick PS-pyrene layer inserted at distances away from the free surface deeper into the PS matrix, Ellison and Torkelson were the first to measure a local T_g gradient emanating from the free surface of PS, finding that PS bulk T_g is only recovered 30 to 40 nm deep into the film. Additionally, samples with a 14 nm thick PS-pyrene layer sandwiched between two neat bulk PS layers and a 12 nm thick PS-pyrene layer next to a silicon substrate, capped with a neat PS bulk layer, showed no T_g reductions relative to bulk T_g. These control experiments showed that there are no artifacts upon breaking the film into individual layers (albeit the layers were thermally annealed to create a consolidated sample) and that there is a neutral interaction between PS and the silica substrate. Following this set of experiments, over the past decade the Torkelson group measured physical aging at interfaces and bulk,[11-13] effects of plasticization,[14] nanocomposite content in PS thin films,[15] polymer fragility[16,17] and the effects of dissimilar polymer-polymer interfaces on T_g,[18-21] all upon confinement of polymer films using fluorescence techniques.

2.3 SAMPLE PREPARATION

2.3.1 Polymerization and Sample Build

For fluorescence measurements, PS was synthesized via free radical polymerization for 24 h at 50 ^{o}C with azobisisobutyronitrile (AIBN) as initiator, including trace amounts of 1-pyrenyl butyl methacrylate monomer that was synthesized by esterification of 1-pyrenebutanol and methacryloyl chloride.[1,22] PnBMA used for single layer fluorescence measurements was also synthesized via free radical polymerization with 1-pyrenyl butyl methacrylate monomer and AIBN as the initiator, but for 2 h at 50 ^{o}C. Post thermal termination, the PS-pyrene and PnBMA-pyrene polymer were subsequently reprecipitated in their respective methanol baths 7 times to remove any unreacted monomer and to reduce the polydispersity. Since the bulk PnBMA-pyrene T_g is close to room temperature, the methanol bath for PnBMA-pyrene was chilled to 10 ^{o}C. The resulting PS-pyrene molecular weight (M_w = 580 kg/mol, M_w/M_n = 1.6) and PnBMA-pyrene molecular weight (M_w = 1400 kg/mol, M_w/M_n = 1.7) was measured by gel permeation chromatography with tetrahydrofuran (THF) as eluent. The pyrene-label content in PS-pyrene of 0.34 mol% and in PnBMA-pyrene of .7 mol% was determined by ultraviolet-visible spectroscopy in spectroscopic grade THF. For ellipsometry measurements, PS with M_w = 934 kg/mol, M_w/M_n = 1.14 was purchased from Polymer Source and used as received.

Bilayer samples were made by spin-coating neat PnBMA (M_w = 319 kg/mol, M_w/M_n = 2.58, Scientific Polymer Products) from toluene solutions onto silicon for ellipsometry or quartz slides for fluorescence. The surface chemistry of quartz substrates ending in –OH surface groups is equivalent to that of silicon wafers containing a native oxide layer. PS-pyrene films spun onto freshly-cleaved mica were then floated atop the

PnBMA films via a water transfer procedure. All individual layers were annealed under vacuum for at least 18 h at 80 ^{o}C for PnBMA or 120 ^{o}C for PS-pyrene prior to bilayer assembly, and the thickness of each layer was independently measured by ellipsometry. Prior to fluorescence measurements, all bilayer films were directly annealed in the Peltier cooled Instec TS62 heater at 120 ^{o}C for 20 min to reset the sample's thermal history, dry out any remaining water, and create a well-defined PS/PnBMA interface. The interfacial width of PS/PnBMA bilayer films has been previously measured to be 7 nm for comparable molecular weights.[23]

2.3.2 Fluorescence Measurements

Fluorescence measurements on PS-pyrene, PnBMA-pyrene, and on PS-pyrene/PnBMA bilayers were performed with a Photon Technology International QuantaMaster spectrofluorometer with samples mounted in a Peltier-cooled Instec (TS62) hot stage. Before starting a fluorescence measurement, both single layer and bilayer films were thermally equilibrated at 120 ^{o}C for 20 min. The emission band-pass was set to 5 – 6 nm depending on PS or PnBMA film thickness to ensure that the raw intensity at the first pyrene emission peak remained less than 30 thousand counts with the voltage from the reference detector (correlated data) set to .9 $\pm$ .1 volts. The 5 – 6 nm emission band pass was set by first starting at 6 nm, then reducing the band pass in increments of .5 nm if the first pyrene emission peak was still above 30 thousand counts when the excitation mechanical shutter was closed to the point of distorting the excitation beam and if the emission mechanical shutter was closed more than 50 percent. The excitation band-pass was kept at 5 nm for all polymers labeled with pyrene (see Figure 2.2b for the chemical

structure of this specific pyrene label). Bilayer or single layer PS-pyrene and PnBMA-pyrene films were excited with a xenon arc lamp filtered to 330 nm with a monochromator, while the fluorescence intensity was collected on cooling at 1 K/min, averaging the peak emission intensity (peak at 379 nm for PS-pyrene and 377 nm for PnBMA-pyrene) for 3 s every 27 s. Samples were then reheated to the starting temperature and a full emission scan was collected to ensure the initial fluorescence intensity prior to the entire measurement cycle was recovered.

2.4 MODIFICATION TO THE FLUORESCENCE METHOD ORIGINALLY DEVELOPED BY THE TORKELSON GROUP

Pyrene is one of the canonical aromatic hydrocarbon small molecules that shows significant fine structure of the vibrational bands (fluorescence spectrum) in the solution phase that is highly sensitive to the nanoscale environment. Though pyrene readily forms excimers through π-π bonds if the monomer aggregates, the short-lived excimer state is typically avoided by using low concentrations of monomer in solutions.[24] Similar to solutions, pyrene doped in a polymer matrix or chemically labeled to a polymer backbone shows similar sensitivity to the nanoscale environment,[3,9] however the length of the tether between the polymer backbone and pyrene also determines the sensitivity.[24,25]

The solvent dependence on the intensity of the various vibrational bands was first realized in the 1970s where the intensity of certain bands (emission peaks) correlated well with the polarity of the media.[26,27] For example, it was recognized that the first peak showed overall increasing intensity with increasing polarity of the solvent at the expense

of the intensities of the higher energy bands.[27] The first peak of the pyrene fluorescence emission spectrum is well known to correspond to the 0-0 vibrational band where the singlet ground state transitions to the excited 0-0 singlet state.[10] In particular, the third peak of the emission spectrum showed minimal intensity variation with polarity. The ratio of the third to first peak was subsequently recognized as a measure of solvent polarity or qualitatively a local, nanoscopic measure of the interaction between dipoles of the media with the excited singlet state of pyrene.[27] The third to first peak ratio of pyrene served as a measure of the critical micelle concentration,[27] structural features such as phase transitions,[28] and recently as a self-referencing measure of T_g in free standing PS films.[25]

Because of the 0-0 bands sensitivity to local environment, here I measure the pyrene emission intensity at the 379 nm first peak of PS chemically labeled with pyrene and similarly at the 377 nm first peak of PnBMA chemically labeled with pyrene. The emission spectra of pyrene chemically labeled to PS and PnBMA, with the first vibrational bands identified by dashed vertical lines, is shown in Figure 2.2a and 2.2b for PS-pyrene and PnBMA-pyrene respectively. Since pyrene is sensitive to the polarity of its local environment, the peaks of pyrene labeled to PnBMA are slightly blue shifted relative to pyrene labeled PS.

In contrast, the experimental protocol developed by the Torkelson group typically integrates the intensity collected for the entire emission spectrum (usually taking over 60 s to acquire) every 5 ^{o}C on cooling, which helps to minimize noise associated with fluctuations in fluorescence intensity,[1] although early measurements did use the intensity at a single wavelength (374, 384 and 395 nm).[3,9] After collecting an emission spectrum, the temperature is subsequently dropped by 5 ^{o}C and equilibrated for 5 min prior to taking

a new emission spectrum at the new lower temperature. The 5 °C temperature jump followed by a 5 min equilibration step was meant to mimic the 1 K/min cooling rates from the original work by Keddie, Jones, and Cory.[5] Integrating over the entire spectrum is generally very laborious for the user since the software interfacing with the fluorescence system did not allow acquisition protocols, nor is the software easily modifiable due to company patents. The heaters were not interfaced with the fluorescence system so each temperature jump and equilibration step was done manually prior to taking a full emission spectrum, resulting in hours of time necessary for the user to measure a single sample.

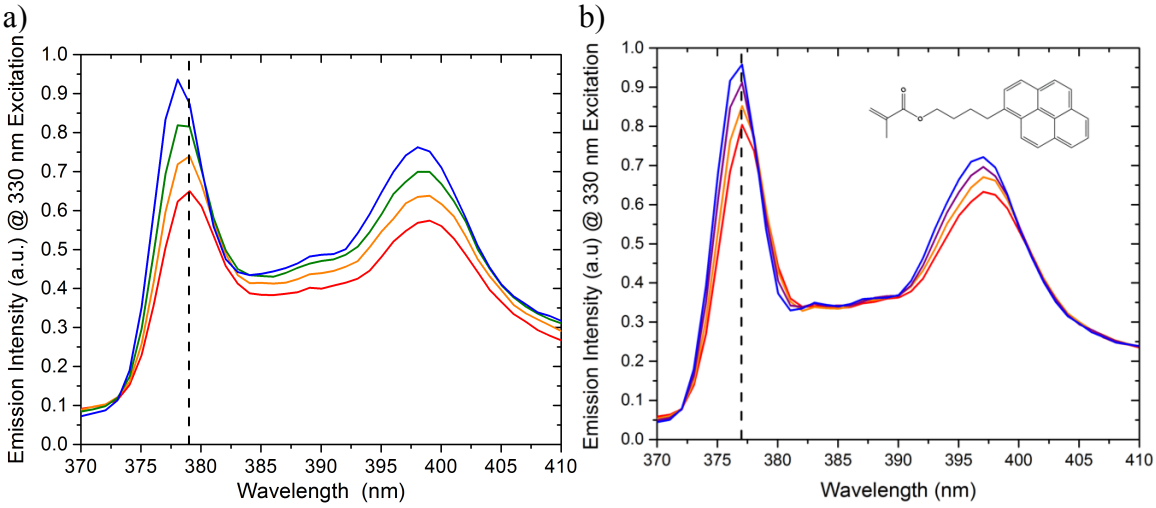

Figure 2.2: (a) Pyrene fluorescence spectra collected from a 16-nm thick single-layer PS film shown at representative temperatures (50, 80, 100, 115 °C from top to bottom) with the 379 nm wavelength used for T_g-ramping measurements indicated. (b) Pyrene emission spectra collected from a 430-nm thick single-layer PnBMA film is shown for a series of different temperatures (–10, 10, 30, 50 °C). Overall the pyrene spectra in both PS and PnBMA pyrene labeled single layer films primarily shifts uniformly up and down with temperature. Inserted is the chemical structure of the pyrene monomer chemically labeled to the PS and PnBMA backbone.

Here, we minimize fluctuations in fluorescence intensity by focusing on a single wavelength just off the first peak of the pyrene emission spectra and averaging over a 3 s acquisition window. Measuring the sample for 3 s per 0.5 ^{o}C greatly reduces the amount of time pyrene is exposed to UV light, especially at temperatures above 100 ^{o}C where the dye is particularly sensitive to photobleaching. For example, when measuring from 120 to 100 ^{o}C (typical starting temperature post thermal annealing of PS) and collecting for 3 s every .5 ^{o}C exposes the pyrene dye a total of 2 min of irradiation over that temperature range compared to 5 min of exposure if a full emission spectrum was integrated (60 seconds per spectrum) every 5 min for the same 120 to 100 ^{o}C temperature range. In addition, because the acquisition window is short, we can continuously ramp the temperature at 1 K/min, while sampling the fluorescence intensity every 27 s, dramatically increasing the amount of data collected for a single T_g measurement. Not only does ramping the temperature save the user time, the frequency of data points is greatly increased, from 1 data point per 5 ^{o}C as measured by the integration of the emission spectrum to 2 data points per 1 ^{o}C while ramping at 1 K/min. Ramping not only reduces photobleaching, but also leads to a 10-fold increase in data per temperature window compared to acquiring full pyrene emission spectra with temperature jumps. Data showing T_g reductions of single layer supported PS films collected by temperature ramping match those collected with the procedure described by the Torkelson group, and agrees with data previously reported.[1,4]

2.5 COMPARISON AND VERIFICATION OF THE MODIFIED FLUORESENCE METHOD TO LITERATURE: SINGLE LAYER PS FILMS

Figure 2.3 plots the measured fluorescence intensity at 379 nm as a function of temperature collected on cooling 1 K/min for single layer PS films on quartz. On cooling, the fluorescence intensity increases with decreasing temperature, reflecting that the amount of non-radiative decay from the pyrene excited state is reduced at lower temperatures. Non-radiative decay of the pyrene dye is influenced by the local density of the PS units surrounding it such that as PS transitions from the melt to glassy state, a change in the slope of the temperature-dependent intensity data is observed that can be used to measure T_g.[1,3] Representative data for thick and thin films are presented in Fig. 2.3 with a bulk 196 nm (circles) thick single layer PS film measuring a T_g = 98 ^oC consistent with bulk T_g for PS, and a thin 21.5 nm (triangles) thick single-layer PS film measuring a significantly reduced T_g = 80 ^oC, consistent with existing literature.[1,4] The T_g for each data set was identified by preforming linear fits to the data on either side of the transition and determining the intersection of the best fit lines. The data chosen on either the glassy or rubbery side of the transition was selected by optimizing the R^2 of the fit and also maintaining a distance of at least 10 ^oC away from the transition thereby avoiding data that contains curvature upon entering the transition from the rubbery to glassy regions.

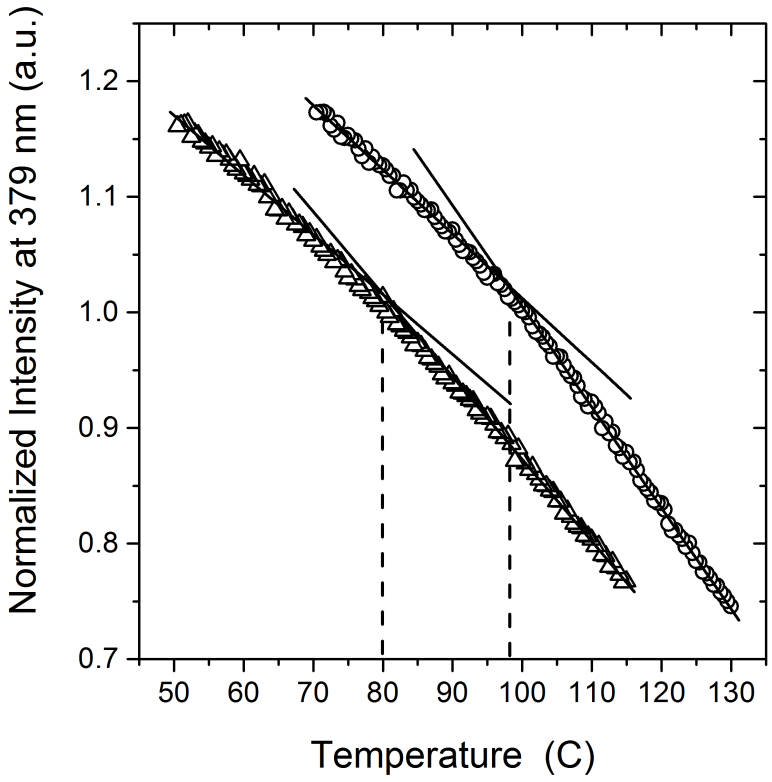

Figure 2.3: Fluorescence intensity as a function of temperature for single layer PS bulk 196 nm (circles) and thin 21.5 nm (triangles) thick films on quartz. The bulk PS film reports a T_g of 98 ^{o}C consistent with literature values while the 21.5 nm thick film show an 20 ^{o}C T_g depression also matching literature values of PS T_g upon confining the films to thin geometries.[1,4]

Figure 2.4 plots the single layer pyrene labeled PS average T_g as a function of PS film thickness, where the average T_g is the T_g of the entire film. To clarify, most common experimental techniques that measure T_g such as ellipsometry and differential scanning calorimetry are forced to measure the T_g across the whole film or material, whereas fluorescence measurements can be targeted to local measurements of T_g such as isolating the perturbation from a polymer-air interface, from finite size effects or substrate interactions.[1] Localization of the pyrene probe will be discussed in more detail in Chapter 3. All the PS and subsequent PnBMA T_g data shown has been collected by our revised

fluorescence ramping method at 1 ^{o}C per/min on cooling. The data for single layer PS films are compared to the existing data from the research literature, represented by the solid curve that is the best fit of the original empirical Keddie, Jones and Cory equation,[5] $T_g(h) = T_g^{bulk}\,[1 - (A/h)^{\delta}]$, given by Ellison et al.[4] to their fluorescence data for single-layer PS films with parameters of $T_g^{bulk} = 100$ ^{o}C, $A = 3.2$ nm, and $\delta = 1.63$. To within experimental error, the PS T_g collected by my modified fluorescence method matches the PS labeled data collected by integration of the pyrene emission spectrum by Ellison et al.[4]

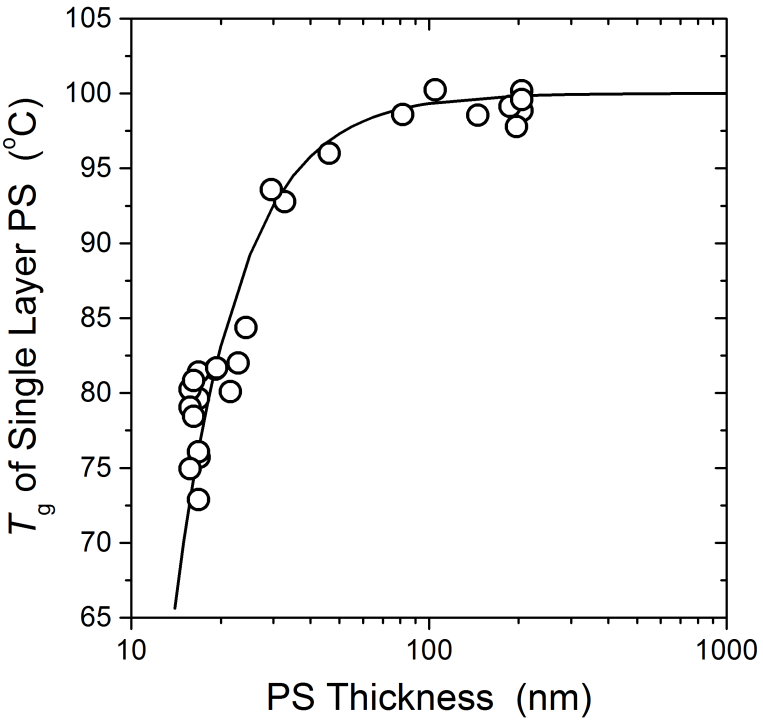

Figure 2.4: Average single layer PS T_g as a function of PS film thickness as measured by the modified fluorescence method. The solid curve is a fit to the empirical equation originally introduced by Keddie, Jones, and Cory[5] to characterize T_g depressions. The parameters used in the fit are from Ellison and Torkelson[4] where they have successfully shown that fluorescence technique reproduce T_g depressions as measured by ellipsometry (see Fig. 2.1).[1] The changes to the original fluorescence method clearly reproduce data available in the literature.

2.6 FLUORESCENCE T_g OF SUPPORTED SINGLE LAYER PnBMA FILMS

Figure 2.5 plots the single layer PnBMA average T_g as a function of PnBMA film thickness. Interestingly, single layer PnBMA T_g data shown in Fig. 2.5 exhibits a much weaker T_g depression compared to the PS T_g data in Fig. 2.4. Methacrylates, specifically poly(methyl methacrylate) PMMA, does not contain a T_g depression when the film thickness is lowered down to 10 nm, rather PMMA has a slight T_g increase below approximately 30 nm.[29] It is commonly recognized that the two oxygen atoms, each having an electron lone pair, in the PMMA methacrylate group can interact with the silicon oxide substrate and pin PMMA at the polymer-substrate interface. The competing effects at the polymer-air and polymer-substrate interfaces then generally cancel out each other's T_g perturbations in PMMA.[2] Though PnBMA possesses the same two oxygen atoms, both also with electron lone pairs in its butyl methacrylate side group, data from Priestley et al.[2] for different methacrylates would suggest that a long n-butyl group could limit the hydrogen bonding at the substrate. It is important to note that the pyrene used in this thesis is chemically attached to the PS or the PnBMA backbone by a butyl methacrylate group. The T_g depressions in Figure. 2.4 are highly weakened if the polymer is spun directly onto the substrate. Therefore, all of the single layer PS and PnBMA films containing a pyrene label were first spin cast onto freshly cleaved mica, annealed at T_g + 20 K for 18 hours to alleviate stresses due to spin coating, and only then successively transferred onto quartz via a water transfer process. The interaction of pyrene with the quartz substrate during spin coating polymer with pyrene label was first realized by Ellison and Torkelson.[14]

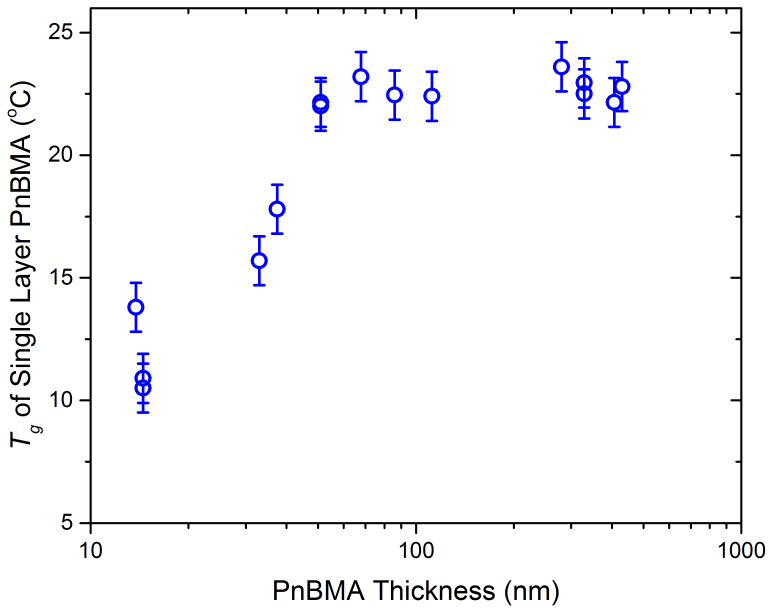

Figure 2.5: Average single layer PnBMA T_g as a function of PnBMA film thickness measured by the modified fluorescence technique. The PnBMA T_g depression upon confining the film is much weaker when compared to single layer PS T_g measurements.

2.7 PS/PnBMA BILAYER: AVERAGE $T_g(h)$ OF PS

The average PS layer T_g in a PS/PnBMA bilayer containing a static 7 nm glassy-rubbery PS/PnBMA polymer-polymer interface is plotted in Figure 2.6 as a function of the PS layer thickness atop a bulk > 450 nm thick PnBMA underlayer. In the present Chapter, I do not isolate the effects from one interface, i.e., the effects of a dissimilar polymer-polymer interface from a polymer-air interface as reported later in Chapters 3, 4, and 5. Instead the average PS layer T_g in the PS/PnBMA bilayer reflects a convolution of both polymer-air and polymer-polymer perturbations to the PS layer.

Stamm and coworkers have measured the interfacial width of PS/PnBMA bilayers using neutron reflectivity finding a slight temperature dependence with annealing temperature, (6.4 ± 0.2) nm at 120 °C and (8.6 ± 0.2) nm at 156 °C.[23] These data were

collected on PS/PnBMA bilayer films with molecular weights of PS M_w = 720 kg/mol, M_w/M_n = 1.13 and PnBMA M_w = 150 kg/mol, M_w/M_n = 1.03, that are not very different from those of the present study. A note of caution that the above studies using neutron scattering involve deuterated PS, which might be expected to alter the immiscibility slightly resulting in a small difference in interfacial width for an undeuterated system compared with that measured by Stamm et al.[30,31] Regardless, the specific absolute value of the interfacial width formed and that used in the ellipsometry layer model does not alter the measured physical aging rate.

Studies have shown that PS and PnBMA are weakly immiscible with small, but positive interaction parameter χ at all temperatures.[32] Only for low molecular weights is the entropy of the system enough to overcome the repulsive enthalpic interactions common in most high molecular weight polymer pairs. For example, Russell et al. reported a miscibility gap in PS-*b*-PnBMA diblock copolymers with total chain lengths of $M_w \leq 99$ kg/mol, but found that for M_w = 170 kg/mol the system ordered at all temperatures.[33] In comparison, blends of homopolymers will be even less miscible, with reports stating that PS and PnBMA blends phase separated for molecular weights as low as 20-30 kg/mol.[32] Thus, we can safely assume that the high molecular weights used in the present study, PnBMA M_w = 319 kg/mol and PS M_w = 934 kg/mol and 582 kg/mol, are immiscible. Additionally, studies by Forrest and Dalnoki-Veress investigated the interface formation between PS/PnBMA at various temperatures below and above the bulk T_g value of PS.[34-36] They reported the formation of an interfacial width of 2 nm for temperatures as low as 92 ^oC (8 ^oC below the bulk T_g of PS), "consistent with a reduction of the T_g of PS in the interfacial region of ~20 K". At lower temperatures, below 87 ^oC, no evolution of the

PS/PnBMA interface was observed.[37] These studies were for molecular weights of PS M_w = 120 kg/mol and PnBMA M_w = 182 kg/mol, which are significantly lower than that used in the present study. Thus, the interface can be taken to be effectively frozen at 65 °C when we will be comparing PS T_g measurements of the PS/PnBMA bilayer to PS aging measurements in the same sample geometry later in this chapter.

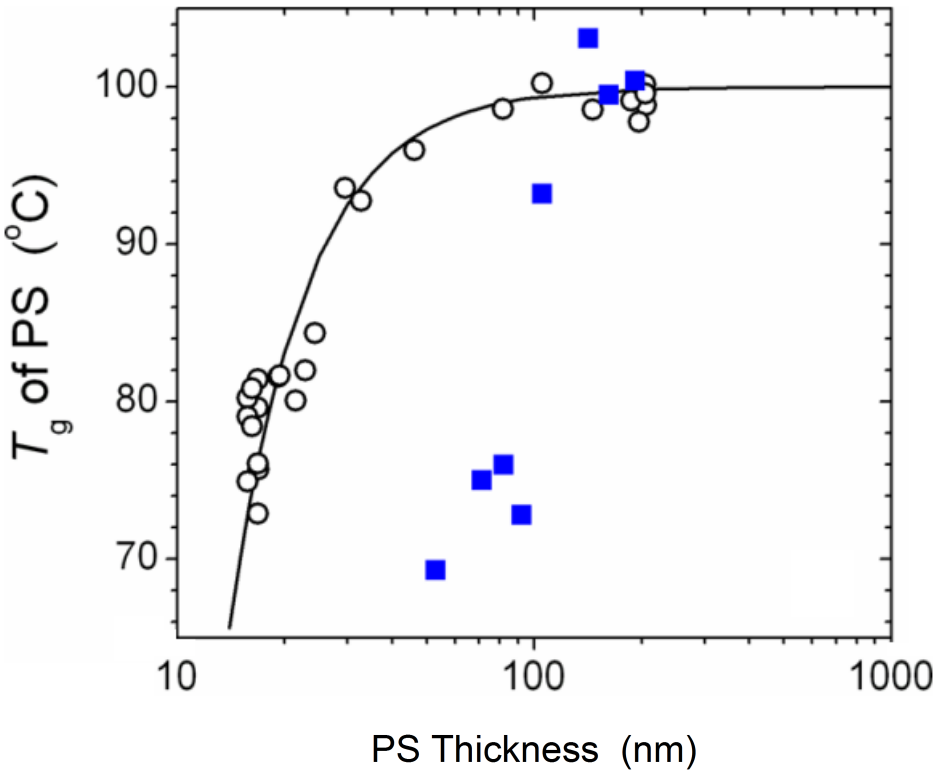

Figure 2.6: Average T_g of single layer PS (black circles, see Figure 2.4) compared to the average T_g of PS bilayers atop PnBMA underlayers in the PS/PnBMA bilayer system (blue squares). The PS/PnBMA bilayer shows an additional PS T_g reduction aside from the polymer-air interface. The further reduction is attributed to the presence of a 7 nm dissimilar polymer-polymer interface with PnBMA behaving as a soft underlayer during the course of the measurements in the PS/PnBMA bilayer. Perturbative effects due to only a dissimilar polymer-polymer interface will be discussed in Chapter 3.

In Figure 2.6 the sharp decrease in the PS T_g values for the PS/PnBMA bilayer films with decreasing PS layer thickness appears reminiscent of the sharp molecular-weight dependent T_g reductions in high molecular weight free standing (no substrate) films.[38] However, note that the *x*-axis in Fig. 2.6 is on a log scale, rather than linear. In addition, Pye and Roth[39] recently showed that such large T_g reductions in free standing PS films only comprise a small portion of the film and that the dominant transition is still molecular-weight independent, similar to that observed in supported films[1,4,5] and identical to that observed in low molecular weight free-standing films.[40] Recent work by Wang and McKenna have found that T_g reductions of ultrathin PS films floating on a liquid surface such as glycerol appear similar to that for supported films on silicon.[41,42] Thus, the nature of how a supposedly "soft interface", such as a free surface, monomeric liquid or lower T_g polymer, imparts T_g reductions to thin glassy films all appear to act quite differently. The large T_g reductions observed here are quite surprising suggesting that polymer-polymer interfaces may be quite different perhaps because they are not sharp, but several nanometers in width. Tito et al.[38] have recently developed a lattice mobility model that can make direct comparisons of local mobility near and across different interfaces including bilayers, which should be able to provide insight into the fundamental differences between these types of interfaces. Perhaps the extent to which local mobility is coupled across a boundary differs between a free surface, monomeric liquid, and polymer interface in a manner analogous to impedance matching. The behavior of these different interfaces generate interesting and puzzling questions that will be addressed in Chapters 3 and 4.

2.8 PHYSICAL AGING OF PS/PnBMA BILAYER

2.8.1 Experimentally Determining Aging: Ellipsometry of PS/PnBMA Bilayer

Ellipsometry physical aging measurements were done by Phillip Rauscher,[7] where physical aging was initiated by thermally quenching the bilayer films on silicon from equilibrium at 120 ^{o}C to room temperature at a cooling rate of ~50 ^{o}C/min.[43] The samples were then placed on the ellipsometer (Woollam M-2000) hot stage pre-equilibrated to the aging temperature of 65 ^{o}C. At this aging temperature, the PS layers are nominally in a glassy state (PS T_g^{bulk} = 101 ^{o}C), while the PnBMA layers are in their rubbery state above T_g (PnBMA T_g^{bulk} = 21 ^{o}C). This study focused on the physical aging behavior at 65 ^{o}C because it represents the peak in aging rate for bulk PS.[6,44] Dry nitrogen gas was flowed through the sample chamber at 1.8 L/min throughout the aging run to prevent uptake of water by the PnBMA layer. During the aging run, raw data of the amplitude ratio, $\Psi(\lambda)$, and phase shift, $\Delta(\lambda)$, of p- to s- polarized light was collected every minute (averaging over a 40 s time window) for a total aging time of 6 hours. This measurement procedure follows previous work developed by our group for physical aging studies on single layer films.[6,43,44] In our initial studies,[44] we demonstrated by comparing aging data for a variety of different aging times out to a total of 24 hours that a reliable measure of the aging rate can be obtained from aging runs as short as 6 hours. This was done to address concerns, discussed in the review by Hutchinson,[45] that aging measurements made for short aging times at temperatures far below T_g can be affected by an initial plateau in the aging data. We also routinely do measurements for longer aging times on new types of samples to ensure that these conditions are still valid. The ellipsometry data were analyzed by modeling the bilayer films as two Cauchy layers, with index of refraction $n(\lambda) = A + B / \lambda^2$ for λ = 400-

1000 nm, containing a 7 nm intermix layer between them, all atop a silicon substrate with a 2 nm native oxide layer. The thickness of the intermix layer was held fixed at 7 nm during fitting of the $\Psi(\lambda)$ and $\Delta(\lambda)$ data to correspond to the interfacial width measured by ref.[23], but setting this interface thickness to any equally reasonable value did not alter the measured aging rate.

Figure 2.7 (a) graphs the total bilayer film thickness as a function of aging time for a sample consisting of 415 nm of PS atop 524 nm of PnBMA supported on silicon. Both these layer thicknesses are considered to be thick enough to exhibit bulk glass transition and aging characteristics.[6,18,19] After a thermal quench from equilibrium at 120 ^{o}C, the bilayer sample is held at an aging temperature of 65 ^{o}C such that the PS layer will be in its glassy state (PS T_g^{bulk} = 101 ^{o}C), while the PnBMA layer will be in its rubbery state above T_g (PnBMA T_g^{bulk} = 21 ^{o}C). Observed here is a logarithmic decrease in the total bilayer thickness of the film as a function of aging time characteristic of physical aging in polymer films, which we ascribe to the physical aging of the glassy PS layer. Control measurements following the same experimental protocol on single layer PnBMA films show a stable rubbery PnBMA thickness as expected for films held in equilibrium above their T_g, as demonstrated in Figure 2.7 (b).

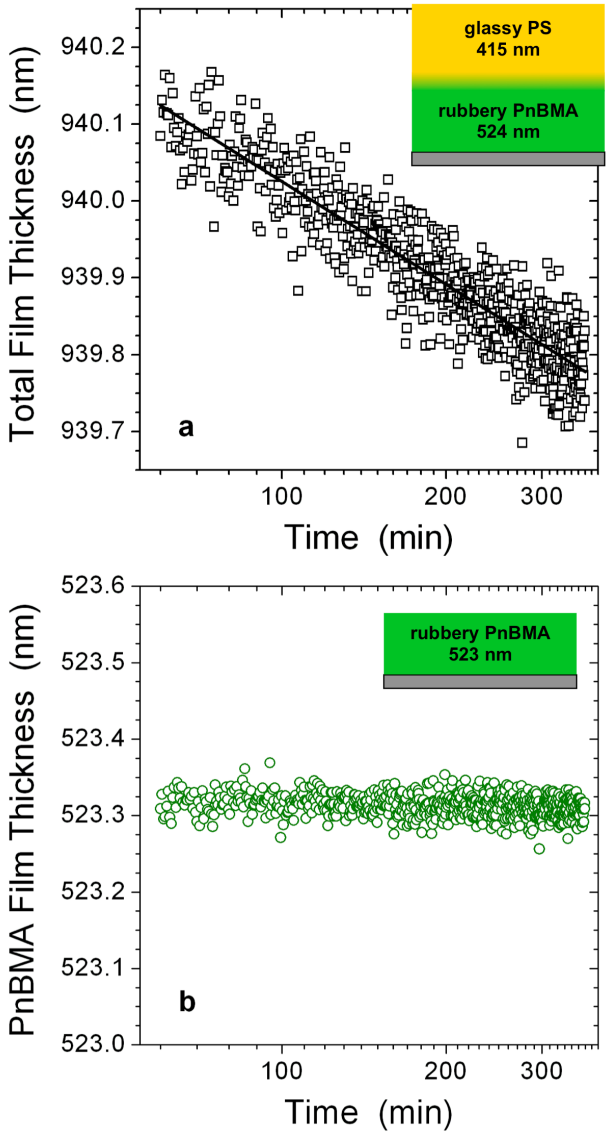

Figure 2.7: Film thickness over a 6 hour period for samples on silicon held at 65 ^{o}C following a thermal quench from equilibrium at 120 ^{o}C. (a) PS/PnBMA bilayer film with 415 nm of glassy PS atop 524 nm of rubbery PnBMA, and (b) PnBMA single layer film of 523 nm thickness. Note that the vertical scale intervals are identical in both graphs facilitating direct comparison.

In our previous work from the group we have shown that the physical aging rate of polymer films can be calculated from[44]

$$\beta = -\frac{1}{h_0}\left(\frac{dh}{d\log t}\right), \quad (1)$$

where h_0 was taken as the film thickness at an aging time of 10 min.[6,43,44,46] This was demonstrated to be equivalent to more sophisticated efforts of normalizing the thickness $h(t)$ data to an extrapolated equilibrium film thickness h_∞ to more closely match the original volumetric aging rate definition by Struik, $\beta = -1/V_\infty \, dV/d(\log t)$.[47] Several control measurements on single layer PnBMA films showed that the PnBMA thickness can take ~30 min to stabilize once placed on the ellipsometer hot stage (data not shown). This was believed to result from the slow relaxation dynamics of the rubbery PnBMA to both the dry nitrogen flow and the large temperature jumps associated with initiating the aging measurements. In order to be certain that the rubbery PnBMA layer is stable during the period in which the aging rate was calculated, the first 60 min of data were cropped and subsequent data were normalized to an initial thickness h_0 taken as a 10-min average of the thickness centered about the 60-min time mark.

2.8.2 Comparison of Fluorescence T_g to Physical Aging of PS in PS/PnBMA Bilayers

A comparison of PS T_g behavior as a function of PS layer thickness in PS/PnBMA bilayers to the physical aging rate β of PS also as a function of PS layer thickness in PS/PnBMA bilayers is plotted in Figure 2.8 (blue symbols) alongside T_g and physical aging of a single PS layer films (open black circles). The β(h) curve fitting the aging rate data for single layer PS films in Fig. 2.8 (b) was developed by Pye et al.[6] based on there being

a reduced T_g near the free surface. Using a simple two-layer model, similar to that used by Keddie, Jones and Cory for their $T_g(h)$ equation,[5] Pye et al.[6] assumed that a liquid-like layer of thickness $A(T)$ near the free surface with a T_g reduced below that of the aging temperature would have zero aging rate, while the remainder of the film would have a bulk-like aging rate $\beta_{bulk}(T)$. This assumption agreed with separate fluorescence measurements by Ellison and Torkelson[1] showing that the T_g of a 14-nm thick surface layer is reduced by –32 ^{o}C, while the T_g of an equivalent layer near the substrate interface still reported bulk T_g. Such a simple two-layer model resulted in a fitting equation for the aging rate, $\beta(h,T) = \beta_{bulk}(T)\,[1 - A(T)/h]$, that was shown to be a good fit to the aging data for single-layer PS films.[6] The temperature-dependent thickness $A(T)$ of the near surface layer agreed very well with a similar layer model applied to $T_g(h)$ reductions in single-layer free-standing films of low molecular weight PS[40,48] demonstrating that the same enhanced surface dynamics were responsible both for the $T_g(h)$ reductions and $\beta(h,T)$ reductions.[6] A more sophisticated analysis was also done by Pye et al. assuming a continuous change in aging rate with depth $\beta(z)$ that more realistically modeled the gradient in dynamics near the free surface, which produced equally good fits to the $\beta(h,T)$ data.[6] As can be seen in Fig. 2.8, the decrease in $T_g(h)$ and $\beta(h)$ for single-layer PS films occurs at roughly the same PS thickness (~80 nm). In contrast, the $T_g(h)$ and $\beta(h)$ for PS/PnBMA bilayer films are not correlated in the same manner.

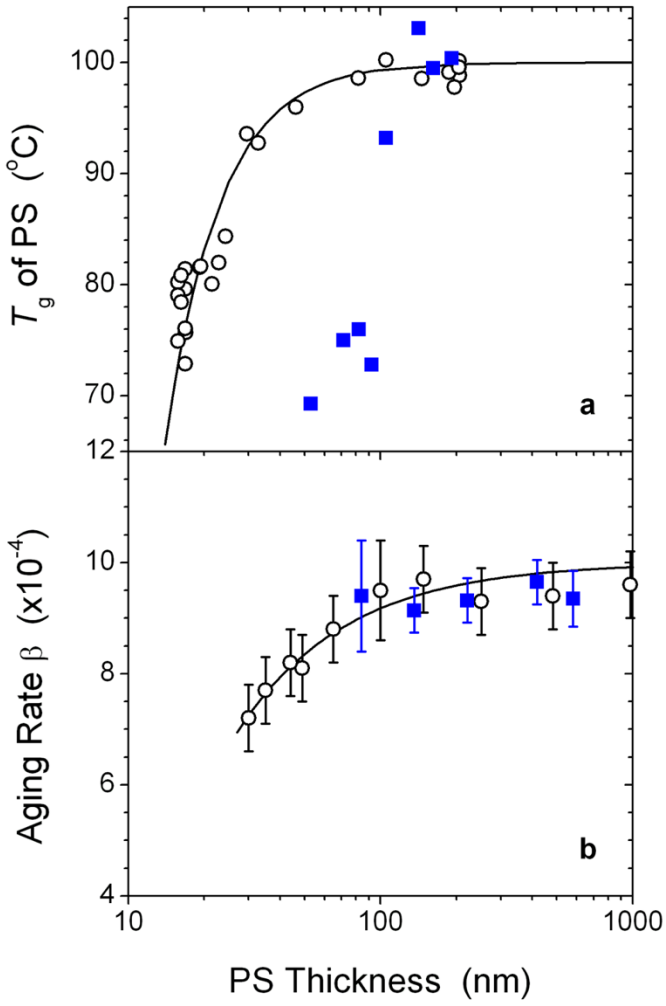

Figure 2.8: Comparison of the PS thickness dependence of PS T_g (a) and physical aging rate β at an aging temperature of 65 °C (b) for single-layer PS films (open circles) and PS/PnBMA bilayer films (closed squares) with bulk (~500 nm) PnBMA layers. (a) The T_g data presented were collected with our fluorescence ramping method, while the solid curve represents the fluorescence data given by Ellison et al[4]. for single-layer PS films. (b) The bilayer aging rate data were collected with the ellipsometry method, while the single-layer PS aging rate data was taken from Pye et al.[6] along with the fit curve (see text for details). Note that the 65 °C aging temperature is only 5-10 °C below the average T_g of an 84 nm PS layer atop PnBMA preventing us from decreasing the PS layer further without changing the aging temperature.

It is clear from the data presented in Fig. 2.8 that the aging rate of the PS layer in the PS/PnBMA bilayer films do not decrease with decreasing PS thickness when the fluorescence T_g data measures a very large decrease in the average T_g of the layer. The large error bars for the bilayer aging rate data at 84 nm PS layer thickness is typical of measurements on nanoconfined layers measured close to T_g and was also observed for single layer PS films.[6] For the bilayer aging data presented in Fig. 2.8 (b), each datapoint represents the average and standard deviation of 2-4 measurements, with the datapoint at 84 nm corresponding to an average of 4 measurements. Large sample-to-sample variability occurs for the aging rate of these thin PS layers because the T_g varies strongly with only a few nanometer change in PS layer thickness. Despite the large error bar for this data, the average of multiple measurements finds the aging rate for 84 nm thick PS layers atop PnBMA to be $\beta = 9.4 (\pm 0.9) \times 10^{-4}$, significantly and notably above the predicted value of $\beta \leq 7 \times 10^{-4}$ needed to correlate with the measured T_g reductions. Note that the 65 ^{o}C aging temperature is only 5-10 ^{o}C below the average T_g of an 84 nm PS layer preventing us from decreasing the PS layer further without changing the aging temperature as well. Thus, the bilayer aging rates stand in direct contrast with data for single-layer PS films, where the physical aging rate reductions accompany the T_g reductions seen at comparable film thickness.[6,11,12,49-52] For example, at an aging temperature of 65 ^{o}C, the 29 nm thick single-layer PS film in Fig. 2.8b shows a decrease in physical aging rate of $\Delta\beta \approx -3 \times 10^{-4}$ relative to bulk when the film had an average T_g reduction of 8-10 ^{o}C . In contrast, the bilayer films show no corresponding reduction in aging rate for the 84 nm thick PS layer despite an average T_g reduction of 25-30 ^{o}C. These results, while unexpected, are not necessarily inconsistent with previous observations in related multilayer systems. Gas

permeation and DSC studies on alternating glassy-rubbery multilayers formed by the forced-assembly process showed no change in aging rate as the glassy layer thickness was decreased down to 185 nm.[53,54] However, direct comparison between the present study and these alternating glassy-rubbery multilayers formed by forced-assembly should be done with care because different sample fabrication methods may cause important differences. For instance, the low viscosities and high processing temperatures needed to make the forced-assembly process work could result in differences in the local equilibrium of the interface and the possible formation of chemical bonds between polymers across the interface. How the presence of a chemical bond between the two polymers across the interface alters the local T_g and aging dynamics is an interesting and little explored issue, but of significant importance given the prevalence of block copolymer systems. The one study to make such a direct comparison between the local T_g of block copolymers and homopolymer multilayers found no difference in the local T_g between the two systems,[19] despite the well documented differences in local chain confirmations.

2.8.3 Open Questions

What factors could be altering the local aging rate near the glassy-rubbery interface is unclear. We can speculate that the presence of the much more flexible PnBMA units intermixed with the PS segments near the interfacial region might locally facilitate structural relaxation of the PS. Free volume diffusion type models have been popular in explaining accelerated aging in a number of different systems where free volume "holes" are thought to diffuse to and locally annihilate at interfaces.[55-62] Perhaps the nearby rubbery PnBMA domain provides a readily available sink for such local free volume. However,

several studies have shown that glassy dynamics do not correlate with free volume because mechanical deformation is found to lead to faster physical aging even in compression.[63-65] This type of behavior has been interpreted in terms of stress or stain facilitating energy barrier hopping[66,67] or equivalently tilting of the energy landscape,[68,69] such that glassy mobility is found to depend on the glass' position[69,70] within the potential energy landscape frequently used to describe glass formation.[71] It is possible that the presence of the PnBMA interface is altering the local stress of the nearby glassy PS. Pye and Roth[46] have recently shown that the physical aging rate of single layer PS films are strongly affected by stress imparted to the film during thermal cooling resulting from differences in thermal expansion between the film and underlying support. The bulk aging rate for single layer PS films on silicon (9.0-9.5 $\times$ 10^{-4} at 65 ^{o}C) is partially induced by a 5.3 MPa stress imparted to the film on cooling due to the thermal expansion mismatch between PS and silicon, while the zero stress aging rate is only ~4×10^{-4}.[46] How a rubbery underlayer with an elastic modulus on the order of MPa might alter this behavior is not necessarily trivial due to the presence of a broad 7 nm PS/PnBMA interface in the PS/PnBMA bilayer. The uniqueness of polymer-polymer interfaces will be discussed in detail in Chapters 3 and 4. If anything, one might suspect that the rubbery PnBMA would reduce the stress imparted to the PS film on cooling, which would be expected to lower the aging rate, contrary to what we observe. In the next Chapter we will focus on isolating the effects of just the glassy-rubbery interface in order to quantify its perturbation to the glass transition.

2.9 REFERENCES

[1] C.J. Ellison and J.M. Torkelson, Nat Mater **2**, 695 (2003).

[2] R.D. Priestley, M.K. Mundra, N.J. Barnett, L.J. Broadbelt, and J.M. Torkelson, Aust. J. Chem. **60**, 765 (2007).

[3] C.J. Ellison and J.M. Torkelson, J Polym Sci, Part B: Polym Phys **40**, 2745 (2002).

[4] C.J. Ellison, M.K. Mundra, and J.M. Torkelson, Macromolecules **38**, 1767 (2005).

[5] J.L. Keddie, R.A.L. Jones, and R.A. Cory, Europhys. Lett. **27**, 59 (1994).

[6] J.E. Pye, K.A. Rohald, E.A. Baker, and C.B. Roth, Macromolecules **43**, 8296 (2010).

[7] P.M. Rauscher, Honors Thesis: Effect of Adjacent Rubbery Layers on the Physical Aging of Polymer Glasses, 2013.

[8] P.M. Rauscher, J.E. Pye, R.R. Baglay, and C.B. Roth, Macromolecules **46**, 9806 (2013).

[9] C.J. Ellison, S.D. Kim, D.B. Hall, and J.M. Torkelson, Eur. Phys. J. E **8**, 155 (2002).

[10] B. Valeur, *Molecular Fluorescence: Principles and Applications* (Wiley-VCH, Weinheim, 2001).

[11] R.D. Priestley, L.J. Broadbelt, and J.M. Torkelson, Macromolecules **38**, 654 (2005).

[12] R.D. Priestley, C.J. Ellison, L.J. Broadbelt, and J.M. Torkelson, Science **309**, 456 (2005).

[13] P. Rittigstein and J.M. Torkelson, J Polym Sci, Part B: Polym Phys **44**, 2935 (2006).

[14] C.J. Ellison, R.L. Ruszkowski, N.J. Fredin, and J.M. Torkelson, Phys. Rev. Lett. **92**, 095702 (2004).

[15] P. Rittigstein, R.D. Priestley, L.J. Broadbelt, and J.M. Torkelson, Nat Mater **6**, 278 (2007).

[16] C.M. Evans, H. Deng, W.F. Jager, and J.M. Torkelson, Macromolecules **46**, 6091 (2013).

[17] C.M. Evans and J.M. Torkelson, Macromolecules **45**, 8319 (2012).

[18] C.B. Roth, K.L. McNerny, W.F. Jager, and J.M. Torkelson, Macromolecules **40**, 2568 (2007).

[19] C.B. Roth and J.M. Torkelson, Macromolecules **40**, 3328 (2007).

[20] C.M. Evans, R.W. Sandoval, and J.M. Torkelson, Macromolecules **44**, 6645 (2011).

[21] C.M. Evans, S. Kim, C.B. Roth, R.D. Priestley, L.J. Broadbelt, and J.M. Torkelson, Polymer **80**, 180 (2015).

[22] A. Kriisa, S.S. Park, and C.B. Roth, J Polym Sci, Part B: Polym Phys **50**, 250 (2011).

[23] D.F. Siqueira, D.W. Schubert, V. Erb, M. Stamm, and J.P. Amato, Colloid Polym Sci **273**, 1041 (1995).

[24] P. Chen, editor, *Molecular Interfacial Phenomena of Polymers and Biopolymers* (Woodhead Publishing, Cambridge, 2005), pp. 214–263.

[25] S. Kim, C.B. Roth, and J.M. Torkelson, J Polym Sci, Part B: Polym Phys **46**, 2754 (2008).

[26] A. Nakajima, Journal of Luminescence **11**, 429 (1976).

[27] K. Kalyanasundaram and J.K. Thomas, J. Am. Chem. Soc. **99**, 2039 (1977).

[28] D.J.W. Barber, D.A.N. Morris, and J.K. Thomas, Chemical Physics Letters **37**, 481 (1976).

[29] J.L. Keddie, R.A.L. Jones, and R.A. Cory, Faraday Disc. **98**, 219 (1994).

[30] G.H. Fredrickson and H.C. Andersen, Phys. Rev. Lett. **53**, 1244 (1984).

[31] G.H. Fredrickson and H.C. Andersen, J Chem Phys **83**, 5822 (1985).

[32] S. Butler and P. Harrowell, J Chem Phys **95**, 4466 (1991).

[33] S. Butler and P. Harrowell, J Chem Phys **95**, 4454 (1991).

[34] S. Mirigian and K.S. Schweizer, J. Phys. Chem. Lett. **4**, 3648 (2013).

[35] S. Mirigian and K.S. Schweizer, J Chem Phys **140**, 194507 (2014).

[36] S. Mirigian and K.S. Schweizer, J Chem Phys **141**, 161103 (2014).

[37] G. Adam and J.H. Gibbs, J Chem Phys **43**, 139 (1965).

[38] N.B. Tito, J.E.G. Lipson, and S.T. Milner, Soft Matter **9**, 9403 (2013).

[39] J.E. Pye and C.B. Roth, Phys. Rev. Lett. **107**, 235701 (2011).

[40] J. Mattsson, J.A. Forrest, and L. Borjesson, Phys. Rev. E **62**, 5187 (2000).

[41] J. Wang and G.B. McKenna, Macromolecules **46**, 2485 (2013).

[42] J. Wang and G.B. McKenna, J Polym Sci, Part B: Polym Phys **51**, 1343 (2013).

[43] L.A.G. Gray, S.W. Yoon, W.A. Pahner, J.E. Davidheiser, and C.B. Roth, Macromolecules **45**, 1701 (2012).

[44] E.A. Baker, P. Rittigstein, J.M. Torkelson, and C.B. Roth, J Polym Sci, Part B: Polym Phys **47**, 2509 (2009).

[45] J.M. Hutchinson, Prog in Polym Sci **20**, 703 (1995).

[46] J.E. Pye and C.B. Roth, Macromolecules **46**, 9455 (2013).

[47] L.C.E. Struik, *Physical Aging in Amorphous Polymers and Other Materials* (Elsevier Scientific Publishing Company, Amsterdam, 1978).

[48] J.A. Forrest and J. Mattsson, Phys. Rev. E **61**, R53 (2000).

[49] S. Kawana and R.A.L. Jones, Eur. Phys. J. E **10**, 223 (2003).

[50] Y.P. Koh and S.L. Simon, J Polym Sci, Part B: Polym Phys **46**, 2741 (2008).

[51] B. Frieberg, E. Glynos, and P.F. Green, Phys. Rev. Lett. **108**, 268304 (2012).

[52] B. Frieberg, E. Glynos, G. Sakellariou, and P.F. Green, ACS Macro Lett. **1**, 636 (2012).

[53] T.M. Murphy, D.S. Langhe, M. Ponting, E. Baer, B.D. Freeman, and D.R. Paul, Polymer **53**, 4002 (2012).

[54] T.M. Murphy, D.S. Langhe, M. Ponting, E. Baer, B.D. Freeman, and D.R. Paul, Polymer **52**, 6117 (2011).

[55] D. Cangialosi, M. Wübbenhorst, J. Groenewold, E. Mendes, H. Schut, A. van Veen, and S.J. Picken, Phys Rev B **70**, 224213 (2004).

[56] V.M. Boucher, D. Cangialosi, A. Alegría, and J. Colmenero, Macromolecules **45**, 5296 (2012).

[57] M.S. McCaig and D.R. Paul, Polymer **31**, 629 (2000).

[58] M.S. McCaig, D.R. Paul, and J.W. Barlow, Polymer **41**, 639 (1999).

[59] Y. Huang, X. Wang, and D. Paul, J Membrane Sci **277**, 219 (2006).

[60] A.W. Thornton and A.J. Hill, Ind. Eng. Chem. Res. **49**, 12119 (2010).

[61] V.M. Boucher, D. Cangialosi, A. Alegría, J. Colmenero, J. González-Irun, and L.M. Liz-Marzan, Soft Matter **6**, 3306 (2010).

[62] D. Cangialosi, V.M. Boucher, A. Alegría, and J. Colmenero, J Chem Phys **135**, 014901 (2011).

[63] D.M. Colucci, P.A. OConnell, and G.B. McKenna, **37**, 1469 (1997).

[64] R.A. Riggleman, H.-N. Lee, M.D. Ediger, and J.J. de Pablo, Phys. Rev. Lett. **99**, 215501 (2007).

[65] T.L. Smith, G. Levita, and W.K. Moonan, J Polym Sci, Part B: Polym Phys **26**, 875 (1988).

[66] K. Chen and K.S. Schweizer, Europhys. Lett. **79**, 26006 (2007).

[67] K. Chen and K.S. Schweizer, Macromolecules **44**, 3988 (2011).

[68] D.J. Lacks and M.J. Osborne, Phys. Rev. Lett. **93**, 255501 (2004).

[69] Y.G. Chung and D.J. Lacks, J. Phys. Chem. B **116**, 14201 (2012).

[70] R.A. Riggleman, K.S. Schweizer, and J.J. de Pablo, Macromolecules **41**, 4969 (2008).

[71] P.G. Debenedetti and F.H. Stillinger, Nature **410**, 259 (2001).

Chapter 3

Experimentally Determined Profile of Local Glass Transition Temperature Across a Glassy-Rubbery Polymer Interface with a T_g Difference of 80 K

A version of this chapter was published as Roman R. Baglay and Connie B. Roth, *Journal of Chemical Physics*, 143, 11110, 2015.

3.1 SYNOPSIS

For decades the glass transition in confined systems has been studied with the hopes of uncovering the governing length scales that impact these dynamics. Most efforts have focused on the effects of the free surface, however the theoretical treatment of such interfaces relies on the assumption of a set of dynamics at the polymer-air interface. In this Chapter we will explore the impact of a dissimilar polymer-polymer interfacial boundary with a bulk T_g difference of 80 K on the local glass transition temperature $T_g(z)$ as a function of depth z away from the polymer-polymer interface. It is clear that such a system possesses asymptotics, where bulk dynamics must be recovered far from the polymer-polymer interface on both sides of the model semi-infinite bilayer. We will further investigate the characteristic length scales of cooperative dynamics imparted by a dissimilar polymer-polymer interface and show that unlike polymer-air, polymer-substrate, or polymer-liquid

interfaces, the dynamics across a dissimilar polymer-polymer interface are smooth and continuous.

High molecular weight polymers have a large separation in time scales between cooperative segmental motion (α-relaxation) and chain diffusion allowing these series of measurements to map out a local $T_g(z)$ profile across a glassy (high T_g component)/rubbery (low T_g component) interface of polystyrene (PS)/poly(*n*-butyl methacrylate) (PnBMA) using fluorescence. In this Chapter we will find that a dissimilar polymer-polymer interface produces unexpected results when compared to expectations based on the existing literature on miscible polymer blends. In contrast to expectations based on miscible blends, which would predict a sharp transition in dynamics across a dissimilar polymer-polymer interface with a strong correlation to the composition profile, the measured cooperative dynamics do not correlate with the 7 nm wide symmetric composition profile of the interface. Instead I find that the cooperative dynamics linking local T_g are very broad, spanning 350-400 nm from one bulk T_g value to another, and highly asymmetric, extending further into the glassy side (PS side of the PS/PnBMA system) of the semi-infinite bilayer.

3.2 INTRODUCTION

Glassy materials reveal a rich dynamic heterogeneity, both spatially and temporally, on cooling close to the glass transition temperature (T_g).[1,2] In this supercooled region, local rearrangements are thought to be facilitated through cooperative motion amongst neighboring units, such that the dynamics are coupled to their surrounding environment.[3,4] Upon vitrification, the glass former enters a dynamically frustrated state where the available thermal energy is insufficient to activate this cooperative motion

among multiple constituents. The length scales and mechanisms underlying these interactions that induce cooperative motion are still highly debated.[1,3,5]

One promising approach to understanding cooperative dynamical length scales associated with the glass transition is to introduce a local perturbation to the system, typically a boundary with faster or slower dynamics, and investigate how this perturbation alters the local dynamics. Variations on this type of approach have been treated both experimentally[6-10] and theoretically,[11-17] particularly investigating glass formers confined to nanoscopic dimensions.[6-9,11,18,19] Because of their ubiquity and technological importance, the majority of such studies have been done on thin polymer films. One can separate the effects of a perturbing interface into two parts: (1) Molecules or segments located at the interface have their dynamics enhanced or suppressed, depending on the particular interaction. For example, at a free surface (e.g., a polymer-air interface) the dynamics are typically enhanced, believed to result from the partial absence of contacts with surrounding units.[13,15,20] (2) This difference in local mobility at the interface is then propagated into the material by some yet not well understood mechanism. For dynamics connected to the glass transition, there is evidence that this mechanism is associated with cooperative motion.[10,17,21,22] This central idea suggests that the study of how a local dynamical perturbation to T_g propagates into the material can provide insight into the nature of how cooperative motion is coupled and transferred across neighboring cooperatively rearranging regions (CRRs). A single CRR, an idea originally introduced by Adam and Gibbs,[23] is defined as the minimum number of units necessary to undergo a collective local rearrangement.[3] Most estimates place the size of a single CRR at approximately 3 nm for typical glass formers, including polymers.[2,24,25] Yet studies of glassy dynamics in

nanoconfined systems suggest that dynamical perturbations of an interface persist much deeper into the material than a single CRR, several tens of nanometers in some cases before local bulk-like dynamics are recovered.[8,10,26] Such studies have primarily focused on the presence of a free surface as the source of dynamical perturbation to the system. However, the difficulty with determining a dynamical length scale when investigating the polymer-air interface is how to theoretically quantify the magnitude of the enhanced dynamics at the free surface.[13,14,20,27,28] Some studies have estimated the free surface T_g at ~300 K,[29,30] while others have suggested that the free surface may always be liquid-like.[31-33] To avoid these ambiguities of how to treat the free surface and subsequent polymer-air interface, we instead investigate here how the local T_g and associated dynamics transition from one well-defined T_g value to another.

In the present Chapter, we take advantage of the large separation of time scales in high molecular weight polymers between cooperative segmental motion (α-relaxation) and chain diffusion. For example, at temperatures of T_g + 15-20 K, chain diffusion occurs on time scales of many hours to days for molecular weights of 700-2000 kg/mol,[34-36] while the α-relaxation time is on the order of milliseconds at such temperatures.[37] This decoupling of local vs. global chain dynamics in polymers is well known and has been frequently exploited. Here, I employ this strategy to create an interface with a large 80 K step-change in T_g from one side to the other between two dissimilar polymers: polystyrene (PS) with bulk glass transition temperature $T_g^{bulk}{}_{PS}$ = 101 ^oC, and poly(*n*-butyl methacrylate) (PnBMA) with $T_g^{bulk}{}_{PnBMA}$ = 21 ^oC. I utilize a fluorescence method to measure the local T_g of a layer a fixed distance z from this interface, whose chains have been covalently tagged with a fluorescent pyrene butyl methacrylate probe. By assembling

multilayer stacks of spin-coated polymer films with specific layer thicknesses via a water transfer process, and subsequently annealing them carefully to consolidate the sample into a single material while still limiting macroscopic diffusion of the high molecular weight chains, it is possible to create samples where the fluorescence signal originates from a 10-15 nm thick layer at a known distance z from the interface. Iterating this process to create many samples with varying values of z allows us to measure the local $T_g(z)$ at different distances from this interface. As the position z of the pyrene labeled PS or PnBMA layer is varied, the local $T_g(z)$ measured must clearly transition from $T_g^{bulk}{}_{PS}$ = 101 ^oC far from the interface on one side to $T_g^{bulk}{}_{PnBMA}$ = 21 ^oC far from the interface on the other. Surprisingly, I find that the local $T_g(z)$ takes approximately 350-400 nm to transition between these two extremes, with an asymmetric profile propagating deeper into the glassy PS side of the bilayer system.

3.3 EXPERIMENTAL METHODS

High molecular weight pyrene-labeled polystyrene (PS-Py) with 1.4 mol% pyrene content (M_w = 672 kg/mol, M_w/M_n = 1.3) and high molecular weight pyrene-labeled poly(*n*-butyl methacrylate) (PnBMA-Py) with 0.7 mol% pyrene content (M_w = 1400 kg/mol, M_w/M_n = 1.7) were synthesized by bulk free radical polymerization as follows. 1-pyrenylbutyl methacrylate monomer was synthesized by esterification of 1-pyrenebutanol and methacryloyl chloride.[8,38] This pyrene monomer was then copolymerized at 50 ^oC with styrene for 24 h or *n*-butyl methacrylate for 2 h under a nitrogen environment using azobisisobutyronitrile (AIBN) as initiator. In each case, the resulting polymer was dissolved in tetrahydrofuran (THF) and subsequently re-precipitated in methanol at least

seven times to remove unreacted monomer and chromophores. For the PnBMA-Py, the methanol was chilled to 10 ^{o}C as the T_g of this polymer is close to room temperature. This washing procedure helps reduce polydispersity, while retaining the higher molecular weight chains. The label content of PS-Py and PnBMA-Py was characterized by ultraviolet-visible spectroscopy in spectroscopic grade THF. Unlabeled (neat) PnBMA was synthesized alongside the labeled PnBMA with the same synthesis protocols yielding M_w = 1210 kg/mol, M_w/M_n = 1.7. Unlabeled (neat) polystyrene (PS) with M_w = 1920 kg/mol, M_w/M_n = 1.26 was purchased from Pressure Chemical and used as received.

To create the multilayer structures shown in Figure 3.1, individual layers of the various polymers were made by spin-coating from toluene solutions either onto freshly-cleaved mica or quartz slides for the base underlayers. The spin speed and solution concentrations were carefully adjusted to produced films with known and reproducible thicknesses. Films were either floated or spin-coated onto silicon wafers for determination of film thickness by ellipsometry.[10,39,40] All individual layers were annealed under vacuum for at least 18 h at 120 ^{o}C for PS or 80 ^{o}C for PnBMA to remove any residual solvent and relax spin-coating induced stresses. Multilayers are then assembled by successively floating each layer onto room temperature deionized water and capturing the layer onto the multilayer sample starting from the base underlayer spun directly onto the quartz slide needed for fluorescence measurements.[40] Between each successive floating, the sample is allowed to thoroughly dry. Figure 3.1 provides an exploded sample view where each individual layer and thickness are identified. The outer, bulk layers were made >450 nm in thickness to ensure that the pyrene-labeled probe layer is unaffected by the free surface or underlying substrate interface.

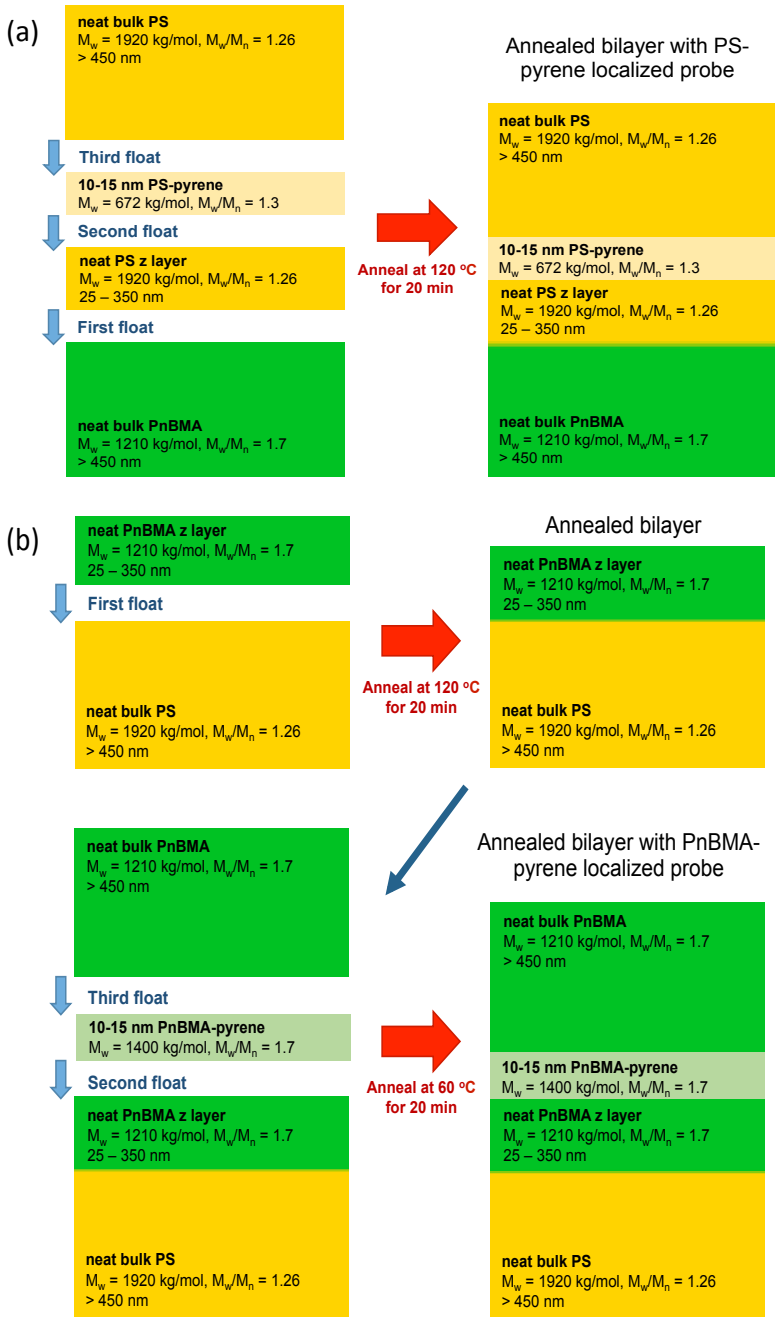

Figure 3.1: Exploded sample view identifying each individual layer prior to assembly and the annealing succession for each given sample. (a) PS-Py labeled layer used to measure $T_g(z)$ on the PS side (positive z) assembled by one annealing step; (b) PnBMA-Py labeled layer used to measure $T_g(z)$ on the PnBMA side (negative z) assembled by a two step annealing process where the PS/PnBMA interface was annealing independently from the PnBMA/PnBMA-Py/PnBMA interfaces prior to measuring the sample.

Because of the specific requirements needed to anneal the PS/PnBMA interface thoroughly to achieve an equilibrium interface and a consolidated sample, while simultaneously limiting the annealing time for PS/PS-Py or PnBMA/PnBMA-Py interfaces to ensure that the pyrene-labeled layers stay localized within the multilayer stack, the multilayer assembly and annealing protocols were different for measuring the PS side compared to the PnBMA side. As PS has the higher T_g ($T_g^{bulk}{}_{PS}$ = 101 ^oC), the multilayer stack in Fig. 3.1a could be assembled as shown and then annealed at 120 ^oC for 20 min prior to the fluorescence measurements. This annealing protocol is sufficient to create a well-annealed PS/PnBMA interface with equilibrium interfacial width of 7 nm,[40-42] yet still limit the overall diffusion of the high molecular weight PS/PS-Py interfaces to a couple of nanometers,[34-36] forming a consolidated interface and keeping the pyrene-labeled layer localized.[8] In contrast, because of the low T_g of PnBMA ($T_g^{bulk}{}_{PnBMA}$ = 21 ^oC), the multilayer stack in Fig. 3.1b was assembled and annealed in two steps. First, the neat PnBMA layer of thickness z was floated atop the base PS underlayer supported on the quartz slide. This PnBMA/PS bilayer film was then annealed in a vacuum oven at 120 ^oC for 20 min to ensure that the PS/PnBMA interface reaches its equilibrium width of 7 nm. Then, the remaining layers, PnBMA-Py (10-15 nm thick) and bulk neat PnBMA, were floated on. The final annealing step at 60 ^oC for 20 min to create a consolidated sample, but limit the diffusion of the PnBMA/PnBMA-Py interfaces, was done just prior to starting the fluorescence measurements. Once annealed to equilibrium by this procedure, the 7 nm PS/PnBMA interfacial width remains effectively static during the course of the fluorescence measurements.[40-42]

The different annealing temperatures for the PS side ($T_g^{bulk}{}_{PS}$ + 20 K) versus the

PnBMA side ($T_g^{bulk}{}_{PnBMA}$ + 40 K) was chosen to accommodate the weaker Vogel-Fulcher-Tammann (VFT) temperature-dependence of PnBMA than for PS.[43] In addition, the molecular weight for the PnBMA-Py (M_w = 1400 kg/mol) is essentially double that for the PS-Py (M_w = 672 kg/mol). Use of high molecular weight polymers effectively localizes the labeled layer within the multilayer structure during the course of the experiment.

Fluorescence measurements were performed using a Photon Technology International QuantaMaster spectrofluorometer with samples mounted in a Peltier-cooled Instec TS62 temperature stage. For measurements of the PnBMA side, dry nitrogen gas was flowed continuously across the temperature stage window (at 2.7 L/min) to prevent moisture condensation below room temperature. The pyrene-labeled probe layers were excited at a wavelength of 330 nm using a xenon arc lamp with an excitation band-pass of 5.5-6.0 nm and an emission band-pass of 5.0 nm. After annealing above T_g as described above and in Fig. 3.1, pyrene fluorescence intensity was collected for 3 s every 27 s, at an emission wavelength of 379 nm for PS-Py or 377 nm for PnBMA-Py, while the sample temperature was ramped down at 1 ^oC/min. As PnBMA is more polar that PS, the overall pyrene emission spectra is blue shifted slightly, with an emission wavelength of 377 nm for PnBMA corresponding to the same location on the first peak as 379 nm for PS. This ramped fluorescence procedure was previously reported in Rauscher et al.,[40] and is based on the method originally developed by the Torkelson group.[8,9,44-46] In Chapter 2, I demonstrated that data of film-thickness dependent $T_g(h)$ reductions for single-layer PS films collected with this temperature-ramping protocol match those collected with the procedure described by the Torkelson group,[8,44,47] and agree with $T_g(h)$ data previously reported by other techniques such as ellipsometry.[7,48,49] At the end of each cooling run, the

samples were reheated to the starting temperature to ensure that the same initial fluorescence intensity was recovered. For the PnBMA-Py samples, data were also collected on heating at 1 °C/min after the initial cooling run at 1 °C/min. The data on heating were found to match that collected on cooling allowing the high temperature range to be extended well above the measured $T_g(z)$ (as shown in Fig. 3.4 for $z = -160$ nm data, green circles) to demonstrate that no additional transition is present at higher temperatures. Figure 3.2 shows the emission spectra for a pyrene-labeled PnBMA film collected at a series of different temperatures, demonstrating that the overall pyrene spectra primarily shifts uniformly up and down with temperature.

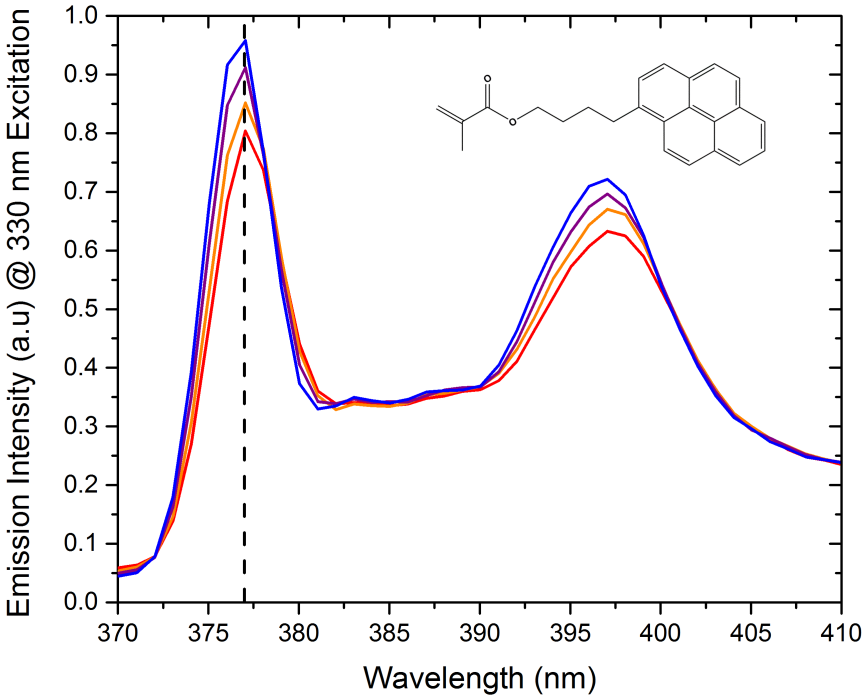

Figure 3.2: Pyrene emission spectra from a 430-nm thick single-layer pyrene-labeled PnBMA film are shown for a series of different temperatures: 50, 30, 10, and –10 °C (bottom to top), with the 377 nm wavelength used for the ramping T_g measurements indicated. Inset shows the chemical structure for the 1-pyrenylbutyl methacrylate monomer used.

The $T_g(z)$ of the pyrene-labeled probe layer located at a distance z away from the PS/PnBMA interface was determined from the change in the linear temperature dependence of the fluorescence intensity as shown in Figure 3.4. Linear fits of the data well above and well below the transition were done, and T_g was identified as the intersection point of these two fits. The data range for the linear fits was optimized by initially selecting all the data above (or below) the transition, staying a minimum of 10 ^oC away from the transition temperature on both sides of the transition. The data range was then reduced to maximize the R^2 value of the fit. As demonstrated in Figures 3.4 and 3.5, the $T_g(z)$ values recover the bulk T_g of each polymer when far from the PS/PnBMA interface. This confirms that the act of confining such dye-labeled chains to 10-15 nm thick probe layers, annealed within such neat polymer matrices, do not affect the measured T_g, as previously shown in work by Ellison and Torkelson[8] for a 12-nm pyrene-labeled PS layer sandwiched between bulk PS layers.

3.4 RESULTS AND DISCUSSION

Figure 3.3 illustrates the layer structures assembled for the samples used in this Chapter. It is important to note that each $T_g(z)$ value is measured from a separate sample, and that samples are not run again to ensure that interdiffusion of the pyrene labeled layer is limited and do not cause a smearing of the local $T_g(z)$ profile. The basic structure consists of two semi-infinite slabs (each >450 nm in thickness) to create a well-defined 7 nm interface between the high-T_g glassy polymer (PS) and low-T_g rubbery polymer (PnBMA). A 10-15 nm thick probe layer containing pyrene of either PS or PnBMA is inserted, where fluorescent pyrene has been covalently attached along the backbone of the chain at a level

of one dye for every 70-145 monomers. On the glassy PS side, I use pyrene-labeled PS (M_w = 672 kg/mol, M_w/M_n = 1.3, with 1.4 mol% pyrene), whereas on the rubbery PnBMA side, I use pyrene-labeled PnBMA (M_w = 1400 kg/mol, M_w/M_n = 1.7, with 0.7 mol% pyrene). To vary the distance of the probe layer to the PS/PnBMA interface, the thickness z of a neat (unlabeled) PS (M_w = 1920 kg/mol, M_w/M_n = 1.26) or PnBMA (M_w = 1210 kg/mol, M_w/M_n = 1.7) spacer layer next to the interface (see Fig. 3.3) is varied. Each layer is individually spin-coated to desired thickness and annealed prior to successively floating each layer atop the next. The annealing time and temperature above T_g of the multilayer stacks are carefully controlled to ensure that the PS/PnBMA interface reaches its equilibrium interfacial thickness, while still limiting the macroscopic diffusion of the pyrene-labeled layers to only a few nanometers. When measuring the low T_g PnBMA side, this necessitated assembling and annealing the multilayer structures of Fig. 3.3b in two stages as annealing the PS/PnBMA interface to equilibrium requires going above the bulk T_g of PS. (Explicit details of the sample preparation and annealing protocols for each type of sample are explained in the Experimental Methods section.) After annealing, this weakly immiscible system forms a stable, well-defined dissimilar polymer-polymer interface of 7 nm for such high molecular weight polymers.[40-42,50,51] The interfacial width $w_I \sim \frac{1}{\sqrt{6\chi}}$ formed between two high-molecular weight polymers is determined by the unfavorable interaction parameter χ,[36] which has been well characterized for a PS/PnBMA system in agreement with the experimentally measured interfacial width.[41,50,51] Thus, this protocol creates a stable sample with an 80 K step-change in local T_g from the glassy-PS side to the rubbery-PnBMA side, whose geometry remains effectively static during the course of the experiment.[40,42]

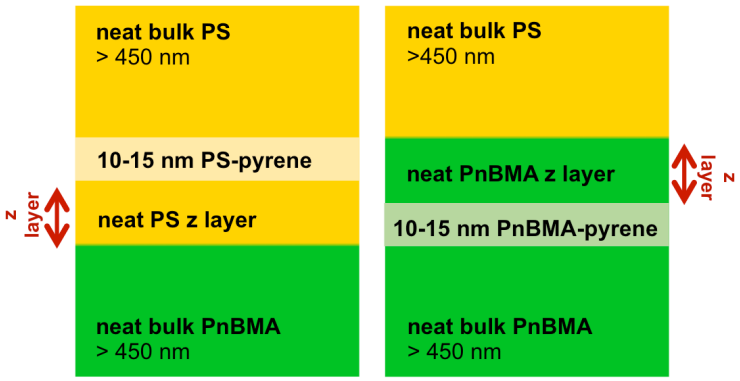

Figure 3.3: Schematic illustrating sample geometries comprised of four individually spin-coated layers of either polystyrene (PS) or poly(*n*-butyl methacrylate) (PnBMA) assembled and annealed to form a consolidated material with a 10-15 nm thick pyrene-labeled layer located at a variable distance *z* from the PS/PnBMA interface (7-nm wide). High molecular weight polymers ensure assembled morphology remains static throughout the experiment.

Use of pyrene-labeled polymers allows us to perform fluorescence measurements to determine the local $T_g(z)$ of this layer at a given distance *z* from the interface. Numerous previous studies have established that the fluorescence intensity of pyrene (when covalently attached as 1-pyrenylbutyl methacrylate monomer) provides a good measure of T_g in agreement with other experimental measures such as differential scanning calorimetry (DSC) and ellipsometry in thin films.[8,9,40,45] Pyrene fluorescence intensity exhibits a different linear temperature dependence in the glassy and rubbery regimes such that T_g can be identified from the intersection of two linear fits as the temperature at which this change in slope occurs. It is well known that pyrene fluorescence intensity and spectral shape vary with local polarity and mobility of the material surrounding the dye.[52] The sensitivity of pyrene to local T_g derives from the change in the relative amount of radiative vs. non-

radiative decay of the dye as a function of temperature affected by the local density and rigidity of the surrounding polymer matrix.[8,53] At higher temperatures, the higher mobility of the surrounding matrix increases the amount of non-radiative decay, showing a stronger temperature dependence in the melt region above T_g. Specific details of how I perform these fluorescence measurements are outlined in Chapter 2. In short, we monitor the fluorescence intensity, every 30 s on cooling at 1 ^oC/min, at a single wavelength corresponding to the first peak in the pyrene spectra,[40] which is known to show the most sensitivity to its local environment.[52]

Normalized fluorescence intensity as a function of temperature for four different samples, each with the pyrene-labeled layer located at a different position z from the glassy-rubbery PS/PnBMA interface is plotted in Figure 3.4. Each dataset exhibits a break in the linear temperature-dependence of the fluorescence intensity identifying the local glass transition temperature $T_g(z)$ at that distance z from the interface. The top curves were collected using a pyrene-labeled PS layer located on the glassy-PS side at a distance: z = 356 nm far from the PS/PnBMA interface reporting $T_g = 99 \pm 2$ ^oC consistent with bulk PS, and z = 64 nm closer to the interface reporting a significantly reduced $T_g = 63 \pm 2$ ^oC. Remarkably, I find the local $T_g(z)$ on the PS side to be reduced by more than 35 K from its bulk value at a distance still more than 60 nm from the PS/PnBMA interface. As we have seen in Chapter 2, such a reduction in T_g for a single PS layer would be akin to a 12 nm thick PS film with a polymer-air interface providing the perturbative effect, highlighting that that cooperative length scales associated with a dissimilar polymer-polymer interface might be globally much longer ranged than a polymer-air interface. Further discussion of an apparent universality of coupling across polymer-polymer interfaces will be addressed

in Chapter 4. The bottom curves were collected using a pyrene-labeled PnBMA layer located on the rubbery-PnBMA side at a distance: $z = -160$ nm far from the PS/PnBMA interface reporting $T_g = 20 \pm 2\ ^oC$ consistent with bulk PnBMA, and $z = -36$ nm closer to the interface reporting $T_g = 29 \pm 2\ ^oC$. Each dataset displayed only a single T_g value for each location z, even when the temperature range was significantly extended. This measurement has been repeated with many different samples, varying z to map out the profile in local $T_g(z)$ across the PS/PnBMA interface.

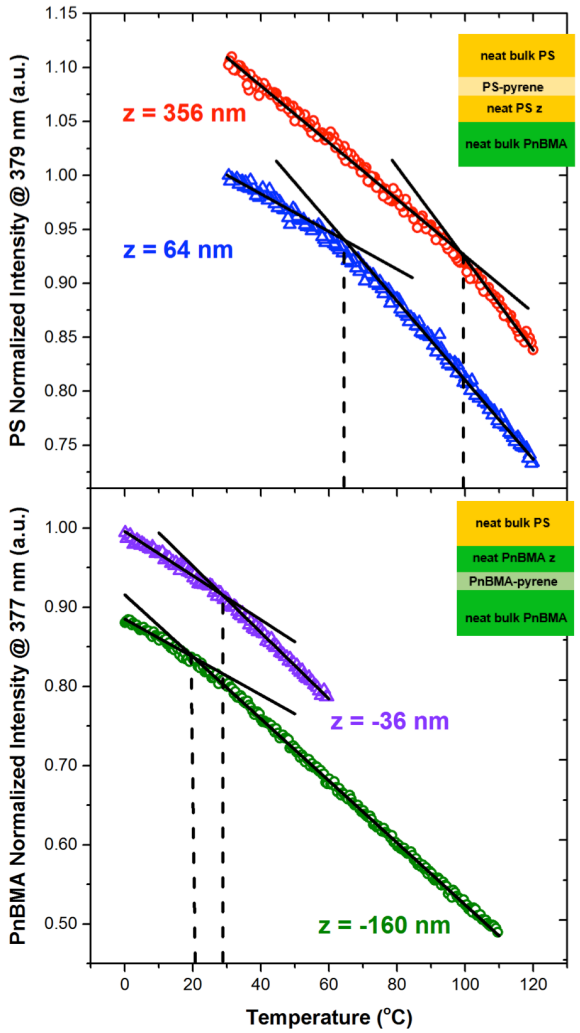

Figure 3.4: Fluorescence intensity as a function of temperature collected at 1 °C/min for four different samples. (Top) Pyrene-labeled PS layer located at a distance z = 356 nm away from PS/PnBMA interface reporting local $T_g(z) = 99 \pm 2$ °C consistent with bulk PS, and at a distance z = 64 nm reporting a significantly reduced $T_g(z) = 63 \pm 2$ °C when closer to the PS/PnBMA interface. (Bottom) Pyrene-labeled PnBMA layer located at a distance of 160 nm from the PS/PnBMA interface reporting local $T_g(z) = 20 \pm 2$ °C consistent with bulk PnBMA, and at a distance of 36 nm reporting local $T_g(z) = 29 \pm 2$ °C when closer to the interface.

Figure 3.5 graphs all the local $T_g(z)$ values measured as a function of the labeled-layer's position z from the interface, where positive z values denote the glassy-PS side and

negative z values denote the rubbery-PnBMA side. The $T_g(z)$ values smoothly transition from the bulk T_g of PnBMA, average $T_g(z < -150$ nm) = 20.9 ± 2.0 °C, to the bulk T_g of PS, average $T_g(z > 250$ nm) = 100.8 ± 2.0 °C. Two features of the data are surprising: (1) the transition from one bulk T_g value to the other occurs over a very large distance 350-400 nm, and (2) the $T_g(z)$ profile is asymmetric with the perturbation in local mobility at the interface propagating much further into the glassy-PS side than the rubbery-PnBMA side. To obtain a quantitative measure of these two factors, we have fit the $T_g(z)$ data to a hyperbolic tangent:

$$T_g(z) = T_g^{av} + \frac{1}{2}\Delta T_g \tanh\left[\frac{2(z-\gamma)}{w}\right] \qquad (1)$$

where the difference $\Delta T_g = T_g^{bulk}{}_{PS} - T_g^{bulk}{}_{PnBMA} = 79.9$ K and average $T_g^{av} = ½ (T_g^{bulk}{}_{PS} + T_g^{bulk}{}_{PnBMA}) = 60.8$ °C were determined from the asymptotes (measured T_g bulk values) of the data at large $|z|$ and held fixed during the fit. The best fit values for the profile width w = 231 ± 5 nm and asymmetry γ = 79 ± 3 nm demonstrate that the T_g-mobility gradient is broad and strongly biased towards the (positive z) glassy-PS side. Intriguingly, a recent limited mobility model by Tito et al.[15] investigating local mobility profiles near free surfaces and glassy-rubbery interfaces predicted an asymmetric mobility profile biased towards the lower-mobility (glassy) side consistent with our experimental results. The infusion of enhanced mobility at a boundary propagates a significantly larger distance into glassy material.

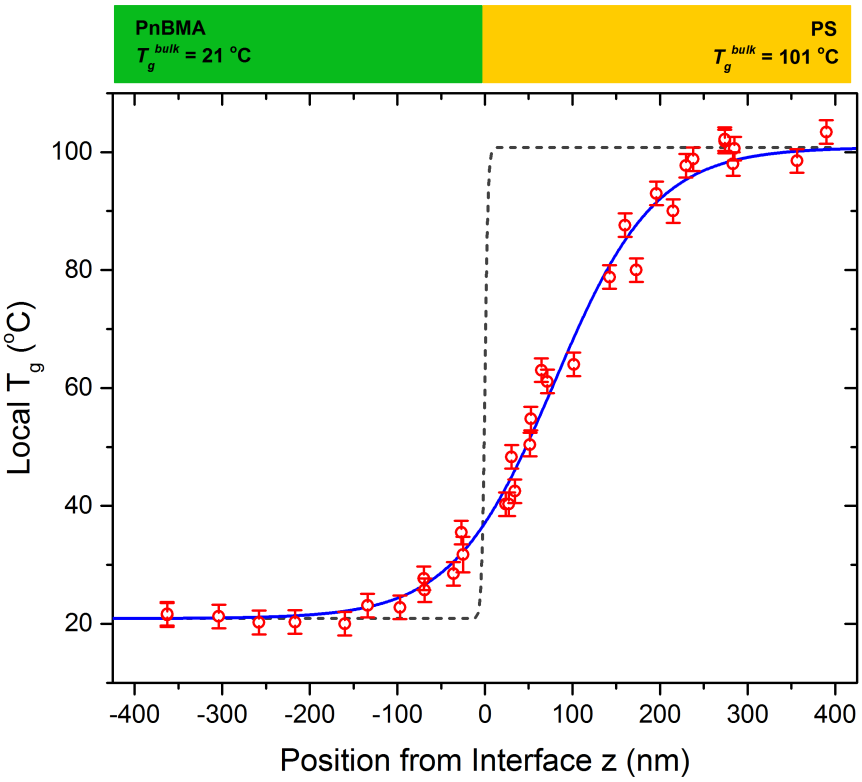

Figure 3.5: Measured local $T_g(z)$ as a function of the pyrene-labeled layer's position from the PS/PnBMA interface (positive z = glassy-PS side, negative z = rubbery-PnBMA side). $T_g(z)$-profile fit to hyperbolic tangent (solid-blue curve) demonstrating mobility-gradient is broad and strongly biased toward glassy-PS side. Grey-dashed curve indicates local composition profile $\phi(z)$ with 7 nm interfacial width.

It is important to recognize that the T_g-mobility gradient does not correlate at all with the local composition profile $\phi(z)$ of the two polymers across the interface. The composition profile $\phi(z) \approx \tanh(2z/w_I)$ of PS/PnBMA interfaces has been measured by Stamm et al.[41] using neutron reflectivity. For PS/PnBMA layers of comparable thickness and annealing conditions to our own work, and with a slightly smaller molecular weight to the high molecular weights used in the present study, they found the interfacial width w_I = 7 nm for PS/PnBMA.[41] To illustrate this composition profile, a gray-dashed curve has been added to Fig. 3.5 with width w_I = 7 nm. If the local cooperative segmental motion

associated with T_g were independent on either side of the polymer-polymer interface, the local $T_g(z)$ would follow the local composition profile transitioning sharply at $z = 0$. Consider a value of $z \approx 100$ nm, the local PS segments exhibit a T_g reduced by ~30 K from its bulk $T_g^{bulk}{}_{PS}$ value, despite all PnBMA segments being over 100 nm away. These results are in strong contrast with the present views of how local T_g is expected to correlate with local composition ϕ within a small region of a few nanometers.[54-56] The long length scale over which the local $T_g(z)$ is correlated demonstrates that cooperative segmental dynamics associated with T_g can be coupled over large distances and across polymer-polymer interfaces.

Because PS/PnBMA is only very weakly immiscible, we have addressed possible concerns that low molecular weight PnBMA chains could possibly penetrate the glassy PS side of the PS/PnBMA interface leading to plasicization of the PS side of the sample. Plasticization of the PS matrix by such diffusion of low molecular weight PnBMA chains within the PS matrix could then be a likely candidate to explain the asymmetry and extended length scales of the local $T_g(z)$ associated with the PS/PnBMA polymer-polymer interface. To address this possible concern, some measurements of the glassy-PS side of the $T_g(z)$ profile were done using two different unlabeled PnBMA for the underlayer domains with very different molecular weights and distributions: M_w = 319 kg/mol with M_w/M_n = 2.6 (purchased from Scientific Polymer Products and used as received) and M_w = 1400 kg/mol with M_w/M_n = 1.7 (synthesized by free radical polymerization and washed 7 times). To within experimental error, the same local $T_g(z)$ values were measured despite the difference in molecular weight and polydispersity of the PnBMA used. If the locally reduced $T_g(z)$ value of the PS matrix next to PnBMA were caused by plasticization from

low molecular weight PnBMA chains, then the lower molecular weight and higher dispersity PnBMA, with a larger amount of low molecular weight chains, would be expected to give a different $T_g(z)$ profile. The results presented in Chapter 4 will also present similarly broad $T_g(z)$ profiles for dissimilar polymer-polymer pairs that are more strongly immiscible where plasticization effects are not a concern. These types of control experiments, alongside other studies regarding the evolution of a PS/PnBMA interface,[40-42] give confidence that the PS/PnBMA interface remains static after it has reached thermal equilibrium under the time and temperature conditions used in this study. For example, Figure 3.6 demonstrates that the measured $T_g(z)$ values for the PS side near the PS/PnBMA interface are the same within experimental error after annealing for 20 min at an elevated temperature of $T_g{}^{bulk}{}_{PS}$ + 40 K instead of $T_g{}^{bulk}{}_{PS}$ + 20 K. Not only do these data show that localization of the PS-Py and PnBMA-Py layers is robust under more aggressive annealing conditions, but the annealing conditions for $T_g{}^{bulk}{}_{PS}$ + 40 K and $T_g{}^{bulk}{}_{PnBMA}$ + 40 K would not alter the local $T_g(z)$ even though PnBMA has weaker VFT temperature dependence relative to PS. Also note that the scale of the *x*-axis in Figures 3.5 and 3.6 is very large with the width of each $T_g(z)$ data point spanning ~20 nm, approximately the width of the labeled layer after annealing. Further discussion of various possible factors dictating the $T_g(z)$ profile behavior will be discussed in greater detail in Chapter 4.

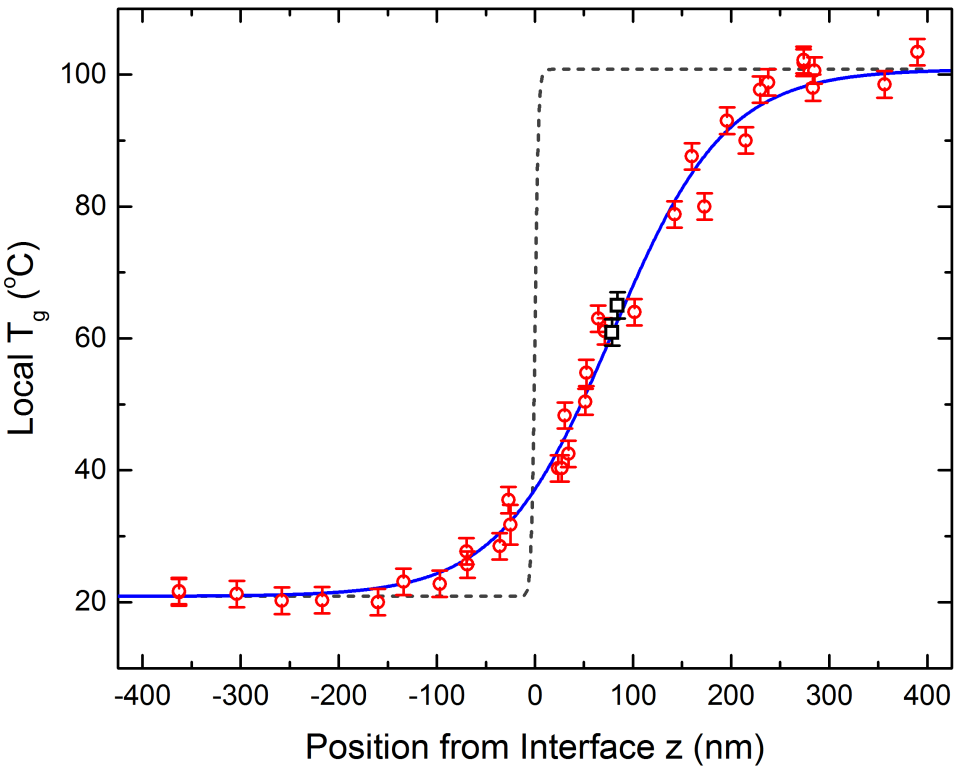

Figure 3.6**:** Figure 3.5 with additional $T_g(z)$ data points (open black squares) on the PS side near the PS/PnBMA interface that were annealed for 20 min at $T_g{}^{bulk}{}_{PS}$ + 40 K (140 °C) instead of $T_g{}^{bulk}{}_{PS}$ + 20 K.

A central question associated with the glass transition is the spatial extent over which cooperative dynamics are correlated. Although most studies focus on the length scale associated with a single CRR, the size over which neighboring units undergo collective rearrangements typically of order a few nanometers, we are instead interested over what larger distance are dynamics correlated across neighboring CRRs. *How far away must two CRRs be to exhibit completely independent motion?* The results from Figure 3.5 suggest that this length scale, the distance from where one region exhibits bulk dynamics to the other, is 350-400 nm. As local rearrangements occur in one CRR, its neighbor is affected by this local disturbance at its boundary altering its dynamics, which in turn

influences its neighbor. This idea of there existing a dynamical length scale larger than that associated with a single CRR has been incorporated into some theoretical models of the glass transition.[1,3,12,13,57] A recent unified theory of activated relaxation by Mirigian and Schweizer[4,58] provides some insight into why the influence of the perturbing interface has longer range effects on the glassy side. They added a nonlocal character to the α-relaxation event incorporating a cage expansion to facilitate local hopping in highly densified systems. The free-energy barrier for this cage expansion scales with the local elastic displacement field resulting in a length scale for collective rearrangements that grows with increasing rigidity (modulus) of the system. Factors that might be causing such enormous length scales and apparent profile asymmetry with be further explored in Chapters 4 and 5.

Various theoretical models have been applied to the study of how a dynamical perturbation at an interface propagates into glassy material.[12-15,27] To keep the analysis as general as possible, I choose to focus on the facilitated kinetic Ising spin model, originally billed as the simplest model of cooperative dynamics.[59] The two-spin facilitated Ising model (2SFM) by Fredrickson and Andersen[59,60] contains no equilibrium phase transition and no inherent static correlation length, yet with only nearest-neighbor dynamical interactions it displays a spectrum of relaxation times and dynamic arrest as the effective temperature is reduced, characteristic of the glass transition. Butler and Harrowell[12] have investigated how the 2D 2SFM behaves near a layer of pinned spins representing an interface. They found that the temperature-dependence of a dynamical correlation length $\xi_{dyn}(T)$, defined as the distance from the boundary over which bulk behavior is recovered, matched the temperature-dependence of the mean relaxation time $\tau(T)$ in the bulk.[57] This suggests that investigations of dynamical gradients near an interface can be used to learn

about the dynamic length scale associated with cooperative motion. Specifically, Butler and Harrowell[12] defined a surface-influence function $si(n) = \frac{(\tau_{bulk} - \tau_n)}{(\tau_{bulk} - \tau_1)}$ with the dynamical correlation length $\xi_{dyn}(T)$ corresponding to the distance (layer number n) when the relaxation time of the n^{th} layer (τ_n) was midway between the surface value (τ_1) and the bulk (τ_{bulk}), $si(n=\xi) = 0.5$. $\xi_{dyn}(T)$ grew with decreasing temperature becoming much larger than a single nearest-neighbor interaction. In analogy, we can define an equivalent dynamic correlation length $\xi_{dyn}(T)$ as the distance from the interface at which the local $T_g(z)$ value is midway between the interface value $T_g(z=0) = 37\ ^oC$ and the bulk:

$$si(z = \xi) = \frac{|T_g^{bulk} - T_g(z)|}{|T_g^{bulk} - T_g(z=0)|} = 0.5 \qquad (2)$$

For the glassy-PS side $\xi_{PS/PnBMA} = 103$ nm, while for the rubbery-PnBMA side $\xi_{PnBMA/PS} = 50$ nm. We suspect that the difference in these values reflect in some measure the temperature dependence of $\xi_{dyn}(T)$ based on whether the interface has a lower or higher local T_g value than the bulk. Chapter 4 will unify the ideas presented in this Chapter by comparing a series of different systems and show an apparent universal behavior of dynamical perturbations across dissimilar polymer-polymer interfaces.

3.5 CONCLUSIONS

In this Chapter, I have shown the first experimentally determined local $T_g(z)$ gradient spanning and originating from a dissimilar PS/PnBMA glassy-rubbery polymer-polymer interface with a T_g difference of 80 K. By using a localized fluorescence probe that is sensitive to the local density and rigidity of the surrounding polymer matrix, and exploiting the decoupling of α-relaxations and chain diffusion in high molecular weight

polymers, I was able to experimentally measure the local gradient in dynamics for this weakly immiscible polymer pair. The results are surprising in two parts: (1) the local cooperative dynamics between the glassy-PS and rubbery-PnBMA sides of the semi-infinite bilayer are coupled over 350-400 nm before bulk dynamics are recovered on both sides of the system, suggesting some other long range cooperative mechanism other than a singe CRR is responsible for understanding local glassy dynamics; (2) as opposed to the current paradigm that local dynamics are correlated with the composition profile between polymer pairs, I find the local $T_g(z)$ profile to be highly asymmetric, penetrating much further into glassy-PS side of the system.

A recent theoretical treatment of the glass transition has been proposed by Mirigian and Schweizer,[4,27,58] where particle hopping between cages or CRRs is facilitated by an additional longer range term related to elastic distortion (local modulus) of the system. This treatments has received success modeling polymer-air interfacial perturbations to bulk T_g dynamics. Though the theory by Mirigian and Schweizer does not yet have the capability to model polymer-polymer interfaces, the theory does depend on an additional long range mechanism to model glassy dynamics, suggesting that the Adam and Gibbs[23] hypothesis needs to be revisited to further our understanding of glassy phenomenon. In addition, the kinetic limited mobility model of low-mobility/high-mobility/low-mobility slabs proposed by Tito *et. al*[15] shows a strong mobility gradient with an asymmetric bias toward the low-mobility slab at the low-mobility/high-mobility interfaces, akin the asymmetry of the local cooperative dynamics in a glassy-PS/rubbery-PnBMA interface system explored in this Chapter.

3.6 REFERENCES

[1] L. Berthier and G. Biroli, Rev. Mod. Phys. **83**, 587 (2011).

[2] M.D. Ediger, Annu Rev Phys Chem **51**, 99 (2000).

[3] F.W. Starr, J.F. Douglas, and S. Sastry, J Chem Phys **138**, 12A541 (2013).

[4] S. Mirigian and K.S. Schweizer, J Chem Phys **140**, 194507 (2014).

[5] M.D. Ediger and P. Harrowell, J Chem Phys **137**, 080901 (2012).

[6] M. Alcoutlabi and G.B. McKenna, J Phys: Condens Matter **17**, R461 (2005).

[7] C.B. Roth and J.R. Dutcher, Journal of Electroanalytical Chemistry **584**, 13 (2005).

[8] C.J. Ellison and J.M. Torkelson, Nat Mater **2**, 695 (2003).

[9] C.B. Roth, K.L. McNerny, W.F. Jager, and J.M. Torkelson, Macromolecules **40**, 2568 (2007).

[10] J.E. Pye, K.A. Rohald, E.A. Baker, and C.B. Roth, Macromolecules **43**, 8296 (2010).

[11] J. Baschnagel and F. Varnik, J Phys: Condens Matter **17**, R851 (2005).

[12] S. Butler and P. Harrowell, J Chem Phys **95**, 4466 (1991).

[13] J.D. Stevenson and P.G. Wolynes, J Chem Phys **129**, 234514 (2008).

[14] J.E.G. Lipson and S.T. Milner, Eur. Phys. J. B **72**, 133 (2009).

[15] N.B. Tito, J.E.G. Lipson, and S.T. Milner, Soft Matter **9**, 9403 (2013).

[16] C. Cammarota, G. Gradenigo, and G. Biroli, Phys. Rev. Lett. **111**, 107801 (2013).

[17] P.Z. Hanakata, J.F. Douglas, and F.W. Starr, Nat Commun **5**, 4163 (2014).

[18] J.E. Pye and C.B. Roth, Phys. Rev. Lett. **107**, 235701 (2011).

[19] R.J. Lang, W.L. Merling, and D.S. Simmons, ACS Macro Lett. **3**, 758 (2014).

[20] R.P. White and J.E.G. Lipson, Phys. Rev. E **84**, 041801 (2011).

[21] R.J. Lang and D.S. Simmons, Macromolecules **46**, 9818 (2013).

[22] A. Shavit and R.A. Riggleman, J. Phys. Chem. B **118**, 9096 (2014).

[23] G. Adam and J.H. Gibbs, J Chem Phys **43**, 139 (1965).

[24] U. Tracht, M. Wilhelm, A. Heuer, K. Schmidt-Rohr, and H.W. Spiess, Phys. Rev. Lett. **81**, 2727 (1998).

[25] E. Hempel, G. Hempel, A. Hensel, C. Schick, and E. Donth, J. Phys. Chem. B **104**, 2460 (2000).

[26] R.D. Priestley, C.J. Ellison, L.J. Broadbelt, and J.M. Torkelson, Science **309**, 456 (2005).

[27] S. Mirigian and K.S. Schweizer, J Chem Phys **141**, 161103 (2014).

[28] J.A. Forrest and K. Dalnoki-Veress, ACS Macro Lett. **3**, 310 (2014).

[29] J.A. Forrest and J. Mattsson, Phys. Rev. E **61**, R53 (2000).

[30] Y.C. Jean, R.W. Zang, H. Cao, J.P. Yaun, C.M. Huang, B. Nielsen, and P. Asoka-Kumar, Phys

Rev B **56**, R8459 (1997).

[31] M.D. Ediger and J.A. Forrest, Macromolecules **47**, 471 (2014).

[32] E.C. Glor and Z. Fakhraai, J Chem Phys **141**, 194505 (2014).

[33] G.F. Meyers, B.M. DeKoven, and J.T. Seitz, Langmuir **8**, 2330 (1992).

[34] A. Karim, A. Mansour, G.P. Felcher, and T.P. Russell, Phys Rev B **42**, 1 (1990).

[35] M. Stamm, S. Huttenback, G. Reiter, and T. Springer, Europhys. Lett. **14**, 451 (1991).

[36] R.A.L. Jones and R.W. Richards, *Polymers at Surfaces and Interfaces* (Cambridge University Press, 1999).

[37] T. Inoue, M.T. Cicerone, and M.D. Ediger, Macromolecules **28**, 3425 (1995).

[38] A. Kriisa, S.S. Park, and C.B. Roth, J Polym Sci, Part B: Polym Phys **50**, 250 (2011).

[39] E.A. Baker, P. Rittigstein, J.M. Torkelson, and C.B. Roth, J Polym Sci, Part B: Polym Phys **47**, 2509 (2009).

[40] P.M. Rauscher, J.E. Pye, R.R. Baglay, and C.B. Roth, Macromolecules **46**, 9806 (2013).

[41] D.F. Siqueira, D.W. Schubert, V. Erb, M. Stamm, and J.P. Amato, Colloid Polym Sci **273**, 1041 (1995).

[42] J.A. Forrest and K. Dalnoki-Veress, J Polym Sci, Part B: Polym Phys **39**, 2664 (2001).

[43] D.J. Plazek and V.M. ORourke, Journal of Polymer Science Part a- Polymer Physics **9**, 209 (1971).

[44] C.J. Ellison and J.M. Torkelson, J Polym Sci, Part B: Polym Phys **40**, 2745 (2002).

[45] R.D. Priestley, M.K. Mundra, N.J. Barnett, L.J. Broadbelt, and J.M. Torkelson, Aust. J. Chem. **60**, 765 (2007).

[46] C.B. Roth and J.M. Torkelson, Macromolecules **40**, 3328 (2007).

[47] C.J. Ellison, M.K. Mundra, and J.M. Torkelson, Macromolecules **38**, 1767 (2005).

[48] J.L. Keddie, R.A.L. Jones, and R.A. Cory, Europhys. Lett. **27**, 59 (1994).

[49] S. Kim, S.A. Hewlett, C.B. Roth, and J.M. Torkelson, Eur. Phys. J. E **30**, 83 (2009).

[50] D.W. Schubert, V. Abetz, M. Stamm, T. Hack, and W. Siol, Macromolecules **28**, 2519 (1995).

[51] H. Hammouda, B.J. Bauer, and T.P. Russell, Macromolecules **27**, 2357 (1994).

[52] B. Valeur, *Molecular Fluorescence: Principles and Applications* (Wiley-VCH, Weinheim, 2001).

[53] C.J. Ellison, S.D. Kim, D.B. Hall, and J.M. Torkelson, Eur. Phys. J. E **8**, 155 (2002).

[54] T.P. Lodge and T.C.B. McLeish, Macromolecules **33**, 5278 (2000).

[55] S.K. Kumar, S. Shenogin, and R.H. Colby, Macromolecules **40**, 5759 (2007).

[56] Y. He, T.R. Lutz, and M.D. Ediger, J Chem Phys **119**, 9956 (2003).

[57] S. Butler and P. Harrowell, J Chem Phys **95**, 4454 (1991).

[58] S. Mirigian and K.S. Schweizer, J. Phys. Chem. Lett. **4**, 3648 (2013).

[59] G.H. Fredrickson and H.C. Andersen, Phys. Rev. Lett. **53**, 1244 (1984).

[60] G.H. Fredrickson and H.C. Andersen, J Chem Phys **83**, 5822 (1985).

Chapter 4

Local Glass Transition Temperature $T_g(z)$ of Polystyrene Next to Different Polymers: Hard vs. Soft Confinement

A version of this chapter was published as Roman R. Baglay and Connie B. Roth, *Journal of Chemical Physics*, 146, 203307, 2017.

4.1 SYNOPSIS

The depth to which the local glass transition temperature T_g and alpha-relaxations are perturbed near a boundary is believed to be related to the characteristic length scales associated with cooperative dynamics in dynamically heterogeneous glasses. Following my work outlined in Chapter 3 that measured a very broad 350-400 nm local $T_g(z)$ profile across a glassy-rubbery interface of polystyrene (PS) / poly(*n*-butyl methacrylate) (PnBMA), I compare in Chapter 4 how the $T_g(z)$ profile in PS varies when changing the neighboring polymer from a lower T_g material to a higher T_g material. Here local $T_g(z)$ profiles are reported for PS when in contact with polysulfone (PSF), poly(methyl methacrylate) (PMMA), and poly(isobutyl methacrylate) (PiBMA). I find that the distance from the interface before bulk T_g of PS (T_g^{bulk} = 101 ^oC) is recovered depends on whether PS forms the high-T_g glassy component experiencing so-called soft confinement, $z \approx$ 225-250 nm for PS next to PiBMA (T_g^{bulk} = 62 ^oC) and PnBMA (T_g^{bulk} = 21 ^oC), or PS forms the low-T_g rubbery component experiencing hard confinement, $z \approx$ 100-125 nm for PS next to PSF (T_g^{bulk} = 186 ^oC) and PMMA (T_g^{bulk} = 120 ^oC). The depth to which these $T_g(z)$

gradients persist and the magnitude of the local T_g perturbation at the interface are independent of the difference in T_g^{bulk} between the two polymers, the interaction parameter, and chemical structure. I demonstrate that these broad, extended $T_g(z)$ length scales appear to be universal across these different systems, but show that the strong dynamical coupling across the dissimilar polymer-polymer interface only occurs when this interface has been annealed to equilibrium. I consider why dissimilar polymer-polymer interfaces exhibit continuous local dynamics across the interface in contrast to polymer-free surface, polymer-substrate, or polymer-liquid interfaces that show discontinuous local dynamics.

4.2 INTRODUCTION

Recent trends in polymer blends have been to drive the domain sizes down into the sub 100 nm range to improve material performance, blend uniformity, and to create functionality for particular applications.[1-3] There are now a number of strategies for creating such nanostructured polymer blends: synthesis of multicomponent block copolymers,[4-7] novel cold-state processing methods,[8] and nanolayer stacking and interweaving.[9-13] Of particular interest are co-continuous structures where domains of glassy, rubbery, and crystalline components intertwine while percolating across the material making ideal structures for applications such as filtration, ion conduction, catalysis, photovoltaic technologies, and bioengineering applications.[3,14-17] These are materials whose function and performance will be dictated by the properties of the material near the polymer-polymer interfaces. Historically polymer blends have been treated as a patchwork of different domains with separate properties, where it is often assumed that these domains retain the bulk properties of the individual components.[18] Such approaches

are appropriate for blends with large, micron-sized domains where the relatively small contributions of the regions near polymer-polymer interfaces between the domains can be reasonably ignored. However, when domain sizes become so small that the material becomes dominated by interfaces, it is necessary to understand and incorporate the altered local properties at and near the interfaces. The results I present here demonstrate long length scales for the distance over which local glass transition temperature (T_g) perturbations propagate from polymer-polymer interfaces suggesting that nanostructured polymer blends with domain sizes of order a few hundred nanometers likely have no regions where the local properties remain bulk-like. Instead, nanostructured blends likely exhibit more uniform properties across the different domains and interfaces, which may explain their typically enhanced performance over more traditional blends with large micron-sized domains.

I have recently mapped the local glass transition temperature $T_g(z)$ profile across a glassy-rubbery interface between polystyrene (PS) and poly(*n*-butyl methacrylate) (PnBMA).[19] Focusing on an idealized bilayer-style model system, I used a localized fluorescence method to measure the local $T_g(z)$ at different distances z from the PS/PnBMA interface. The $T_g(z)$ profile transitioned continuously from the bulk T_g value of PnBMA, $T_g^{bulk}{}_{PnBMA} = 21\ ^oC$, to that of PS, $T_g^{bulk}{}_{PS} = 101\ ^oC$, far from the PS/PnBMA interface in either direction, as anticipated. However, unexpectedly, this $T_g(z)$ profile was found to be very broad, spanning 350-400 nm from one extreme to another.[19] In addition, this dynamical $T_g(z)$ profile was asymmetric, being uncorrelated with the local composition profile $\phi(z) \approx \tanh(2z/w_I)$, where the equilibrium interfacial width of PS/PnBMA has been previously characterized at only $w_I = 7$ nm.[20-22] These unexpected results demonstrate that

the local glass transition dynamics are influenced by factors much further away than simply the local composition, which has been the traditional viewpoint in polymer blends.[23-25] These unexpected results of the $T_g(z)$ profile across a PS/PnBMA interface[19] leave many open questions. How universal is this to other polymer systems? What factors are required to get this extraordinary coupling of cooperative segmental dynamics across an immiscible polymer-polymer interface? What controls the length scale over which these dynamics are perturbed away from the interface? Is this length scale a property of the polymer itself, perhaps related to its cooperatively rearranging region (CRR)? What properties of the interface (degree of immiscibility, interaction parameter χ, interfacial width) influence this behavior? To what extent do polymer-polymer interfaces behave similarly or differently to other interfaces (e.g., polymer-substrate, polymer-free surface, polymer-liquid)? Here we consider these various factors.

One way we can begin to understand these results is by analogy to the glass transition behavior in thin films. For over two decades now, studies have found that the average glass transition temperature T_g of thin polymer films supported on various substrates or free-standing with only air interfaces, demonstrate large (tens of degrees Kelvin) deviations in T_g from their bulk values T_g^{bulk} with decreasing film thickness.[26-32] For a variety of polymers such confinement effects begin at film thicknesses ~100 nm.[29,30,33-35] The results of such studies have found that the phenomenon can be understood as the presence of the interfaces (polymer-free surface or polymer-substrate interface) causing a perturbation to the local dynamics that then propagates deep into the material leading to a gradient in local $T_g(z)$ as a function of depth from the interface over some distance before bulk-like properties of the material are recovered.[26,36-45] In general, the

presence of a free surface tends to speed up (enhance) the local mobility, while the presence of a substrate interface can slow down the local dynamics, typically depending on whether attractive interactions such as hydrogen bonding are present between the polymer and substrate interface in question.[28,35,46-49] Such measurements of local T_g near a PS-free surface, using the same localized fluorescence method mentioned above, found that a depth of 30-40 nm from the free surface is required before the bulk T_g of PS was recovered.[50] Some studies investigating polymer-substrate interactions demonstrate even longer length scales spanning several hundred nanometers.[51,52] Though, what factors control this length scale are still not well understood. There is also disagreement about the size of this enhanced mobility region near a free surface, with studies measuring glassy dynamics well below bulk T_g often reporting depths of a few tens of nanometers,[36,50,52,53] while studies measuring liquid-like flow properties above or near bulk T_g only reporting depths of a few nanometers[54-60] before bulk-like properties are recovered. It has been suggested that such differences are associated with what dynamical property is being measured.[41,53,61] Here, we focus on measurements of glassy dynamics and local T_g. Several studies both experimentally[34,50,53,62-65] and theoretically[37-45] suggest that such a length scale is likely related to the length scales involved in describing cooperative motion and dynamic heterogeneity in glasses.

Although the behavior of a polymer-free surface interface has been the most heavily studied, it is informative to make comparisons across different types of interfaces: polymer-substrate, polymer-liquid, and polymer-polymer interfaces. In this regard, other groups have also begun looking at polymer-polymer interfaces and investigating how they differ from that of a free surface or liquid interface. Using MD simulations, Simmons and

coworkers have modeled the T_g of a confined polymer layer in contact with a second different polymer layer.[66] With periodic boundary conditions, this system mimics nanolayered films made by coextrusion.[10,11] They find that both the low-T_g polymer under "hard" confinement and the high-T_g polymer under "soft" confinement exhibit a shift in T_g from their bulk value caused by the presence of the neighboring polymer.[66] The magnitude of the shift for the low-T_g polymer under hard confinement is additionally influenced by the interfacial energy, although in this simulation varying the interfacial energy also varies the amount of interdiffusion at the interface, which I later demonstrate in this Chapter to be an important parameter. Interfacial energy has also been considered an important factor for polymer-substrate[67-69] and polymer-liquid[70] interactions. Tito, Lipson, and Milner have modeled the local mobility profile next to a free surface or glassy-rubbery polymer-polymer interface using a kinetic limited-mobility model that encodes the exchange of local mobility through different types of local free volume ("mobile", "dormant", and "dense") where the interface in question becomes a source or sink of local free volume and hence mobility.[37] Evans and Torkelson have made experimental comparisons between the magnitude of the shift in T_g perturbation for PS with the value of the fragility of the surrounding polymer matrix finding similarities between thin 10-15 nm layers of PS and isolated chains of PS.[71] The idea of differences between so-called hard vs. soft confinement has been around for about a decade. Richert first introduced the concept when comparing small molecule glass formers confined within soft emulsion drops instead of hard nanoporous glasses,[72-74] where, soft confinement referred to a liquid interface instead of that with a hard wall. However, recent studies on polymer-liquid interfaces[70,75-78] seem to suggest that, in some cases, a polymer-liquid interface may not actually behave that

different than a polymer-substrate interface. In contrast, experimental evidence[22,35,79-84] suggests that polymer-polymer interfaces may be distinctly different from that of polymer-free surface or polymer-liquid interfaces.

Here we compare the local $T_g(z)$ profile of PS in contact with several different polymers: polysulfone (PSF), poly(methyl methacrylate) (PMMA), and poly(isobutyl methacrylate) (PiBMA) with that of PnBMA from Chapter 3. I find that the depth to which the local $T_g(z)$ value is perturbed from the polymer-polymer interface is strongly affected by whether the neighboring polymer has a bulk T_g value *higher* or *lower* than that of PS (i.e., whether the confinement is hard or soft), with PS next to PSF behaving remarkably similar to PnBMA next to PS. Following analysis previously employed in Chapter 3 that was based on the efforts of Butler and Harrowell,[43] I characterize the depth to which the local $T_g(z)$ perturbation persists from the interface by $\xi_{½}$, the distance at which the local $T_g(z)$ perturbation has dropped to half the value found at the interface. Butler and Harrowell showed that for a simple two-spin facilitated Ising model such a dynamical length scale $\xi_{½}(T)$ exhibited the same temperature dependence as the mean relaxation time $\tau(T)$ for dynamical heterogeneities in the bulk, suggesting that dynamical gradients near an interface can be used to probe the dynamical length scales associated with cooperative motion.[43,85] I find that these $\xi_{½}$ values are strongly grouped around $\xi_{½}$ = 55 ± 5 nm for polymers next to a *higher* T_g polymer (hard confinement) compared with $\xi_{½}$ = 115 ± 5 nm for polymers next to a *lower* T_g polymer (soft confinement). I suggest that perhaps the distinctiveness of polymer-polymer interfaces may be associated with the extensive breadth (few to several nanometers) of polymer-polymer interfaces in comparison to the breadth of polymer-air or polymer-liquid interfaces (~0.5 nm[86]). As will be demonstrated

later, the extent to which the two dissimilar polymers are allowed to interdiffuse at the polymer-polymer interface is an important factor that affects the extent of dynamical coupling across the interface. If the amount of annealing done at the dissimilar polymer-polymer interface is restricted, I find the $T_g(z)$ profile to be much shorter and not consistently stable as the interface continues to evolve. However, once the dissimilar polymer-polymer interface has been allowed to form to equilibrium, there is no more visible evolution of the $T_g(z)$ profile with further annealing. Interestingly, despite this clear importance of the breadth of interdiffusion of the interface, I do not observe a correlation of the extent of the $T_g(z)$ perturbation from the interface with the equilibrium interfacial width w_I or equivalently the interaction parameter χ between the two polymers. I also note that the breadth of these polymer-polymer interfaces (~5 nm) are all much smaller relative to the large extent of the $T_g(z)$ perturbations (many tens to hundreds of nanometers). Thus, small differences in equilibrium interfacial width do not seem to play a role in the dynamical coupling of cooperative dynamics across the interface provided the dissimilar polymer-polymer interface has been able to anneal to equilibrium.

4.3 EXPERIMENTAL METHODS

High molecular weight pyrene-labeled polystyrene (PS-Py) with 1.4 mol% pyrene content (M_w = 672 kg/mol, M_w/M_n = 1.3) was synthesized by bulk free-radical copolymerization of styrene with a pyrene butyl methacrylate monomer that was synthesized via esterification of 1-pyrenebutanol and methacryloyl chloride.[22,50,87] Polymerization was performed at 50 ^oC for 24 h under a nitrogen environment using azobisisobutyronitrile (AIBN) as initiator. Post thermal termination, the PS-Py polymer

was dissolved in tetrahydrofuran (THF) and subsequently re-precipitated in methanol at least seven times to remove unreacted monomer and chromophores. The washing procedure helps reduce polydispersity, specifically biased towards eliminating low MW PS-Py chains and unreacted monomer, while retaining the higher molecular weight chains. The label content of PS-Py was later characterized by ultraviolet-visible spectroscopy in spectroscopic grade THF. Unlabeled (neat) polystyrene (M_w = 1920 kg/mol, M_w/M_n = 1.26), which was used to sandwich the PS-Py 10-15 nm probe layers on the PS side of the structures, was purchased from Pressure Chemical and used as received. Polysulfone (M_w ≈ 85 kg/mol, Udel P-3500 LCD MB8), poly(methyl methacrylate) (M_w = 1150 kg/mol, M_w/M_n = 1.06), and poly(isobutyl methacrylate) (M_w = 295 kg/mol, M_w/M_n = 1.83) were purchased from Solvay Advanced Polymers, Pressure Chemical, and Scientific Polymer Products, respectively, and used as received.

Individual layers of PS-Py, PS, PMMA, and PiBMA were made by spin-coating from toluene solutions either onto freshly-cleaved mica or quartz slides, depending on if the polymer was used as an underlayer or a PS/PS-Py/PS T_g reporting multilayer stack. All PSF films were prepared in the same manner but from cyclopentanone solutions. Film thickness was determined via ellipsometry after the films were either floated or spin-coated onto silicon wafers. The spin speed and solution concentrations were adjusted to produce films with known reproducible thicknesses and minimal surface roughness (on the order of <1 nm). All individual layers were annealed under vacuum for at least 18 h at T_g + >20 K to facilitate the removal of any residual solvent and relaxation of spin-coating induced stresses. Multilayers were then assembled by successively floating each layer onto room temperature deionized water and capturing the layer onto the multilayer sample starting

from a given base underlayer spun directly onto the quartz slide needed for fluorescence measurements. Between each successive floating, the sample is allowed to thoroughly dry. Bulk polymer underlayers and bulk PS capping layers were made > 450 nm in thickness to ensure that the pyrene-labeled probe layer is unaffected by the free surface or underlying substrate interface.

Multilayer structures with polymer underlayers containing a polymer with a T_g *higher* than that of PS were constructed in a two-step annealing process, as illustrated in Figure 4.1, to limit the interdiffusion of the PS-Py probe layer into the surrounding neat PS matrix, while still ensuring that the polymer-polymer interface of interest has reached equilibrium, ensuring good coupling of the cooperative dynamics across the interface. The variable thickness PS *z*-layer was floated onto a PMMA or PSF coated substrate (post initial vacuum annealing of each layer) and annealed to consolidate this bilayer and thereby form a PS/PMMA or PS/PSF interface that had reached equilibrium prior to floating the remaining PS layers. The PS/PMMA and PS/PSF bilayers were annealed under vacuum at 150 ^{o}C for 30 min and at 210 ^{o}C for 90 min, respectively. After these polymer-polymer interfaces were consolidated, the remaining PS-Py and capping neat PS layers were floated atop the PS/PMMA or PS/PSF samples. The remaining PS/PS-Py/PS interfaces were then annealed in an Instec HCS402 heater immediately prior to the fluorescence measurements by heating to 170 ^{o}C and holding for 5 min prior to dropping the temperature to 150 ^{o}C and holding for 2 min. This annealing protocol ensured that the PS/PS-Py/PS layers formed consolidated interfaces, while still limiting diffusion of the PS-Py probe layer. Multilayer structures with polymer underlayers containing a polymer with a T_g *lower* than that of PS could be fabricated with a single annealing process because the polymer-polymer interface

of interest easily reaches equilibrium for annealing conditions that are appropriate for the PS/PS-Py/PS interfaces.[19] The PS and PS-Py films in multilayer samples containing PiBMA as the underlayer were floated directly atop each other in succession, and then only annealed together immediately prior to the fluorescence measurement for 20 min at 120 ^{o}C.

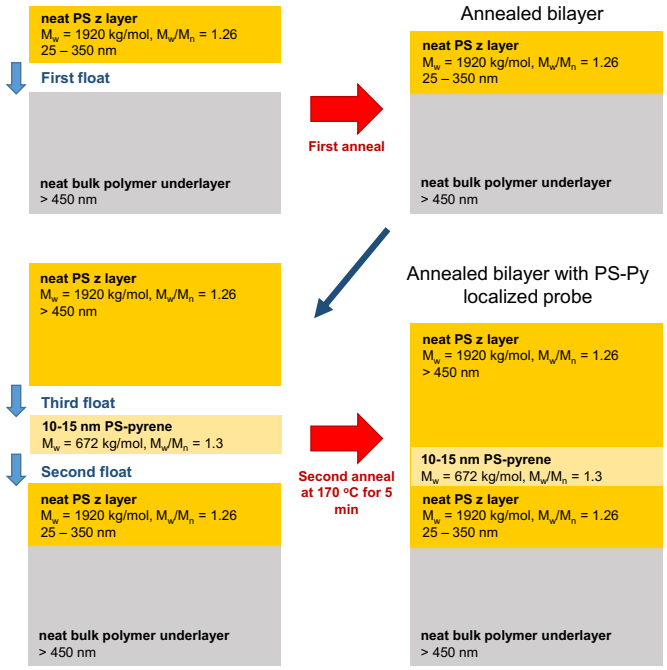

Figure 4.1: Exploded view of the two-step annealing process for multilayer samples containing PMMA or PSF as the polymer underlayer that have a T_g *higher* than that of PS. The two-step annealing process ensures that the PS/PMMA or PS/PSF interface has reached equilibrium without allowing interdiffusion of the PS-Py reporting layer.

Fluorescence measurements were performed using a Photon Technology International QuantaMaster spectrofluorometer with samples mounted in an Instec HCS402 heater. The pyrene-labeled probe layers were excited at a wavelength of 330 nm using a xenon arc lamp with an excitation band-pass of 5.5-6.0 nm and an emission band-

pass of 5.0 nm. After the final sample annealing as described above, the sample temperature was ramped down at 1 ^{o}C/min while pyrene fluorescence intensity was collected for 3 s every 27 s, at an emission wavelength of 379 nm. All samples were reheated to the starting temperature after each run to ensure that the same initial fluorescence intensity was recovered, verifying that the sample had remained stable during the course of the experiment and no photobleaching occurred. This ramped fluorescence procedure for measuring T_g was further described in Chapter 2[22] and utilized for the data collection in Chapter 3.[19] Bulk T_g values measured by fluorescence and ellipsometry are for PMMA T_g^{bulk} = 120 ^{o}C, PiBMA T_g^{bulk} = 62 ^{o}C, and PSF T_g^{bulk} = 186 ^{o}C.

4.4 RESULTS AND DISCUSSION

4.4.1 Comparing PS/PSF to PS/PnBMA: Hard vs. Soft Confinement

In the following two sections I will show that the asymmetry and the extended length scale of the local glass transition $T_g(z)$ profile recently reported in the polystyrene/poly(*n*-butyl methacrylate) (PS/PnBMA) system[19] is not unique to this single polymer-polymer system. We start by comparing my previously measured PS/PnBMA system to one that is effectively reversed, where PS now forms the rubbery component next to a glassy polymer, polysulfone (PSF). The bulk glass transition temperature value of PSF is T_g^{bulk} = 186 ^{o}C resulting in an 85 K difference across the PS/PSF interface (T_g^{bulk} = 101 ^{o}C for PS). This PS/PSF system is analogous to that of PS/PnBMA, but reverses the role of the PS component. In the PS/PnBMA system, the PS component was the hard glassy material that underwent soft confinement by the rubbery PnBMA, whereas in the PS/PSF system, the PS component is the soft rubbery material undergoing hard confinement by the

glassy PSF. In both cases, there is an 80-85 K difference in bulk T_g between the two components. A comparison between these two systems will allow us to test whether the penetration depth of the dynamical T_g perturbation from the dissimilar polymer-polymer interface is polymer specific (e.g., related to chemical structure) or determined by the glassy vs. rubbery role played by the component (i.e., whether the confinement is soft vs. hard).

Figure 4.2 illustrates the sample geometries of the two systems being compared. Each geometry is comprised of four individually constructed films of designed thickness that were assembled and carefully annealed to form a consolidated material with an effectively static geometry as illustrated. I employ a temperature-dependent fluorescence method to measure the local $T_g(z)$ at different distances z from the glassy-rubbery polymer-polymer interface. The multilayer sample geometries are constructed via a floating procedure where a 10-15 nm pyrene-labeled PS probe layer (PS with a fluorescent 1-pyrenylbutyl methacrylate monomer chemically attached to the PS backbone at a label content of ~1:70 monomers, designated PS-Py) is placed at a known distance z from the dissimilar polymer-polymer interface in question by inserting a neat (unlabeled) PS layer of thickness z between the pyrene-probe layer and the dissimilar polymer layer (PSF or PnBMA in Fig. 4.2). As previously discussed in Chapter 3, high molecular weight polystyrenes are used to limit interdiffusion of the PS/PS-Py/PS interfaces and keep the T_g-reporting PS-Py layer localized a fixed distance z from the dissimilar polymer-polymer interface of interest. One of the advantages of using polymers for this type of study is that chain diffusion is effectively decoupled from more local cooperative segmental α-relaxations associated with T_g in high molecular weight entangled polymers such that the

morphology of the layers assembled will remain static during the course of the experiment. As we will explore in more detail below, a key factor in measuring a reproducible and reliable value of $T_g(z)$ is that the dissimilar polymer-polymer interface has been annealed to equilibrium. Immiscible polymer-polymer interfaces initially interdiffuse quite readily by local Rouse modes, but stabilize quickly at an equilibrium interfacial width $w_I \sim \chi^{-\frac{1}{2}}$ of only a few nanometers limited by the unfavorable interactions χ between the two materials.[88] Unless otherwise indicated, all the $T_g(z)$ values presented are measured ensuring that the dissimilar polymer-polymer interface has been annealed to equilibrium prior to the start of the fluorescence data collection.

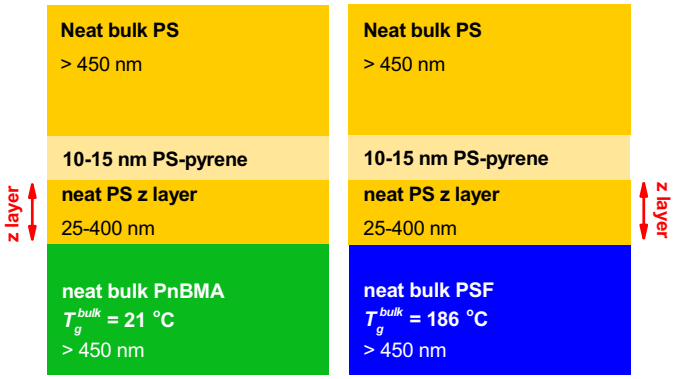

Figure 4.2: Sample geometries comprised of four individually spin-coated layers of polystyrene (PS), and poly(*n*-butyl methacrylate) (PnBMA) or polysulfone (PSF), assembled and annealed to form a consolidated material with a 10-15 nm thick local T_g-reporting pyrene-labeled PS layer. The neat PS *z*-layers varied the distance *z* of the pyrene-labeled PS layer relative to the PS/PnBMA (7 nm wide) or PS/PSF (6 nm wide) interface. High molecular weight polymers ensure that the assembled morphology remains static throughout the experiment.

Figure 4.3 shows the temperature-dependent fluorescence intensity measured for four different samples where the PS-Py probe layer has been placed at specific distances *z*

from either a PS/PnBMA or PS/PSF interface. Vitrification in polymers is characterized by the dynamic arrest of cooperative segmental motion as the material enters the glassy state. It is well known that pyrene is sensitive to the local density and rigidity of the surrounding polymer matrix.[22,35,50,89] As the temperature is lowered and the local polymer matrix surrounding the pyrene dye becomes more rigid, the probability of radiative compared with non-radiative decay of the pyrene fluorescence increases, where a break in the slope of the signal intensity is manifested when crossing from the liquid to glassy state as the temperature dependence of the density changes. Previous works have demonstrated that this measure of T_g via fluorescence matches that by differential scanning calorimetry (DSC) in bulk materials and by ellipsometry in thin films.[50,89] I measure the fluorescence intensity on cooling at 1 ^{o}C/min where the intensity at a single wavelength (first emission peak of pyrene at 379 nm that is the most sensitive to its local environment[90,91]) is sampled every 30 s (averaging signal intensity over a 3 s time window) resulting in a data point collected every 0.5 ^{o}C, with no additional smoothing performed to the temperature-dependent intensity data.[19,22] To facilitate comparisons, each dataset shown in Fig. 4.3 is normalized and then vertically shifted for clarity. The top panel graphs the temperature-dependent intensity for PS-Py probe layers located at different distances from a PS/PSF interface where PS forms the rubbery, lower T_g component: at a distance z = 139 nm (far from the PS/PSF interface), the local $T_g(z)$ = 103 ± 2 ^{o}C, consistent with the T_g of bulk PS, but at a distance z = 51 nm (closer to the PS/PSF interface), the local $T_g(z)$ = 120 ± 2 ^{o}C, significantly increased relative to T_g^{bulk} of PS. For comparison, the bottom panel graphs the temperature-dependent intensity for PS-Py probe layers located at different distances from a PS/PnBMA interface where PS forms the glassy, higher T_g component: at a distance

z = 356 nm (far from the PS/PnBMA interface), the local $T_g(z) = 99 \pm 2$ °C, consistent with the T_g of bulk PS as expected, but at a distance z = 64 nm (closer to the PS/PnBMA interface), the local $T_g(z) = 63 \pm 2$ °C, significantly decreased relative to T_g^{bulk} of PS.[19] Decreasing the separation distance (z layer thickness) of the pyrene-labeled PS layer in relation to the dissimilar polymer-polymer interface drastically changes the local T_g at that location relative to PS bulk T_g. The magnitude of the T_g perturbation is large (+19 K and –38 K) at a distance (51 and 64 nm) that is still quite far from the dissimilar polymer-polymer interface. As discussed in Chapter 3, these perturbations in local T_g occur far from the polymer-polymer interface such that locally only PS segments are present at the position z. The local $T_g(z)$ near the PS/PnBMA interface is not at all correlated with the local composition $\phi(z)$, which has been the traditional view in understanding local T_g in miscible polymer blends.[23-25] These distances (z = 51 and 64 nm) are also quite large compared to the observed perturbation length scales associated with the PS-free surface,[50,53] but are comparable to systems with highly chemically-interactive substrates.[49,51,52]

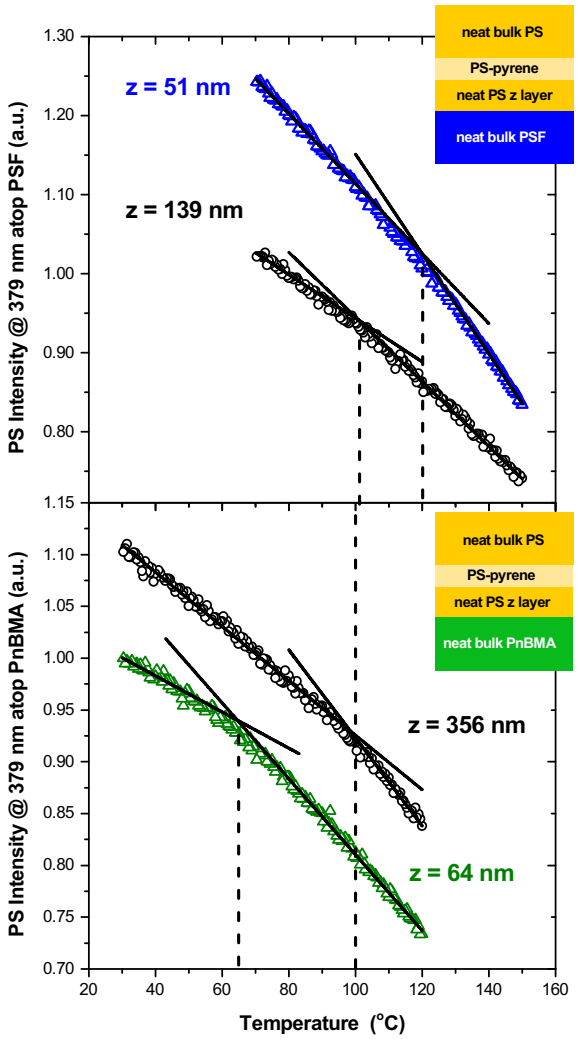

Figure 4.3: Normalized fluorescence intensity as a function of temperature collected on cooling at 1 °C/min for four different samples. (Top) PS/PSF system: pyrene-labeled PS probe layer located at a distance z = 139 nm away from the PS/PSF interface reports a local $T_g(z)$ = 103 ± 2 °C in agreement with T_g^{bulk} of PS, while at a distance z = 51 nm, the local $T_g(z)$ = 120 ± 2 °C significantly increased by the presence of the PS/PSF interface. (Bottom) PS/PnBMA system:[19] at a distance z = 356 nm, the local $T_g(z)$ = 99 ± 2 °C in agreement with T_g^{bulk} of PS, while at a distance z = 64 nm, the local $T_g(z)$ = 63 ± 2 °C significantly decreased by the presence of the PS/PnBMA interface. In both cases, the large perturbation in local $T_g(z)$ occurs at distances that are many tens of nanometers away from the change in composition.

To further investigate the length scale of the dynamical T_g perturbation near the PS/PSF interface, Figure 4.4 graphs the local $T_g(z)$ values measured for many different samples where the thickness of the neat PS z-layer between PSF and the PS-Py probe reporting layer was varied. Error bars of ± 2 ^oC were determined based on the standard deviation of multiple measurements at comparable z values as the largest experimental error is associated with sample-to-sample variability. It is not possible to polymerize PSF with a pyrene label; thus, I am restricted to only mapping the PS side of the PS/PSF $T_g(z)$ profile. However, all data collected indicate that the $T_g(z)$ profile behaves similarly to the full $T_g(z)$ profile collected previously[19] for PS/PnBMA where the data are well fit by a hyperbolic tangent function, which asymptotes to the bulk T_g values far from the interface on either side, with a broad mobility-gradient, strongly biased toward the glassy PS side. The PS/PSF $T_g(z)$ data can be similarly fit to a hyperbolic tangent showing the broad mobility-gradient is now strongly biased toward the glassy PSF side. The local T_g-dynamics transition smoothly from one extreme to the other across the interface, in contrast to the composition. The dashed curves in the figure represent the composition profiles of the two systems, $\phi(z) \approx \tanh(2z/w_I)$, with equilibrium interfacial width w_I = 7 nm for PS/PnBMA[19-22] and w_I = 6 nm for PS/PSF (estimated based on solubility parameters[92-94]). On the scale of Fig. 4.4, the two composition profiles look similar and nearly vertical, starkly defining the location of the interface. In comparing directly the $T_g(z)$ profiles of the PS/PSF system with that measured previously for the PS/PnBMA system, we can observe two distinct behaviors: (1) The magnitude of the T_g reduction or enhancement from bulk T_g dynamics is not dependent on the relative T_g difference at the polymer-polymer interface. In both the PS/PnBMA and PS/PSF systems, the difference in T_g is 80-85 K, yet

the PS-Py probe layers close to the PS/PnBMA interface experience more than twofold greater deviation in local $T_g(z)$ from the bulk T_g of PS for a given distance z, as compared to the PS-Py probe layers close to the PS/PSF interface. The local $T_g(z=0)$ at the interface is consistently closer to the lower T_g component in both systems: $T_g(z=0) = 37 \pm 2\ ^oC$ for PS/PnBMA and $T_g(z=0) = 130 \pm 3\ ^oC$ for PS/PSF. (2) The z-distance at which the perturbation in local $T_g(z)$ begins on the PS side as the PSF or PnBMA interface is approached is significantly different: at $z \approx 125$ nm as PSF is approached and at $z \approx 250$ nm as PnBMA is approached. In addition, the propagation of the $T_g(z)$ perturbation is uncorrelated with the magnitude of the T_g difference between the two polymers and is independent of the magnitude in $T_g(z)$ perturbation at the interface. Below I discuss separately these two factors, the magnitude of the perturbation in local T_g at the interface and the distance of propagation away from the interface that the dynamical perturbation persists. By comparing a series of polymer systems, I will show that these behaviors of the broad $T_g(z)$ profile appear to be universal across different systems and are grouped in behavior by whether the neighboring interface has a higher or lower T_g, i.e., hard vs. soft confinement.

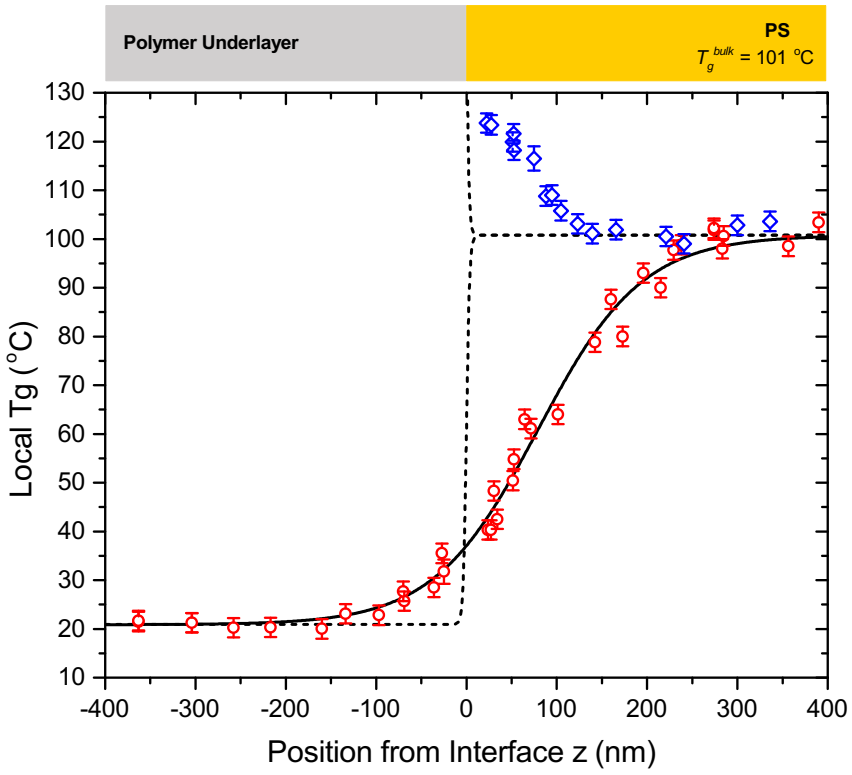

Figure 4.4: Experimentally measured local $T_g(z)$ profile of PS/PSF (open blue diamonds), compared with that previously measured[19] for PS/PnBMA (open red circles), as a function of z, the pyrene-labeled layer's position from the PS/PSF or PS/PnBMA interface. In the PS/PSF system, the PS layer is rubbery relative to PSF undergoing hard confinement, while in the PS/PnBMA system, the PS layer is glassy relative to PnBMA undergoing soft confinement. Both PS/PSF and PS/PnBMA systems have a bulk T_g difference of 80-85 K between the two domains that the local $T_g(z)$ must transition between. I previously demonstrated[19] that the PS/PnBMA $T_g(z)$ profile was well fit by a hyperbolic tangent (solid black curve) demonstrating that the mobility-gradient is broad and strongly biased toward the glassy PS side. Grey dashed curves indicate the local composition profiles $\phi(z)$ with an equilibrium interfacial width of 6 nm (PS/PSF) and 7 nm (PS/PnBMA), which appear nearly vertical on this scale unmistakably highlighting the breadth of the T_g mobility gradient.

As it is difficult to precisely identify the location where $T_g(z)$ begins deviating from bulk behavior, I have chosen to quantify the propagation distance of the dynamical $T_g(z)$

perturbation from bulk dynamics by identifying the distance from the interface $\xi_{½}$ at which the magnitude of the $T_g(z)$ perturbation at the interface $\left|T_g(z=0) - T_g^{bulk}\right|$ decays to half its value, $\xi_{½} = z$ when $\frac{\left|T_g(z) - T_g^{bulk}\right|}{\left|T_g(z=0) - T_g^{bulk}\right|} = 0.5$. This quantification of a length scale for the dynamical perturbation follows from my previous work[19] and is based on an original definition of a kinetic correlation length in glassy systems put forward by Butler and Harrowell.[43] In 1991, Butler and Harrowell[85] explored the temperature dependence of the mean spin relaxation times $\tau(T)$ characterizing dynamical heterogeneity in the 2D two-spin facilitated Ising model (2FSM) of Fredrickson and Andersen.[95,96] This simple facilitated kinetic Ising spin model exhibits heterogeneous dynamics, a broad spectrum of relaxation times, and undergoes dynamic arrest when the effective temperature is decreased. These characteristic hallmarks of the glass transition are achieved with only nearest-neighbor dynamical interactions; yet, this simple system otherwise does not contain an equilibrium phase transition or an inherent static correlation length. As a separate consideration to their main work,[85] Butler and Harrowell also explored how the local relaxation time τ_n for a given layer *n* would behave when next to a surface layer of all up spins.[43] Butler and Harrowell[43] characterized the dynamical influence of a surface of all up spins on the glassy kinetics of this simple Ising model as a function of layer distance *n* away from the surface by defining a kinetic correlation length $\xi_{½}(T)$ as the distance from the surface (*n*=1) at which the perturbation to the local relaxation time τ_n relative to bulk decayed to half its value, $\xi_{½}(T) = n$ when $\frac{\left|\tau_n - \tau_{bulk}\right|}{\left|\tau_1 - \tau_{bulk}\right|} = 0.5$. Having full access to the temperature-dependent relaxation time $\tau_n(T)$ from their simulations, Butler and Harrowell were able to determine values of $\xi_{½}(T)$ for different temperatures. They

found that the temperature dependence of $\xi_{½}(T)$ matched the temperature dependence of the mean relaxation times $\tau(T)$ previously determined for the bulk system and argued that such a surface decay kinetic correlation length $\xi_{½}(T)$ was a reflection of kinetic correlations of glassy dynamics in bulk systems.[43] In their simulations, Butler and Harrowell found values of $\xi_{½}(T)$ up to 5-6 spin-layers as the glass transition was approached from above, meaning deviations from bulk dynamics could persist to a depth of 10-12 spin-layers from the surface interface of all up spins. Although there is no direct way to convert *n* spin-layers to a physical size in nanometers, we can consider that one spin-lattice site can flip (rearrange) from up to down, corresponding to a coarse-grained measure of a local arrangement of several physical units (polymer segments), representing a local region of the material. With only dynamical correlations between nearest-neighboring spins, the influence of the all-up spin interface persists to depths of many such spin sites.

I recognize that this $\xi_{½}$ length scale is a rather arbitrary definition, but it has the advantage of being robustly quantifiable from the experimentally measured $T_g(z)$ values and according to the work of Butler and Harrowell[43,85] may provide insight into size-scales associated with glassy cooperative dynamics. Thus, I proceed with this measure of quantification for the propagation distance of the dynamical $T_g(z)$ perturbation from bulk dynamics. I previously reported that for the PS/PnBMA system, $\xi_{½} = 103$ nm for glassy PS, while $\xi_{½} = 50$ nm for rubbery PnBMA.[19] From Figure 4.4 I find that in the PS/PSF system, $\xi_{½} = 49$ nm for rubbery PS. Thus, we see that the length scale over which the dynamical $T_g(z)$ perturbation persists depends on whether PS is next to PnBMA (soft confinement) or PSF (hard confinement), and that the length scale in PnBMA next to PS

(hard confinement) is comparable. This suggests that the propagation of the dynamical $T_g(z)$ perturbation does not depend directly on some material property such as chemical structure, but rather on whether the domain in question is in its glassy or rubbery state. As we will see in the next section, PS glassy domains in contact with a rubbery interface (soft confinement) have their local $T_g(z)$ dynamics consistently perturbed out to a further distance from the interface than PS rubbery domains in contact with a glassy interface (hard confinement).

4.4.2 Universal Behavior: Local $T_g(z)$ of PS Next to Different Polymers

Next, we explore how universal this hard vs. soft confinement behavior is by comparing profiles of the local $T_g(z)$ dynamics in the PS domain next to a series of different polymers with higher (hard) and lower (soft) T_g in reference to PS. By making this comparison across different systems, I am able to address possible factors and causes that could affect the strong $T_g(z)$ coupling in cooperative segmental dynamics between domains of dissimilar polymers. Again, for each system presented here, I have made sure that the dissimilar polymer-polymer interface has been annealed to equilibrium. The next section below will address what occurs when the dissimilar polymer-polymer interface has only undergone limited annealing, demonstrating that the strong $T_g(z)$ coupling is significantly reduced or even eliminated if local interdiffusion of the chains has not been allowed to occur.

Figure 4.5 graphs the $T_g(z)$ values within the PS domain next to interfaces with four different polymers: PSF (T_g^{bulk} = 186 ^oC), PMMA (T_g^{bulk} = 120 ^oC), PiBMA (T_g^{bulk} = 62 ^oC), and PnBMA (T_g^{bulk} = 21 ^oC). The bulk T_g of PS = 101 ^oC is identified by the horizontal

dashed black line clearly demarcating which polymers have a higher T_g than PS resulting in hard confinement, and which have a lower T_g than PS resulting in soft confinement. In addition, the $T_g(z)$ data collected on the rubbery PnBMA side from the PS/PnBMA system has been added to Fig. 4.5, but in order to make a comparison of the extended length scale of the $T_g(z)$ perturbation between hard and soft confined systems, I have plotted the magnitude of the $T_g(z)$ perturbation measured in rubbery PnBMA next to PS (hard confinement of PnBMA), on the PS side and elevated it to be referenced to the bulk T_g of PS: $T_g(z) = T_g(z)$ of PnBMA $- T_g^{bulk}{}_{PnBMA} + T_g^{bulk}{}_{PS}$, with $-z \rightarrow z$. In this manner, we can clearly see that the rubbery PnBMA $T_g(z)$ under hard confinement next to glassy PS, behaves very similarly to the rubbery PS $T_g(z)$ under hard confinement next to PSF and PMMA. It is clear from the data that the behavior of the $T_g(z)$ profile near a dissimilar polymer-polymer interface primarily depends on whether the domain in question is experiencing hard confinement next to a polymer with higher T_g than itself or soft confinement next to a polymer with lower T_g than itself. For glassy polymers under soft confinement, the $T_g(z)$ perturbation is much larger and extends to much greater distances ($z \approx$ 225-250 nm before bulk T_g of PS is recovered), compared with rubbery polymers under hard confinement ($z \approx$ 100-125 nm before bulk T_g of PS is recovered). The depth from the dissimilar polymer-polymer interface to which the local $T_g(z)$ is perturbed is independent of the magnitude of the T_g difference between the two polymers in question and the magnitude of the $T_g(z)$ perturbation itself. The behavior depicted by the data appears to be universal to these various polymers, some with very different chemical structures. Note that I have not indicated the composition profiles of the interface in Fig. 4.5, but if included they would resemble a nearly vertical step changes at $z = 0$ on this scale, given the

enormous range of the *x*-axis.

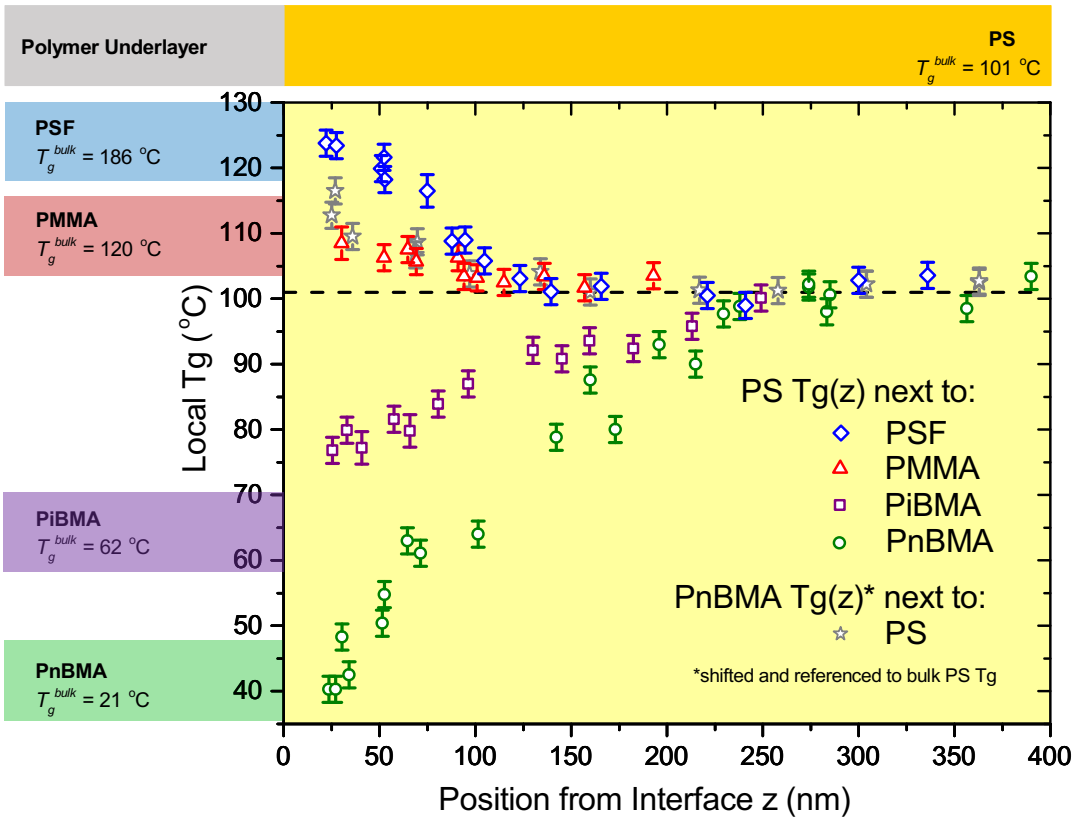

Figure 4.5: Local $T_g(z)$ profile in the PS domain as a function of distance z from the dissimilar polymer-polymer interface with various neighboring polymers: PSF (T_g^{bulk} = 186 °C) shown as blue diamonds, PMMA (T_g^{bulk} = 120 °C) shown as red triangles, PiBMA (T_g^{bulk} = 62 °C) shown as purple squares, and PnBMA (T_g^{bulk} = 21 °C) shown as green circles. The behavior (magnitude and penetration distance) of the $T_g(z)$ profile is primarily dependent on whether PS (T_g^{bulk} = 101 °C, horizontal dashed line) experiences hard confinement next to a polymer with a higher T_g^{bulk} (depth to which perturbation decays to half its value $\xi_{½}$ = 55 ± 5 nm) or soft confinement next to a polymer with a lower T_g^{bulk} ($\xi_{½}$ = 115 ± 5 nm). For comparison, previous data[19] of the magnitude of the $T_g(z)$ perturbation in rubbery PnBMA next to glassy PS (hard confinement) is added as gray stars where the data have been shifted to the T_g^{bulk} of PS as reference.

To make quantitative comparisons between the various $T_g(z)$ datasets shown in Figure 4.5, I calculated the $T_g(z = 0)$ value at the interface between the two dissimilar

polymers and determine the distance $\xi_{½}$ from the interface at which the $T_g(z)$ perturbation decays to half its value. These values are tabulated in Table 4.1 for the various systems, along with the bulk T_g of the polymer in contact with PS, and the difference ΔT_g between the two bulk T_g values. A pattern is clearly observed where polymer domains under soft confinement (next to a polymer interface with a lower T_g than itself) exhibit a large decrease in $T_g(z)$ near the interface over an extremely large length scale $\xi_{½} = 115 \pm 5$ nm, while polymer domains under hard confinement (next to a polymer interface with a higher T_g than itself) exhibit a more modest increase in $T_g(z)$ near the interface over a comparatively smaller length scale $\xi_{½} = 55 \pm 5$nm. For reference I also include values for the equilibrium interfacial width w_I between the two immiscible polymers and the fragility m of the neighboring polymer next to PS. Although the equilibrium interfacial widths of the composition profile $\phi(z)$ vary between 5-7 nm, these are very small differences that appear to have little if any influence on the $T_g(z)$ behavior. (Although there are no reports in the literature of PS/PiBMA equilibrium interfacial widths or even χ values, I suspect it is likely comparable to that between PS/PnBMA as the magnitude and temperature dependence of the surface tension of PiBMA is very similar to that of PnBMA.[97]) Perhaps this is unsurprising given the small size of the composition profile in comparison to the large range of the dynamical $T_g(z)$ profile. However, as is discussed further in the next section, I do believe that the broad nature of polymer-polymer interfaces, in comparison to the sharp ($\leq$ 0.5 nm) polymer-air, polymer-liquid, or polymer-substrate interfaces plays some unique role in leading to the observed enormous dynamical $T_g(z)$ profiles.

Table 4.1: Tabulated values of the experimentally determined $T_g(z = 0)$ at the interface between the two dissimilar polymers, the distance $\xi_{½}$ from the interface at which the $T_g(z)$ perturbation decays to half its value, and for reference the T_g bulk of the polymer in contact with the PS domain, along with the difference ΔT_g between the two bulk T_g values of the system, the equilibrium interfacial width w_I of the composition profile, and the fragility[98] m of the neighboring polymer next to PS. In the lower part of the table are the corresponding values for PnBMA in contact with PS.

	Polymer	T_g^{bulk}	ΔT_g	T_g (z = 0)	Penetration distance $\xi_{1/2}$	Interfacial width	Fragility m
PS/	PSF	186 °C	85 K	130 °C	49 nm	6 nm [1]	141 [4]
	PMMA	120 °C	19 K	112 °C	59 nm	5 nm [2]	145 [5]
	PiBMA	62 °C	39 K	75 °C	127 nm	——	67 [6]
	PnBMA	21 °C	80 K	37 °C	103 nm	7 nm [3]	56 [4]
PnBMA/	PS	101 °C	80 K	37 °C	50 nm	7 nm [3]	139 [7]

[1] Y. Du, et al., in *Physical Properties of Polymers Handbook*, ed. J.E. Mark (AIP Press, New York, 1996), pp. 227–239.
[2] J. Brandrup et al. Eds., *Polymer Handbook*, 4th ed. (Wiley: New York, 1999).
[3] D. F. Siqueira et al., *Colloid Polym. Sci. 273*, 1041 (1995).
[4] D. Huang and G. B. McKenna, *J. Chem. Phys. 114*, 5621 (2001).
[5] A. P. Sokolov et al., *J. Phys.: Condens. Matt. 19*, 205116 (2007).
[6] K. L. Ngai et al., *Polymer 47*, 7222 (2006).
[7] R. Böhmer et al., *J. Chem Phys. 99*, 4201 (1993).

Evans et al. have recently measured the experimental T_g value of thin PS layers surrounded by large (500-nm thick) bulk layers of different polymers.[71] They found that as the PS layer thickness decreased the T_g of the PS layer increased or decreased relative to $T_g{}^{bulk}{}_{PS}$ and approached the bulk T_g value of the surrounding polymer in their trilayer systems. For the thinnest films of 14-nm PS, the maximum shift in T_g of the PS domain was equivalent to previous measurements[99,100] of the component T_g of isolated PS chains (0.1 wt% blends at near-infinite dilution) in a matrix of different polymer that was the same as the surrounding polymer in the trilayer system. Evans et al. argued that the magnitude

of the perturbation to the PS T_g in these trilayer and near-infinite dilution systems were correlated with the fragility value of the neighboring (surrounding) polymer.[71,100] We consider now if my experimentally measured magnitude of the perturbation in local T_g is correlated with the fragility of the neighboring domain. My observed maximum perturbation in local T_g occurs at the dissimilar polymer-polymer interface (z = 0). Following Evans et al.,[71] I calculate the relative shift in the magnitude of the T_g perturbation at the interface as $\left|T_g(z=0) - T_g^{bulk}\right|/\Delta T_g$ from the data presented in Table 4.1. For the perturbation to the PS component in my systems, at best only a loose correlation between fragility of the neighboring domain with the magnitude of the T_g perturbation is found. However, it is not consistent with PSF and PMMA, which have comparable fragilities[101,102] (141 and 145), but significantly different magnitudes in perturbation (35% and 60% of maximum, respectively). An estimate of how universal this correlation with neighboring fragility might be by determining the magnitude of the T_g perturbation for the other polymers at the dissimilar polymer-polymer interface caused by the presence of the PS domain. The magnitude of the T_g perturbation at the interface (z = 0) varies from 20-65% for the different polymers presented in Table 4.1, while the fragility of the neighboring domain (PS) is a fixed value (m = 139)[103]. Thus, for my systems, it does not appear that fragility is a key parameter in controlling the magnitude of the T_g perturbation. However, the present geometry is qualitatively different geometry of two semi-infinite domains in contact, instead of isolated chains or small domains of PS surrounded by a dissimilar polymer.

Recently a number of theoretical and computational efforts have explored the dynamics of glassy systems in proximity to high mobility interfaces. Of particular interest

to the present study is a limited mobility model by Tito et al.[37,104] where they have modeled exchanges in local mobility within a heterogeneous glassy material and investigated local mobility profiles near various interfaces. Their 2013 work[37] modeled a slab of a glassy or rubbery domain that was sandwiched by material that had either a lower or higher mobility. Within this kinetic lattice model, probabilities for mobility exchange between neighboring lattice sites transitioned a given site between three different states ("awake", "sleep", or "dense"), where a series of exchange parameters collectively governed the dynamics of the system. Profiles of the local mobility as a function of position across the system showed different penetration depths to which the local dynamics were perturbed by the interface between the glassy-rubbery domains at different temperatures. The Tito et al. work[37] predicted an asymmetric mobility profile at the glassy-rubbery interface that extends further into the glassy (lower mobility side) than into the rubbery (higher mobility side). This prediction of an asymmetric mobility profile is consistent with my experimental results shown in Fig. 4.5 for the various glassy-rubbery polymer-polymer interfaces. This suggests that the observed asymmetry in the $T_g(z)$ profiles (i.e., the difference in penetration depth of perturbed dynamics between the glassy and rubbery sides) may reflect a property of how glassy dynamics behave near interfaces.

Simmons and coworkers have investigated using bead-spring MD simulations the role that interfacial energy between a low T_g and a high T_g polymer domain affect how these two neighboring domains influence each other's dynamics.[66,105] The high T_g domain under soft confinement by the lower T_g polymer had its T_g^{high} reduced relative to its $T_g^{bulk,high}$ and the low T_g domain under hard confinement by the higher T_g polymer had its T_g^{low} increased relative to its $T_g^{bulk,low}$. The T_g shift in the low-T_g domain under hard

confinement was additionally influenced by the magnitude of the interfacial energy between the two domains. One complicating factor in comparing these simulations to my experimental results is that when the interfacial energy was varied in the simulations, it also altered the degree of chain interpenetration between the two domains. In the next section, I demonstrate experimentally that the observed $T_g(z)$ profiles reported in Figures 4.4 and 4.5 are strongly dependent on the amount of annealing of the dissimilar polymer-polymer interface and hence likely the extent of chain interpenetration across this interface. However, of significance, the MD simulations found that the degree to which interfacial energy affected the T_g shift was correlated with the mean-square displacement $\langle u^2 \rangle$ of the neighboring domain, a quantity characterizing the "hardness" or shear modulus of the material.[66] Starr and Douglas have also found that local T_g dynamics near an interface in bead-spring MD simulations correlate with the relative stiffness of the underlying substrate.[38] Perhaps this gives an insight into why my experimental results are separated into longer length scales ($\xi_{½}$ = 115 ± 5 nm) for domains under soft confinement and shorter length scales ($\xi_{½}$ = 55 ± 5 nm) for domains under hard confinement, i.e., it is the softness or hardness of the neighboring domain that influences how local T_g-dynamics are perturbed near these interfaces.

The role that local stiffness or local modulus plays in α-relaxations and T_g has recently received renewed treatment by Mirigian and Schweizer.[106-109] They have proposed that the α-relaxation event can be facilitated by a collective elastic distortion of the surrounding material, where the size of this distortion field is related to the local elastic shear modulus. This would suggest that the local α-relaxations (T_g) would be influenced by its local surroundings out to a greater distance when the material is locally stiffer.

Applying this reasoning to my glassy-rubbery polymer-polymer interface systems might suggest that the higher shear modulus of the glassy side would be altered out to a greater extent than that of the softer rubbery side. This reasoning perhaps provides a qualitative argument for why the direction of the $T_g(z)$ asymmetry is biased towards the glassy side of the dissimilar polymer-polymer interface. Although the Mirigian and Schweizer theory has been successfully applied to model local T_g changes near free surfaces,[44,45] it has not yet been applied to dissimilar polymer-polymer interfaces. None of these theories address the large quantitative size of the length scales observed here in. This is still an outstanding question. It is unclear why polymer-polymer interfaces alter the local T_g value out to hundreds of nanometers in contrast to polymer-air interfaces which typically perturb the dynamics out to only several tens of nanometers at most. This phenomenon will be discussed in more detail in the following section. It should be noted that size scales typically associated with glass transition dynamics ($\xi_{CRR} \approx$ few nanometers) are much smaller than the length scales of interfacial perturbations in confined systems.[19,50,52,53,110] However, a number of theoretical models such as Random First Order Transition (RFOT) theory[42,111] and the Mirigian and Schweizer model just described, incorporate secondary longer-ranged factors where the local cooperative dynamics are influenced by neighboring collective dynamics. Experiments such as in this study demonstrating long-ranged T_g perturbations suggest that factors beyond a single CRR size may be more important than we realize in understanding glassy dynamics.

4.4.3 Varying Annealing Time of PS/PSF Interface: Importance of Reaching Equilibrium

Here I demonstrate the importance of annealing the dissimilar polymer-polymer

interface in establishing the observed $T_g(z)$ profiles. I find that the strong coupling in cooperative segmental dynamics across the interface and the extended length scales over which the $T_g(z)$ perturbation persists from the interface only occur if the dissimilar polymer-polymer interface is annealed to equilibrium. It is easiest to demonstrate this effect by focusing on the PS/PSF system. As described above in the Experimental Methods section and Figure 4.1, when measuring the $T_g(z)$ of a lower T_g component (e.g., PS in PS/PSF), first the PS z-layer and underlying PSF layer are annealed together to ensure that this dissimilar polymer-polymer interface has been annealed to equilibrium. Second, the additional PS-Py labeled-probe layer and top (bulk) PS layer are added, performing a second annealing step of the PS/PS-Py/PS interfaces in order to obtain a consolidated material, while still limiting interdiffusion of the probe layer, prior to the $T_g(z)$ measurement. I find that for a given location z from the interface, the measured $T_g(z)$ value varied with the length of time of the first annealing step (that of the PS/PSF interface) up to some saturation time scale, after which the measured $T_g(z)$ value was reproducible and invariant to further annealing of the PS/PSF interface.

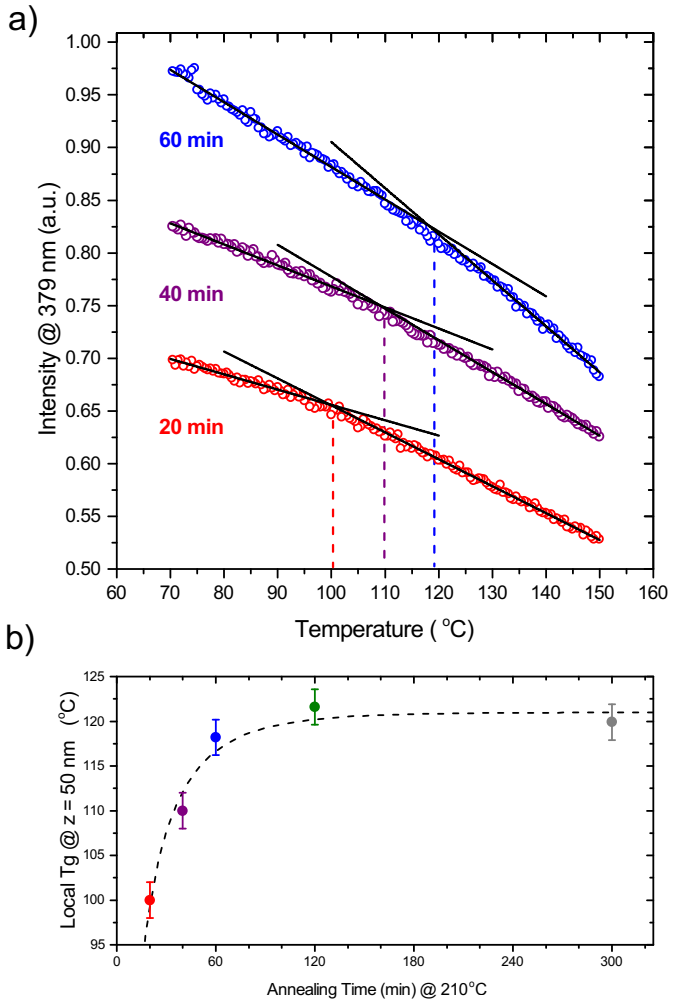

Figure 4.6: (a) Fluorescence intensity at an emission wavelength of 379 nm collected on cooling at 1 °C/min for PS-Py probe layers located at a fixed distance of z = 50 nm from the PS/PSF interface. Data for three different samples are shown where the PS/PSF interface was annealed for various lengths of time (20, 40, and 60 min) at a temperature of 210 °C (above the bulk T_g of both PS and PSF) prior to the $T_g(z)$ fluorescence measurements. With progressively longer annealing times leading to increasing local PS/PSF chain interdiffusion, the $T_g(z = 50$ nm) increases from 100 ± 2 °C, essentially the bulk T_g value of PS for only 20 min of annealing, to 110 ± 2 °C after 40 min and 118 ± 2 °C after 60 min of annealing. (b) Local $T_g(z = 50$ nm) as a function of annealing time of the PS/PSF interface at 210 °C demonstrating that the measured $T_g(z)$ value saturates and becomes invariant after ~60 min of annealing when the PS/PSF interface reaches equilibrium. Dashed curve is a best fit to the data with a stretched exponential decay (see text for details).

Figure 4.6 demonstrates the progression in $T_g(z)$ values at z = 50 nm for the PS/PSF system, where the annealing time of the PS/PSF interface (first annealing step) has been varied during assembly of the multilayered structures. For very limited annealing of the PS/PSF interface, only 20 min, the $T_g(z = 50 \text{ nm}) = 100 \pm 2\ ^{o}\text{C}$, equivalent to the bulk T_g value of PS, indicating that little to no dynamic coupling has occurred across the PS/PSF interface. In contrast, for 40 and 60 min of annealing the PS/PSF interface, the $T_g(z = 50$ nm) increases quickly to $110 \pm 2\ ^{o}\text{C}$ and $118 \pm 2\ ^{o}\text{C}$, respectively. After 60 min, further annealing the PS/PSF interface does little to change the $T_g(z = 50$ nm) value further, with the $T_g(z = 50$ nm) reaching a limiting value of $121 \pm 2\ ^{o}\text{C}$. It is important to note, that this annealing of the PS/PSF interface was done at 210 ^{o}C, above to the bulk T_g values of both polymers.

Figure 4.6b plots these local $T_g(z = 50$ nm) values as a function of annealing time of the PS/PSF interface at 210 ^{o}C. The data are reasonably well fit to a stretched exponential decay with an average relaxation time τ = 8 min and stretching exponent of β = 0.6. Such values are consistent with the idea that the local $T_g(z = 50$ nm) values are saturating because the PS/PSF interface is annealing further to equilibrium. Polymer-polymer interface annealing occurs initially via Rouse modes, easily leading to equilibrium interfacial widths of several nanometers.[88,112] If the polymers are immiscible such as is the case for the dissimilar polymer pairs in the present study, the equilibrium interfacial width saturates at a maximum value dictated by the unfavorable interaction parameter χ, while in contrast, if the polymers were miscible, further annealing would lead to interdiffusion via reptation. Given the broad spectrum of relaxation times exhibited by the Rouse modes of long chained polymers, it is not surprising that a stretched exponential decay, rather than a

single exponential, was necessary to fit the data in Fig. 4.6b. The $T_g(z)$ values in Fig. 4.6b saturate after approximately 60 min of annealing, a time comparable to that required to obtain equilibrium interfacial widths of 5-7 nm at temperatures of T_g + ~25 K in literature studies.[113-116] I note that I have previously addressed in Chapter 3 the possible suggestion that some small fraction of low MW chains could diffuse across the weakly immiscible dissimilar polymer-polymer interface and possibly plasticize the PS component. I previously demonstrated that the $T_g(z)$ profile, when annealed to equilibrium, is independent of MW and MW distribution of the neighboring polymer next to PS.[19]

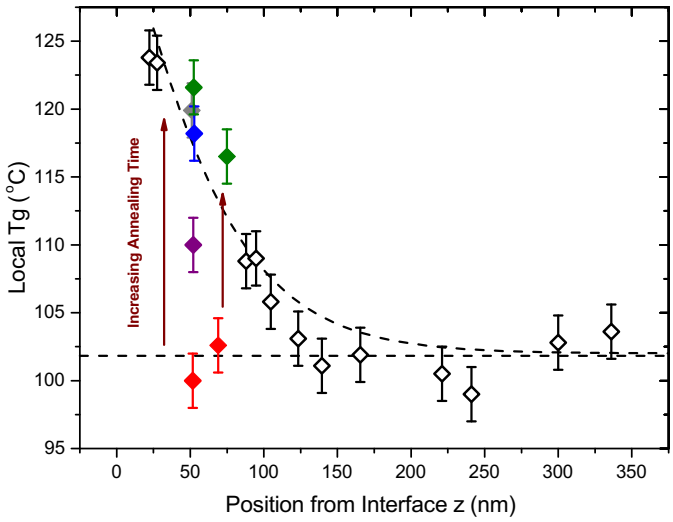

Figure 4.7: Local $T_g(z)$ profiles on the PS side of the PS/PSF system. Data from Figure 4.5, where the PS/PSF interface has been annealed for 90 min to equilibrium are shown as open diamonds. $T_g(z)$ data for z = 50 and 70 nm collected at the different PS/PSF interface annealing times shown in Figure 4.6 are plotted as colored symbols (same color coding as shown in Fig. 4.6): red diamonds indicate that annealing for only 20 min leads to $T_g(z)$ values still close to that of bulk PS with a nearly flat $T_g(z)$ profile, while 40 min of annealing (purple diamonds) shows an intermediate $T_g(z)$ profile compared with that measured for 60+ min of annealing.

Figure 4.7 illustrates how the $T_g(z)$ profile on the PS side of the PS/PSF interface would evolve as a function of annealing time for the PS/PSF interface. The open diamonds plot the data from Fig. 4.5 that was collected after annealing the PS/PSF interface for 90 min, ensuring that equilibrium was reached. $T_g(z)$ data for z = 50 and 70 nm are included in the figure for the different annealing times shown in Fig. 4.6. The data in Fig. 4.7 illustrate that the $T_g(z)$ profile would be nearly flat, remaining at essentially the bulk T_g of PS, at z-values quite close the PS/PSF interface for only 20 min of annealing. In contrast, 40 min of annealing leads to an intermediate $T_g(z)$ profile, compared with the 60+ min of annealing required to obtain an equilibrium PS/PSF interface. From this we can conclude that the amount of local interpenetration of the chains across the dissimilar polymer-polymer interface plays a significant role in creating dynamical coupling of cooperative segmental, T_g-dynamics between the two dissimilar polymers.

One of the major open questions that this work still does not reveal is why polymer-polymer interfaces appear to be so qualitatively different than polymer–free surface, polymer–substrate, and even polymer–liquid interfaces. As demonstrated above, annealing of the dissimilar polymer-polymer interface is necessary to cause the strong dynamical coupling observed. What factors during polymer-polymer interface formation are responsible? During annealing, the interfacial width broadens, the dissimilar polymer chains interpenetrate locally, and the interface roughens, any one of which could be facilitating the dynamical coupling across the interface. Future work is required to disentangle these possible contributing factors. One interesting point is that the breadth or nature of the dissimilar polymer-polymer interface is somehow requiring that the local cooperative segmental dynamics become continuous across the boundary, which may be

responsible for creating the large breadth of the $T_g(z)$ profile. For only limited (20 min) amounts of annealing, the data shows that the $T_g(z)$ profile appears very narrow and could possibly be discontinuous at the dissimilar polymer-polymer interface. This would be more like polymer–free surface, polymer–substrate, and polymer–liquid interfaces (all ~0.5 nm) where the molecular dynamics from one phase to another are locally discontinuous.

4.5 CONCLUSIONS

I have used a localized fluorescence probe to measure local glass transition temperature $T_g(z)$ profiles in PS domains near interfaces with different polymers. This work builds on measurements outlined in Chapter 3 where the full dynamical $T_g(z)$ profile across a PS/PnBMA polymer-polymer interface was mapped, finding that the dynamical profile does not correlate with the local composition profile $\phi(z)$. Unexpectedly, the dynamical $T_g(z)$ profile spanned 350-400 nm in extent and was asymmetric with respect to the 7 nm wide composition profile. Here I demonstrate this broad, asymmetric $T_g(z)$ behavior appears to be universal across a number of different systems. Figure 4.5 shows that the distance from the interface over which the $T_g(z)$ profile decays in PS varies depending on if the neighboring domain has a higher T_g (hard confinement) or lower T_g (soft confinement). In addition, I find that the $T_g(z)$ profile in PS (T_g^{bulk} = 101 ^oC) next to PSF (T_g^{bulk} = 186 ^oC) behaves similar to the $T_g(z)$ profile in PnBMA (T_g^{bulk} = 21 ^oC) next to PS. This suggests that the propagation of this dynamical $T_g(z)$ perturbation does not depend on some material property such as chemical structure, but rather on whether the polymer has a higher or lower T_g than its neighbor.

I characterized the penetration depth by the distance $\xi_{½}$ from the interface at which

the $T_g(z)$ perturbation decays to half its value. Such a definition builds on previous work by Bulter and Harrowell[43] who related a similar length scale to the temperature dependence of dynamical heterogeneities in a glassy model system. More recent theoretical efforts have also tied dynamical perturbations near interfaces to glassy dynamics and its associated length scales.[37-42,44,45] This study finds that PS next to PSF and PMMA, so-called hard confinement of PS, shows $\xi_{½} = 55 \pm 5$ nm, compared with PS next to PnBMA and PiBMA, soft confinement of PS, shows $\xi_{½} = 115 \pm 5$ nm. To within experimental error, a difference in $\xi_{½}$ between the PSF and PMMA system, or the PnBMA and PiBMA system, is not observed suggesting that the magnitude of the difference in T_g^{bulk} between the two domains does not dictate the propagation depth in PS. These systems also have slight differences in equilibrium interfacial width, which does not seem to change the length scale of the behavior. However, I find that these large length scales associated with the $T_g(z)$ behavior are only observed when the dissimilar polymer-polymer interface is annealed to equilibrium. I demonstrate using PS/PSF that if the dissimilar PS/PSF interface is minimally annealed for only 20 min at 210 ^oC, compared with the 60+ min required to reach equilibrium, strong dynamical coupling is not observed between the two dissimilar polymer domains and the $T_g(z)$ profile appears nearly discontinuous at the interface. This important observation suggests that the strong dynamical coupling between dissimilar polymer domains, leading to the broad continuous $T_g(z)$ profiles, are caused by some change that occurs during annealing.

Comparing polymer-polymer interfaces to interfacial perturbations near polymer-free surface, polymer-substrate, and polymer-liquid interfaces, I suggest three possible factors that may be responsible for the long range effects. Polymer-polymer interfaces are

typically much wider (~5 nm) compared with the sharp (~0.5 nm) composition profiles associated with the other types of interfaces. Chain connectivity could be also playing a modifying role to dynamical perturbations near interfaces, as has been seen recently in a few studies.[117-119] Alternatively, interfacial roughness, which has been shown in computer simulations to have a modifying effect on local dynamics,[39,120,121] could also be a factor as polymer-polymer interfaces would be expected to experience increased interfacial roughness due to their reduced interfacial energy.[97] Future work will be needed to disentangle these possible factors. The results presented here provide experimental data of a model system for comparison to future theoretical efforts and have implications for how local properties should be considered in polymer blends.

4.6 REFERENCES

[1] C. Harrats, S. Thomas, and G. Groeninckx, *Micro- and Nanostructured Multiphase Polymer Blend Systems: Phase Morphology and Interfaces* (CRC Press, Taylor & Francis Group, Boca Raton, FL, 2006).

[2] L. Leibler, Prog Polym Sci **30**, 898 (2005).

[3] D.A. Bernards and T.A. Desai, Soft Matter **6**, 1621 (2010).

[4] F.S. Bates, M.A. Hillmyer, T.P. Lodge, C.M. Bates, K.T. Delaney, and G.H. Fredrickson, Science **336**, 434 (2012).

[5] T.H. Epps, E.W. Cochran, C.M. Hardy, T.S. Bailey, R.S. Waletzko, and F.S. Bates, Macromolecules **37**, 7085 (2004).

[6] F.S. Bates, MRS Bulletin **30**, 525 (2005).

[7] W.-F. Kuan, R. Roy, L. Rong, B.S. Hsiao, and T.H. Epps III, ACS Macro Lett. **1**, 519 (2012).

[8] Y. Tao, J. Kim, and J.M. Torkelson, Polymer **47**, 6773 (2006).

[9] M.F. Weber, C.A. Stover, L.R. Gilbert, T.J. Nevitt, and A.J. Ouderkirk, Science **287**, 2451 (2000).

[10] R.Y.F. Liu, Y. Jin, A. Hiltner, and E. Baer, Macromol Rapid Comm **24**, 943 (2003).

[11] R.Y.F. Liu, A.P. Ranade, H.P. Wang, T.E. Bernal-Lara, A. Hiltner, and E. Baer, Macromolecules **38**, 10721 (2005).

[12] K. Arabeche, L. Delbreilh, R. Adhikari, G.H. Michler, A. Hiltner, E. Baer, and J.-M. Saiter, Polymer **53**, 1355 (2012).

[13] R. Casalini, L. Zhu, E. Baer, and C.M. Roland, Polymer **88**, 133 (2016).

[14] E.A. Jackson, Y. Lee, and M.A. Hillmyer, Macromolecules **46**, 1484 (2013).

[15] V. Sethuraman, V. Pryamitsyn, and V. Ganesan, J Polym Sci, Part B: Polym Phys **54**, 859 (2016).

[16] R.A. Segalman, B. McCulloch, S. Kirmayer, and J.J. Urban, Macromolecules **42**, 9205 (2009).

[17] H. Sai, K.W. Tan, K. Hur, E. Asenath-Smith, R. Hovden, Y. Jiang, M. Riccio, D.A. Muller, V. Elser, L.A. Estroff, S.M. Gruner, and U. Wiesner, Science **341**, 530 (2013).

[18] L.H. Sperling, *Polymeric Multicomponent Materials: an Introduction* (John Wiley & Sons, 1997).

[19] R.R. Baglay and C.B. Roth, J Chem Phys **143**, 111101 (2015).

[20] D.F. Siqueira, D.W. Schubert, V. Erb, M. Stamm, and J.P. Amato, Colloid Polym Sci **273**, 1041 (1995).

[21] J.A. Forrest and K. Dalnoki-Veress, J Polym Sci, Part B: Polym Phys **39**, 2664 (2001).

[22] P.M. Rauscher, J.E. Pye, R.R. Baglay, and C.B. Roth, Macromolecules **46**, 9806 (2013).

[23] T.P. Lodge and T.C.B. McLeish, Macromolecules **33**, 5278 (2000).

[24] S.K. Kumar, S. Shenogin, and R.H. Colby, Macromolecules **40**, 5759 (2007).

[25] Y.Y. He, T.R. Lutz, and M.D. Ediger, J Chem Phys **119**, 9956 (2003).

[26] M.D. Ediger and J.A. Forrest, Macromolecules **47**, 471 (2014).

[27] J.L. Keddie, R.A.L. Jones, and R.A. Cory, Europhys Lett **27**, 59 (1994).

[28] J.L. Keddie, R.A.L. Jones, and R.A. Cory, Faraday Discuss **98**, 219 (1994).

[29] C.B. Roth and J.R. Dutcher, J Electroanal Chem **584**, 13 (2005).

[30] J.A. Forrest and K. Dalnoki-Veress, Adv Colloid Interfac **94**, 167 (2001).

[31] M. Alcoutlabi and G.B. McKenna, J Phys: Condens Matter **17**, R461 (2005).

[32] O.K.C. Tsui, in *Polymer Thin Films*, edited by O.K.C. Tsui and T.P. Russell (World Scientific, Singapore, 2008), pp. 267–294.

[33] J.E. Pye and C.B. Roth, Phys Rev Lett **107**, 235701 (2011).

[34] C.J. Ellison, M.K. Mundra, and J.M. Torkelson, Macromolecules **38**, 1767 (2005).

[35] C.B. Roth, K.L. McNerny, W.F. Jager, and J.M. Torkelson, Macromolecules **40**, 2568 (2007).

[36] J.E.G. Lipson and S.T. Milner, Eur Phys J B **72**, 133 (2009).

[37] N.B. Tito, J.E.G. Lipson, and S.T. Milner, Soft Matter **9**, 9403 (2013).

[38] P.Z. Hanakata, J.F. Douglas, and F.W. Starr, Nat Commun **5**, 4163 (2014).

[39] P.Z. Hanakata, B.A. Pazmiño Betancourt, J.F. Douglas, and F.W. Starr, J Chem Phys **142**, 234907 (2015).

[40] A. Shavit and R.A. Riggleman, J Phys Chem B **118**, 9096 (2014).

[41] R.J. Lang and D.S. Simmons, Macromolecules **46**, 9818 (2013).

[42] J.D. Stevenson and P.G. Wolynes, J Chem Phys **129**, 234514 (2008).

[43] S. Butler and P. Harrowell, J Chem Phys **95**, 4466 (1991).

[44] S. Mirigian and K.S. Schweizer, J Chem Phys **141**, 161103 (2014).

[45] S. Mirigian and K.S. Schweizer, J Chem Phys **143**, 244705 (2015).

[46] C.B. Roth and J.R. Dutcher, Eur Phys J E **12**, S103 (2003).

[47] R.D. Priestley, M.K. Mundra, N.J. Barnett, L.J. Broadbelt, and J.M. Torkelson, Aust J Chem **60**, 765 (2007).

[48] K. Geng and O.K.C. Tsui, Macromolecules **49**, 2671 (2016).

[49] R.S. Tate, D.S. Fryer, S. Pasqualini, M.F. Montague, J.J. de Pablo, and P.F. Nealey, J Chem Phys **115**, 9982 (2001).

[50] C.J. Ellison and J.M. Torkelson, Nature Materials **2**, 695 (2003).

[51] P. Rittigstein, R.D. Priestley, L.J. Broadbelt, and J.M. Torkelson, Nature Materials **6**, 278 (2007).

[52] R.D. Priestley, C.J. Ellison, L.J. Broadbelt, and J.M. Torkelson, Science **309**, 456 (2005).

[53] J.E. Pye, K.A. Rohald, E.A. Baker, and C.B. Roth, Macromolecules **43**, 8296 (2010).

[54] Z. Yang, Y. Fujii, F.K. Lee, C.-H. Lam, and O.K.C. Tsui, Science **328**, 1676 (2010).

[55] K. Paeng, S.F. Swallen, and M.D. Ediger, J Am Chem Soc **133**, 8444 (2011).

[56] K. Paeng and M.D. Ediger, Macromolecules **44**, 7034 (2011).

[57] K. Paeng, R. Richert, and M.D. Ediger, Soft Matter **8**, 819 (2012).

[58] Z. Fakhraai and J.A. Forrest, Science **319**, 600 (2008).

[59] C.R. Daley, Z. Fakhraai, M.D. Ediger, and J.A. Forrest, Soft Matter **8**, 2206 (2012).

[60] Y. Chai, T. Salez, J.D. McGraw, M. Benzaquen, K. Dalnoki-Veress, E. Raphael, and J.A. Forrest, Science **343**, 994 (2014).

[61] C.B. Roth, J.E. Pye, and R.R. Baglay, in *Polymer Glasses*, edited by C.B. Roth (CRC Press, Taylor & Francis Group, 2016), pp. 181–204.

[62] J.A. Forrest and J. Mattsson, Phys Rev E **61**, R53 (2000).

[63] J. Mattsson, J.A. Forrest, and L. Borjesson, Phys Rev E **62**, 5187 (2000).

[64] C.G. Campbell and B.D. Vogt, Polymer **48**, 7169 (2007).

[65] C.M. Evans, H. Deng, W.F. Jager, and J.M. Torkelson, Macromolecules **46**, 6091 (2013).

[66] R.J. Lang, W.L. Merling, and D.S. Simmons, ACS Macro Lett. **3**, 758 (2014).

[67] J. Torres, P.F. Nealey, and J.J. de Pablo, Phys Rev Lett **85**, 3221 (2000).

[68] D.S. Fryer, R.D. Peters, E.J. Kim, J.E. Tomaszewski, J.J. de Pablo, P.F. Nealey, C.C. White, and W.L. Wu, Macromolecules **34**, 5627 (2001).

[69] O.K.C. Tsui, T.P. Russell, and C.J. Hawker, Macromolecules **34**, 5535 (2001).

[70] D. Christie, C. Zhang, J. Fu, B. Koel, and R.D. Priestley, J Polym Sci, Part B: Polym Phys **54**, 1776 (2016).

[71] C.M. Evans, S. Kim, C.B. Roth, R.D. Priestley, L.J. Broadbelt, and J.M. Torkelson, Polymer **80**, 180 (2015).

[72] R. Richert, Annu Rev Phys Chem **62**, 65 (2011).

[73] L.M. Wang, F. He, and R. Richert, Phys Rev Lett **92**, 095701 (2004).

[74] F. He, L.M. Wang, and R. Richert, Phys Rev B **71**, 144205 (2005).

[75] H. Bodiguel and C. Fretigny, Macromolecules **40**, 7291 (2007).

[76] J. Wang and G.B. McKenna, Macromolecules **46**, 2485 (2013).

[77] J. Wang and G.B. McKenna, J Polym Sci, Part B: Polym Phys **51**, 1343 (2013).

[78] H. Lu, W. Chen, and T.P. Russell, Macromolecules **42**, 9111 (2009).

[79] C.B. Roth and J.M. Torkelson, Macromolecules **40**, 3328 (2007).

[80] C.M. Evans, S. Narayanan, Z. Jiang, and J.M. Torkelson, Phys Rev Lett **109**, 038302 (2012).

[81] Y.P. Koh, G.B. McKenna, and S.L. Simon, J Polym Sci, Part B: Polym Phys **44**, 3518 (2006).

[82] H. Yoon and G.B. McKenna, Macromolecules **47**, 8808 (2014).

[83] M. Wubbenhorst, C.A. Murray, and J.R. Dutcher, Eur Phys J E **12**, S109 (2003).

[84] Y. Rharbi, Phys Rev E **77**, 031806 (2008).

[85] S. Butler and P. Harrowell, J Chem Phys **95**, 4454 (1991).

[86] H.-J. Butt, K. Graf, and M. Kappl, *Physics and Chemistry of Interfaces*, 3rd ed. (Wiley-VCH Verlag GmbH, Weinheim, Germany, 2013).

[87] A. Kriisa, S.S. Park, and C.B. Roth, J Polym Sci, Part B: Polym Phys **50**, 250 (2012).

[88] R.A.L. Jones and R.W. Richards, *Polymers at Surfaces and Interfaces* (Cambridge University Press, 1999).

[89] C.J. Ellison and J.M. Torkelson, J Polym Sci, Part B: Polym Phys **40**, 2745 (2002).

[90] B. Valeur, *Molecular Fluorescence: Principles and Applications* (Wiley-VCH, Weinheim, 2001).

[91] K. Kalyanasundaram and J.K. Thomas, J Am Chem Soc **99**, 2039 (1977).

[92] Y. Du, Y. Xue, and H.L. Frisch, in *Physical Properties of Polymers Handbook*, edited by J.E. Mark (AIP Press, New York, 1996), pp. 227–239.

[93] T. Matsuura, P. Blais, and S. Sourirajan, J Appl Polym Sci **20**, 1515 (1976).

[94] R.Y.F. Liu, T.E. Bernal-Lara, A. Hiltner, and E. Baer, Macromolecules **38**, 4819 (2005).

[95] G.H. Fredrickson and H.C. Andersen, Phys Rev Lett **53**, 1244 (1984).

[96] G.H. Fredrickson and H.C. Andersen, J Chem Phys **83**, 5822 (1985).

[97] A. Falsafi, S. Mangipudi, and M.J. Owen, in *Physical Properties of Polymers Handbook*, edited by J.E. Mark (Springer, New York, 2007).

[98] I caution the reader that fragility values are rarely known to better than 10%, but choose to quote here values from the literature as they were previously cited.

[99] C.M. Evans, R.W. Sandoval, and J.M. Torkelson, Macromolecules **44**, 6645 (2011).

[100] C.M. Evans and J.M. Torkelson, Macromolecules **45**, 8319 (2012).

[101] D. Huang and G.B. McKenna, J Chem Phys **114**, 5621 (2001).

[102] A.P. Sokolov, V.N. Novikov, and Y. Ding, J Phys: Condens Mater **19**, 205116 (2007).

[103] R. Böhmer, K.L. Ngai, C.A. Angell, and D.J. Plazek, J Chem Phys **99**, 4201 (1993).

[104] N.B. Tito, J.E.G. Lipson, and S.T. Milner, Soft Matter **9**, 3173 (2013).

[105] D.S. Simmons, Macromol Chem Phys **217**, 137 (2016).

[106] S. Mirigian and K.S. Schweizer, J Phys Chem Lett **4**, 3648 (2013).

[107] S. Mirigian and K.S. Schweizer, J Chem Phys **140**, 194506 (2014).

[108] S. Mirigian and K.S. Schweizer, J Chem Phys **140**, 194507 (2014).

[109] S. Mirigian and K.S. Schweizer, Macromolecules **48**, 1901 (2015).

[110] Y. Zhang, E.C. Glor, M. Li, T. Liu, K. Wahid, W. Zhang, R.A. Riggleman, and Z. Fakhraai, J

Chem Phys **145**, 114502 (2016).

[111] V. Lubchenko and P.G. Wolynes, Annu Rev Phys Chem **58**, 235 (2007).

[112] I.C. Sanchez, editor, *Physics of Polymer Surfaces and Interfaces* (Butterworth-Heinemann, Reed Publishing, 1992).

[113] A. Karim, A. Mansour, G.P. Felcher, and T.P. Russell, Phys Rev B **42**, 6846 (1990).

[114] S. Huttenbach, M. Stamm, G. Reiter, and M. Foster, Langmuir **7**, 2438 (1991).

[115] M. Stamm and D.W. Schubert, Annu Rev Mater Sci **25**, 325 (1995).

[116] D.W. Schubert, M. Stamm, and A.H.E. Muller, Polymer Engineering and Science **39**, 1501 (1999).

[117] E.C. Glor and Z. Fakhraai, J Chem Phys **141**, 194505 (2014).

[118] E. Glynos, B. Frieberg, H. Oh, M. Liu, D.W. Gidley, and P.F. Green, Phys Rev Lett **106**, 128301 (2011).

[119] L. Zhang, R. Elupula, S.M. Grayson, and J.M. Torkelson, Macromolecules **49**, 257 (2016).

[120] B.A. Pazmiño Betancourt, P.Z. Hanakata, F.W. Starr, and J.F. Douglas, Proc Natl Acad Sci USA **112**, 2966 (2015).

[121] P. Scheidler, W. Kob, and K. Binder, Europhys Lett **59**, 701 (2002).

Chapter 5

Experimental Study of the Influence of Periodic Boundary Conditions: Effects of Finite Size and Faster Cooling Rates on Dissimilar Polymer-Polymer Interfaces

A version of this chapter was published as Roman R. Baglay and Connie B. Roth, *ACS Macro Letters*, 6, 887-891, 2017.

5.1 SYNOPSIS

Building on work presented in Chapters 3 that mapped the local glass transition temperature $T_g(z)$ profile across a single polystyrene (PS) / poly(*n*-butyl methacrylate) (PnBMA) interface, here I explore the impact of limiting domain size and increasing cooling rate in PS/PnBMA multilayer geometries. This study is motivated by traditional computational approaches employed to overcome computer power limitations, where extrapolating short time scales and using periodic boundary conditions allows computer simulations to compare their findings to experimental measurements. However, a consequence of employing periodic boundary conditions is the occasionally unintentional inclusion (discussed in more detail below) of additional interfaces into the system that could potentially introduce further perturbation with length scales comparable to those

observed in Chapters 3 and 4. Along with inadvertent system artifacts discussed above that could be potentially present with periodic boundary conditions, the cooling rates in computer simulations are orders of magnitude faster than anything accessible in current experimental environments. Cooling rate effects have been shown in a limited amount of experimental studies to produce a profound effect on perturbative length scales associated with confinement of supported single layer PS films. Ellipsometry studies by Fakhraai and Forrest[1] were originally proposed to rectify the differences observed in T_g reductions of supported PS thin films reported by high frequency dielectric studies to that of the much slower cooling rates typically utilized in ellipsometry measurements. In this Chapter, I will show how the presences of an additional PS/PnBMA interface, effectively mimicking periodic boundary conditions similar to those used in computer simulations, affects local $T_g(z)$ gradients in PS and how a fixed PS domain sandwiched between two PnBMA domains is additionally affected by increasing cooling rate.

Using the fluorescence method developed in Chapters 2, 3 and 4, I find that the addition of a second PS/PnBMA interface perturbs the local PS $T_g(z)$ at a distance of z = 100 nm from the first PS/PnBMA interface when the second PS/PnBMA interface approaches a distance of approximately 300 nm. I previously showed that the local $T_g(z)$ from one PS/PnBMA interface is observed to perturbed the PS domain over 225-250 nm (see Chapters 3 and 4), and here I demonstrate that the additional perturbative effect attributed to the second PS/PnBMA interface is felt at a distance approximately 300 nm from the first. By then fixing the PS domain to 300 nm, I map out the $T_g(z,y)$ profile for a fixed glassy domain surrounded by two rubbery domains. I show that the interactions between the two PS/PnBMA interfaces seems to be decoupled only very close to each

respective PS/PnBMA interface. The observed local T_g reductions close to each of the two PS/PnBMA interfaces show very similar T_g reductions first observed in Chapter 3 with a semi-infinite bilayer PS/PnBMA system containing only one PS/PnBMA interface. The rest of the 300 nm PS domain sandwiched between two PnBMA domains (far away from the PS/PnBMA interfaces) is perturbed by a non-cumulative combination of two PS/PnBMA interfaces and never recovers PS bulk T_g, even at the center of PS. Additionally, I demonstrate that the local $T_g(z,y)$ profile across a finite PS domain size of 300 nm for a range of cooling rates shows that limiting domain size and increasing cooling rate (faster timescales) diminishes and truncates the profile, weakening the confinement effect for dissimilar polymer-polymer interfaces, consistent with previous studies on single-layer polymer films.

5.2 INTRODUCTION

Studies of glass transition perturbations due to dissimilar polymer-polymer interfaces have recently gained interest.[2-21] Experimentally, these polymer-polymer interfaces show dynamical perturbations persisting to larger distances from the interface compared to systems containing polymer free surface (polymer-air) interfaces.[10,11] Efforts to model such long-ranged effects to slow glass transition dynamics are hampered by typical limitations of computational power. Traditionally these limitations are bypassed by employing periodic boundary conditions[22] and extrapolating the temperature dependence of simulated short time scales down to lower temperatures.[2,23-25] Here I am interested in experimentally exploring what effects these traditional computational strategies have on the observed length scales of dissimilar polymer-polymer interfaces.

Previous studies on single layer polymer films have shown that limiting the system size can lead to a reduction in the gradient in dynamics near a free surface resulting in a more homogeneous profile,[26] and that the use of faster cooling rates[1] or focus on faster time scales[27] can truncate the magnitude and length scales of confinement effects.

Here I build on work presented in Chapter 3 where I employed a localized fluorescence method to map out the full profile in local glass transition temperature $T_g(z)$ across a polystyrene (PS) / poly(*n*-butyl methacrylate) (PnBMA) interface.[10] For this semi-infinite PS/PnBMA bilayer system, the dynamical perturbation is free to extend as far as needed into the material before recovering the bulk T_g value on either side of the interface (PS T_g^{bulk} = 101 °C, PnBMA T_g^{bulk} = 21 °C). Following the results obtained in Chapters 3 and 4, I found this perturbation distance from the interface to be dependent on whether the polymer forms the high T_g glassy component, with dynamical perturbations persisting for 225-250 nm before bulk T_g is recovered, or the low T_g rubbery component, with perturbations persisting for 100-125 nm.[11] I have shown that these broad and asymmetric $T_g(z)$ profiles are common across a number of dissimilar polymer-polymer interfaces and are observed to be much larger and uncorrelated with the 5-7 nm interfacial width in equilibrium composition profile.[10] Furthermore, I have also demonstrated that the extent of chain interpenetration across the dissimilar polymer-polymer interface, or the annealing of dissimilar polymer-polymer interfaces to equilibrium, is important to coupling the dynamics between the two polymers and creating the broad and asymmetric $T_g(z)$ profile observed across the dissimilar polymer-polymer interface.

In this Chapter, I explore the effect of adding a second PS/PnBMA interface, and creating a PS domain of finite size, to the local $T_g(z)$ across the PS component of the

multilayer systems reported in Chapter 3. Molecular dynamics (MD) simulations of a single dissimilar polymer-polymer interface that employ periodic boundary conditions wrap the system in all three dimensions, which extends the system size in two dimensions, but inherently introduces additional perturbative interfaces and limits the domain size in the other dimension.[2] Such simulations are good models of extruded alternating nanolayered systems[15-18] as intended, or perhaps lamellae forming block copolymers, but I believe here that they are distinctly different than my previous experiments on semi-infinite bilayers where the interfacial perturbations can propagate unrestricted into each component of the bilayer. Here I explore the difference between such systems, finding that the addition of a second PS/PnBMA interface already perturbs the local $T_g(z)$ value at z = 100 nm from the first PS/PnBMA interface when the total PS domain size is restricted to approximately 400 nm in size. I then further map out the local $T_g(z)$ profile for a finite PS domain size of 300 nm, observing that bulk T_g of PS is not recovered at any location within the PS domain including at the its center.

Not recovering bulk T_g in systems with multiple perturbative interfaces can be somewhat expected if the total size of the PS domain is not sufficiently large enough compared to the size of each T_g gradient and its respective perturbative length scale emanating from each of the two PS/PnBMA interfaces. If the perturbative length scales from the first and second PS/PnBMA interfaces begin to overlap, we can expect to not necessarily recover bulk T_g, even in the center of the PS domain. In this view, perturbative interfaces and their respective length scales may possibly be treated as simply cumulative, but the idea of how finite size influences the interaction and behavior of multiple perturbative interfaces is inherently neglected.

Over a decade ago it was shown that finite size can play an interesting role in confined polymer thin film systems. Ellison and Torkelson found that interfacial perturbations due to a free surface show non-monotonic T_g reductions upon reducing the total PS domain below 60 nm of a supported PS film with a 14 nm thick capping PS layer labeled with local T_g sensitive pyrene located at the polymer-air interface of the PS domain.[26] Here I will show that interfacial perturbations are not simply cumulative and that finite size of the domain is also important for systems with limiting domain sizes such as the ones present in current computer simulations. In addition, I increase the cooling rate and find that the $T_g(z)$ profile becomes muted and truncated with the most dramatic effect observed near the PS/PnBMA interface. Although I was experimentally limited to cooling rates between 1-15 K/min, I was already able to observe trends consistent with previous experiments[1,28] suggesting simulations focused on faster time scales would similarly observe weakened confinement effects with shorter length scales.

5.3 INTRODUCTION OF A SECOND PS/PnBMA INTERFACE

Following experimental methods developed in Chapters 3 and 4,[10,11] single layer films of neat PS (M_w = 1920 kg/mol, M_w/M_n = 1.26, Pressure Chemical), pyrene-labeled PS (M_w = 672 kg/mol, M_w/M_n = 1.3, free-radically polymerized with 1.4 mol% pyrene content[10]), and PnBMA (M_w = 1210 kg/mol, M_w/M_n = 1.7, free-radically polymerized[10]) were spin-coated from toluene solutions onto freshly-cleaved mica and independently annealed overnight under vacuum at 120 ^oC for PS or 80 ^oC for PnBMA layers. Multilayer stacks, as depicted in Figure 5.1, where then assembled by successively floating layers of

desired thickness (measured by ellipsometry Woollam M-2000) atop each other placing the 11-12 nm PS-Py labeled layer at a distance *z* from the bottom PS/PnBMA interface and a distance *y* from the second, top PS/PnBMA interface. The finite PS domain size is determined from the sum of the PS layers (*z* + PS-Py + *y*). As described previously in Chapters 3 and 4,[10,11] the multilayer stack is then carefully annealed at 120 ^{o}C for 20 min to ensure the PS/PnBMA dissimilar polymer-polymer interfaces are annealed to equilibrium, while consolidating the PS/PS-Py interfaces into a single material, but keeping the PS-Py labeled layer localized. Fluorescence intensity was then collected on cooling using a Photon Technology International QuantaMaster spectrofluorometer (excitation at 330 nm, emission intensity monitored at 379 nm, band-passes of 5-6 nm) with the samples mounted in a Peltier-cooled Instec TS62 temperature stage with dry nitrogen flowing at 2.7 L/min (In *ACS Macro Letters*, 6, 887-891, 2017 the flow is incorrectly written as 1.7 L/min) directly onto the sample cover slip to avoid condensation below room temperature. At the end of the run, all samples were reheated to the initial starting temperature to ensure the same fluorescence intensity was recovered. Intensity data was collected for 3 s every 27 s on cooling at 1 K/min or every 7 s cooling at 10 and 15 K/min. The local T_g of the PS-Py layer is manifested as the intersection of linear fits to the liquid and glassy regimes by maximizing the R^2 on each side of the transition. The largest uncertainty in the measured T_g values comes from sample-to-sample variability, which we find to be ± 2 ^{o}C from an average of multiple samples (typically smaller than the symbol size); the uncertainty in T_g from the fitting is much less.[11]

Figure 5.1 illustrates the different samples I am comparing in this study by plotting the fluorescence emission intensity measured on cooling at 1 K/min for a series of different

representative samples where the local $T_g(z,y)$ measured by the pyrene-labeled layer depends on its distance from the two PS/PnBMA interfaces (z is the distance from the bottom interface and y the distance from the top interface). The top two curves confirm the results from my previous work:[10] far from either interface the bulk T_g value of PS is recovered $T_g(z = 356$ nm, $y > 450$ nm$) = 100 \pm 2$ °C, and when one interface is approached, the local T_g becomes significantly reduced $T_g(z = 100$ nm, $y > 450$ nm$) = 65 \pm 2$ °C. The lower two curves address the question of when the presence of a second PS/PnBMA interface affects these results. From the data we can see that this occurs when the second interface is somewhere between 260-301 nm: $T_g(z = 100$ nm, $y = 301$ nm$) = 66 \pm 2$ °C is consistent with the data when the second y-interface is far away, while $T_g(z = 100$ nm, $y = 260$ nm$) = 63 \pm 2$ °C is now further reduced by the presence of this second y-interface. This distance of ~275 nm is approximately the distance at which bulk T_g of PS was recovered from the single PS/PnBMA interface in our previous study[10] (see inset of Fig. 5.2).

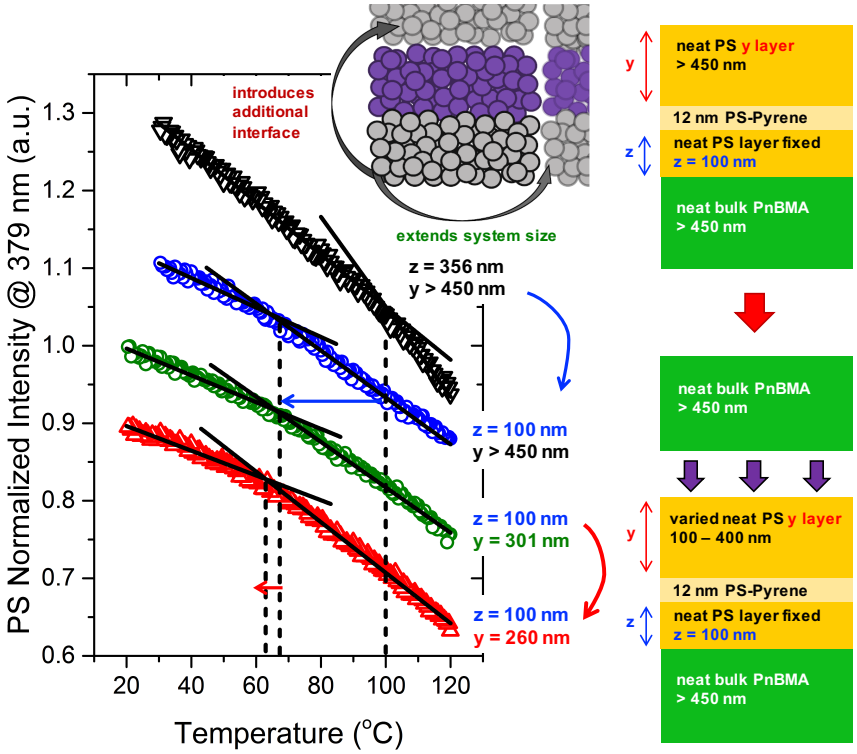

Figure 5.1: Temperature-dependent fluorescence intensity collected on cooling at 1 K/min for a semi-infinite bilayer with a PS-Py layer located at a distance z from the PS/PnBMA interface (black down triangles and blue circles) and a multilayer system with an additional PS/PnBMA interface where the PS-Py layer is now located a distance z from the first and distance y from the second PS/PnBMA interface (green circles and red triangles). For $T_g(z > 350$ nm, $y > 450$ nm) (black triangles), bulk PS T_g is recovered in the semi-infinite bilayer. Reducing the PS z layer to 100 nm, $T_g(z = 100$ nm, $y > 450$ nm) (blue circles), the PS T_g decreases by 35 K as expected from data in Chapter 3. Samples with an additional PS/PnBMA interface with a fixed PS $z = 100$ nm layer and large PS y layer, $T_g(z = 100$ nm, $y > 450$ nm), recover the 35 K T_g reduction observed originating from a single PS/PnBMA interface with comparable PS z layer separation thicknesses. Further reducing the y layer to 260 nm, $T_g(z = 100$ nm, $y = 260$ nm) (red triangles), I observe an 38 K PS T_g reduction relative to PS bulk T_g due to the presence of a second PS/PnBMA.

To more precisely identify when the presence of this second y interface begins to further perturb the local dynamics, we measured a series of different samples all at a fixed

distance z = 100 nm from the bottom PS/PnBMA interface with varying distance y from the top PS/PnBMA interface, as plotted in Figure 5.2. When the top y-interface is far away (y > 300 nm), the local $T_g(z = 100\text{ nm}, y > 300\text{ nm}) = 66 \pm 1.6\ ^oC$ (based on an average of 5 samples) are consistent with the range of local $T_g(z = 100\text{ nm}) = 64\text{-}69\ ^oC$ (represented by the shaded horizontal blue bar) measured in our previous study with only a single interface,[10] as depicted in the inset of Fig. 5.2. Note that this is significantly reduced from the bulk-T_g value of PS = $101 \pm 2\ ^oC$ indicated at the top of the figure. With decreasing y-distance from the second (top) interface, we observe a further decrease in local $T_g(z,y)$ due to the presence of the second interface when $y \leq 290 \pm 10$ nm, a quantitative estimate based on where a linear extrapolation of the data for y < 275 nm intersects with the shaded horizontal-blue bar. These data demonstrate that deviations to the local dynamics from finite domain sizes occur at quite large values relative to free surface length scales for these heterogeneous polymer-polymer systems.

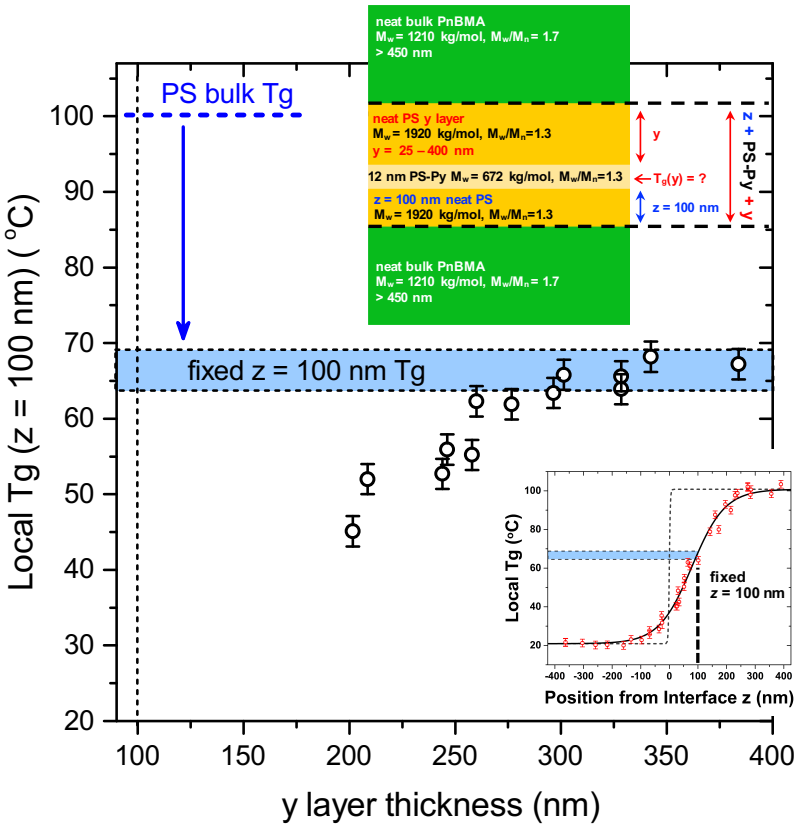

Figure 5.2: Local PS $T_g(z = 100, y)$ profile with a 12 nm T_g reporting PS-Py layer located a fixed distance z = 100 nm from the first and y from the second PS/PnBMA interface. Horizontal-blue bar indicates local PS $T_g(z = 100 \text{ nm})$ = 64-69 °C depression due to a single PS/PnBMA interface identified in ref.[10] (shown in inset). For PS y layer thicknesses above 300 nm $T_g(z = 100, y > 300 \text{ nm})$, the system recovers local T_g perturbations due to only one PS/PnBMA interface in accordance to the semi-infinite bilayer with PS z = 100 nm. Once the PS y layer is decreased below $y = 290 \pm 10$ nm, the second PS/PnBMA interface starts to further decrease PS local T_g, indicated a coupling between the two PS/PnBMA interfaces.

5.4 COOLING RATE EFFECTS ON FINITE SIZE DOMAINS OF PS BETWEEN TWO PnBMA LAYERS

In this final section, I now probe how the local $T_g(z,y)$ profile is altered by a PS domain of finite size sandwiched between two PnBMA layers. Based on the data shown in Fig. 5.2, I chose to focus on a total domain size $z + y = 300$ nm because such a domain size should be small enough to exhibit substantial perturbations to the local $T_g(z,y)$ profile relative to that for a single PS/PnBMA interface, while still remaining large enough such that the two PS/PnBMA interfaces, separated by 300 nm, should not feel each other at or very close to their respective PS/PnBMA interfaces. This means that the local T_g reductions at each of the PS/PnBMA interfaces should be effectively decoupled and match that of the T_g reduction near a single PS/PnBMA interface as discussed in the introduction of this Chapter.

Figure 5.3 plots the local $T_g(z,y)$ profile across a 300 nm PS domain as a function of distance z from the first PS/PnBMA interface. Data were measured for a series of different samples with z varying from 25-150 nm (solid symbols), while the y-layer was correspondingly varied to maintain a total domain size of $z + y = 300$ nm. By symmetry, the $T_g(z,y)$ profile was extended to z = 175-275 nm (open symbols) by mirroring the data about the midpoint of the domain. The open blue symbol at the PS/PnBMA interface was taken from my previous work in Chapter 3,[10] where the local $T_g(z = 0)$ was found to be 37 ^oC at the (single) PS/PnBMA interface of the semi-infinite PS/PnBMA bilayer. The curves through the data are simply a guide to the eye, but highlight how this local $T_g(z,y)$ profile within a finite domain size is flattened and truncated relative to that found for a single PS/PnBMA interface (inset of Fig. 5.2) where the semi-infinite PS domain allowed the

interfacial perturbation to propagate as far as necessary for the dynamics to recover bulk T_g.

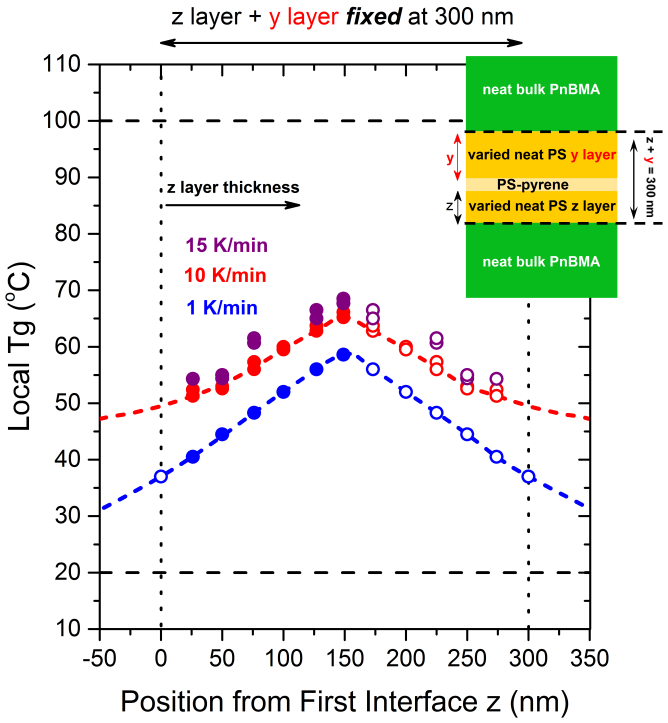

Figure 5.3: Local $T_g(z,y)$ profile with fixed 300 nm PS domain where both the PS z and y layers are varied to retain a total 300 nm PS thickness. The PnBMA/PS/PnBMA sandwich was measured upon cooling at 1 (blue circles), 10 (red circles), and 15 K/min (purple circles). Solid symbols indicate measured data with open symbols mirroring the data about the z or y 150 nm line of symmetry in the geometry. Open blue symbols at the PS/PnBMA interfaces are T_g data obtained from the semi-infinite bilayer PS/PnBMA profile with $T_g(z = 0) = 37$ °C (ref.[10]). T_g data near the PS/PnBMA interface match the trend of the 1 K/min data surprisingly well, supporting that within experimental error, a 300 nm separation between the PnBMA domains is sufficient to decouple the effect from both interfaces. Upon increasing cooling rate to 10 and 15 K/min, a reduction and truncation of the confinement effect is observed, supporting previously observed confinement effects with increasing cooling rates in supported PS thin films.

Figure 5.3 also explores the impact of increasing cooling rate on the measured $T_g(z,y)$ profile, where data collected at cooling rates of 10 and 15 K/min are included. Though I was experimentally limited to a small window of cooling rates, I find that the cooling-rate dependence shown in Fig. 5.3 is empirically equivalent to the film-thickness dependent $T_g(h)$ cooling-rate data reported previously for single layer supported PS films[1,28,29] probing the same underlying physics as fragility.[29] Fakhraai and Forrest originally demonstrated using ellipsometry that increasing the cooling rate from 1-130 K/min resulted in a diminished $T_g(h)$ reduction with a weakened confinement effect.[1] These studies find that the largest change in $T_g(h)$ occurs at smaller cooling rates.[28,29] For example, Glor and Fakhraai[28] see an approximate 10 K increase in $T_g(h)$ for a 10 nm thick film when increasing the cooling rate from 1 to 7 K/min. Similarly, I observe a roughly 10 K increase in local $T_g(z,y)$ near the PS/PnBMA interface when increasing the cooling rate from 1 to 10 K/min. Thus, consistent with these previous works, I also observe a diminished and weakened confinement effect with increased cooling rate in these heterogeneous polymer-polymer systems.

We now consider if the measured $T_g(z,y)$ profiles shown in Figure 5.3 is simply the cumulative $T_g(z) + T_g(y)$ perturbation originating from two PS/PnBMA interfaces. In Figure 5.4, I estimate what a $T_g(z,y) = T_g(z) + T_g(y)$ profile would look like for a 300 PS domain based on the $T_g(z)$ profile measured previously for a single PS/PnBMA interface. In Figure 5.4, I plot two PS/PnBMA local $T_g(z)$ profiles (black dashed curves), originally measured in Chapter 3 for a semi-infinite bilayer PS/PnBMA containing only one PS/PnBMA interface on cooling at 1 K/min, from each of the PS/PnBMA interfaces in Figure 5.3. The T_g reductions from each $T_g(z)$ profile are then simply added to generate

the green dashed curve of an estimated $T_g(z,y)$ profile across a fixed 300 nm PS domain. Now comparing the estimated results of the $T_g(z,y)$ profile to the $T_g(z,y)$ profile measured at 1 K/min (blue circles), it is clear that even though the estimated and measured profiles closely match near each PS/PnBMA interface, the $T_g(z,y)$ profiles bifurcate and show distinctly different T_g reductions deeper into the 300 nm PS domain. Figure 5.4 demonstrates that the measured $T_g(z,y)$ profile is not simply the additive perturbation from two independent interfaces, but suggests some further change to the dynamics occurs at finite domains sizes.

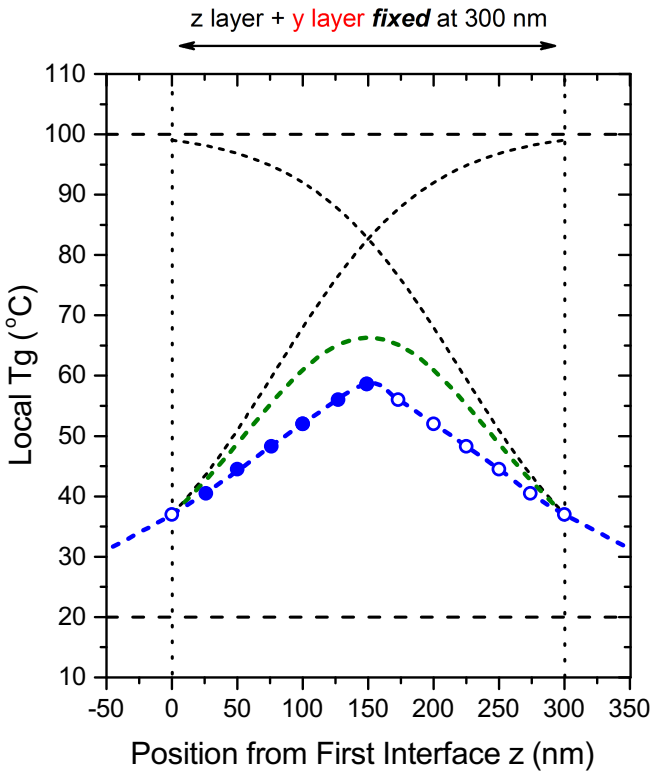

Figure 5.4: Estimated $T_g(z,y)$ profile (green dashed curve) in a fixed 300 nm PS domain from T_g reductions of two cumulative PS/PnBMA $T_g(z)$ profiles (black dashed curves) that were originally measured in a PS/PnBMA semi-infinite bilayer with only one PS/PnBMA interface (see Chapter 3), on cooling at 1 K/min. The estimated $T_g(z,y)$ profile closely matches the measured $T_g(z,y)$ profile collected at 1 K/min (blue circles) only near each PS/PnBMA interface, suggesting another mechanism is responsible for coupling T_g perturbations from multiple perturbative dissimilar polymer-polymer interfaces.

Interestingly I do not observe that PS bulk T_g is recovered in the measured $T_g(z,y)$ profiles found in Figure 5.3, even at the center of the PS 300 nm domain. Previous work comparing pyrene fluorescence to ellipsometry in single layer PS films[30] finds that pyrene fluorescence only identifies a single T_g value, biased towards the low end of the temperature range, even when the ellipsometry data demonstrates a broad transition in thermal expansion coefficient. This suggests there could be a wider distribution of

relaxation times present at a given (z,y) position, but pyrene fluorescence may only be sensitive to what corresponds to a faster subset of such a distribution. At present this pyrene fluorescence method is the only experimental technique able to provide such local, depth dependent information. Previous localized dielectric methods[31,32] have been limited to comparatively fast time scales (>1 Hz) at higher temperatures where such confinement effects would be expected to be weaker. Thus, new experimental techniques with depth dependent, long-time (sub-Hz) resolution are needed.

5.5 CONCLUSIONS

These results of adding a second interface and increasing the cooling rate suggest that if computational studies, necessarily at fast time scales, are going to study such effects with periodic boundary conditions that create finite domain sizes, one would expect to observe shortened length scales and weaker confinement effects. This study has only focused on limiting the PS domain size (similar to the work of Tito et al.[3]); I do not address what impact limiting the domain size of PnBMA would have that is relevant for nanolayered systems with alternating polymer layers[2,15-18] or block-copolymer self-assembled lamellae systems.[19-21] Regardless, the results presented here provide important information about the relevant length scales within materials with dissimilar polymer-polymer interfaces, for picking system sizes where the presence of additional interfaces could be inadvertently affecting the local dynamics. Although the present study does not address the underlying cause for the long length scales observed experimentally, it does provide some reasoning for why computer simulations would see smaller length scales. Experimental efforts are underway to address the underlying cause of the long length scales

in the systems.[11] We believe experiments such as the ones in this study of local properties near dissimilar polymer-polymer interfaces could eventually provide some predictive power to infer the macroscopic properties of heterogeneous polymer-polymer materials with different morphologies.

5.6 REFERENCES

[1] Z. Fakhraai and J.A. Forrest, Phys. Rev. Lett. **95**, 025701 (2005).

[2] R.J. Lang, W.L. Merling, and D.S. Simmons, ACS Macro Lett. **3**, 758 (2014).

[3] N.B. Tito, J.E.G. Lipson, and S.T. Milner, Soft Matter **9**, 9403 (2013).

[4] C.B. Roth, K.L. McNerny, W.F. Jager, and J.M. Torkelson, Macromolecules **40**, 2568 (2007).

[5] C.B. Roth and J.M. Torkelson, Macromolecules **40**, 3328 (2007).

[6] Y.P. Koh and S.L. Simon, J Polym Sci, Part B: Polym Phys **46**, 2741 (2008).

[7] Y. Rharbi, Phys. Rev. E **77**, 031806 (2008).

[8] C.G. Robertson, T.E. Hogan, M. Rackaitis, J.E. Puskas, and X. Wang, J Chem Phys **132**, 104904 (2010).

[9] P.M. Rauscher, J.E. Pye, R.R. Baglay, and C.B. Roth, Macromolecules **46**, 9806 (2013).

[10] R.R. Baglay and C.B. Roth, J Chem Phys **143**, 111101 (2015).

[11] R.R. Baglay and C.B. Roth, J Chem Phys **146**, 203307 (2017).

[12] H. Yoon and G.B. McKenna, Macromolecules **47**, 8808 (2014).

[13] C.M. Evans, S. Kim, C.B. Roth, R.D. Priestley, L.J. Broadbelt, and J.M. Torkelson, Polymer **80**, 180 (2015).

[14] C.M. Evans, S. Narayanan, Z. Jiang, and J.M. Torkelson, Phys. Rev. Lett. **109**, 038302 (2012).

[15] R.Y.F. Liu, Y. Jin, A. Hiltner, and E. Baer, Macromol. Rapid Commun. **24**, 943 (2003).

[16] R.Y.F. Liu, T.E. Bernal-Lara, A. Hiltner, and E. Baer, Macromolecules **38**, 4819 (2005).

[17] K. Arabeche, L. Delbreilh, R. Adhikari, G.H. Michler, A. Hiltner, E. Baer, and J.-M. Saiter, Polymer **53**, 1355 (2012).

[18] R. Casalini, L. Zhu, E. Baer, and C.M. Roland, Polymer **88**, 133 (2016).

[19] V. Sethuraman, V. Pryamitsyn, and V. Ganesan, J Polym Sci, Part B: Polym Phys **54**, 859 (2016).

[20] V. Sethuraman, V. Pryamitsyn, and V. Ganesan, Macromolecules **49**, 2821 (2016).

[21] V. Sethuraman and V. Ganesan, Soft Matter **12**, 7818 (2016).

[22] J. Baschnagel and F. Varnik, J Phys: Condens Matter **17**, R851 (2005).

[23] J.H. Mangalara, M.E. Mackura, M.D. Marvin, and D.S. Simmons, J Chem Phys **146**, 203316 (2017).

[24] P.Z. Hanakata, J.F. Douglas, and F.W. Starr, Nat Commun **5**, 4163 (2014).

[25] P.Z. Hanakata, B.A. Pazmiño Betancourt, J.F. Douglas, and F.W. Starr, J Chem Phys **142**, 234907 (2015).

[26] C.J. Ellison and J.M. Torkelson, Nat Mater **2**, 695 (2003).

[27] K. Fukao and Y. Miyamoto, Phys. Rev. E **64**, 011803 (2001).

[28] E.C. Glor and Z. Fakhraai, J Chem Phys **141**, 194505 (2014).

[29] T. Lan and J.M. Torkelson, Macromolecules **49**, 1331 (2016).

[30] S. Kim, S.A. Hewlett, C.B. Roth, and J.M. Torkelson, Eur. Phys. J. E **30**, 83 (2009).

[31] C. Rotella, S. Napolitano, L. De Cremer, G. Koeckelberghs, and M. Wübbenhorst, Macromolecules **43**, 8686 (2010).

[32] K. Fukao, H. Takaki, and T. Hayashi, in *Dynamics in Geometrical Confinement*, edited by F. Kremer (Springer International Publishing, Cham Heidelberg, 2014), pp. 179–212.

Chapter 6

Characterization of Polystyrene Chemically Labeled with a Photomechanical Azo Dye using Ellipsometry

6.1 SYNOPSIS

In Chapter 1, I introduced glass forming materials and some of their properties. Understanding universal behavior common across glassy systems including granular materials, colloidal suspensions, small molecules, and polymers is a highly sought after theoretical and experimental problem in soft condensed matter physics. I have also discussed that locally, cooperative motion in glassy systems reveals a rich dynamical heterogeneity on multiple length scales, which is still not understood. In the case of polymer glasses, it is relatively easy to shrink system sizes down to thin film geometries with commercialized processing techniques such as spin coating, where polymers can be spin coated to film thicknesses comparable to multiple cooperatively rearranging regions (CRRs), allowing these length scales to be probed above and below T_g with minimal processing of the material.

For the past two decades, the thin film confinement literature has pursued a link between glass transition phenomena on the local length scale of glass formers to some universal dynamics governing glassy behavior. One such dynamical material property is

modulus. In bulk polymers, modulus is molecular weight dependent, typically increasing by 3 orders of magnitude through the transition zone from a polymer melt to a glass in high molecular weight polymers. Though modulus is an important mechanical property of materials, changes to modulus upon confinement (high surface to volume ratio) are still not understood and little studied compared to the glass transition temperature.[1-11]

In this Chapter, I present some preliminary data towards developing a new experimental technique to study modulus of thin polymer films under confinement by chemically labeling polystyrene (PS) with a photomechanical dye that is able to photomechanically generate stress within a film. Here I will be using an azobenzene type molecule, or azo molecule, that undergoes a completely reversible photoisomerization from its *trans* to *cis* conformations when stimulated by an appropriate wavelength of light. Generally, excitation wavelengths depend on the azo subclass and are tunable from UV to infrared, yielding a highly adjustable dye for studying polymer thin films.[12] One of the most interesting features of azo molecules occurs after photoisomerization. When an azo is stimulated by light, the dye requires a substantial .12 – .38 nm^3 amount of "sweep volume," depending on if the dye transverses from the *trans* state into the *cis* state through inversion or rotational pathways.[13-15] This Chapter focuses on characterizing PS polymerized with a commercially available azo dye *N*-ethyl-*N*-(2-hydroxyethyl)-4-(4-nitrophenylazo) aniline, commonly referred to as Disperse Red 1 (DR1), using ellipsometry. I will show how the film thickness, or alternatively strain, of PS labeled with DR1 (PS-DR1) increases with the photoisomerization of DR1 excited by a 532 nm 50 mW laser and a 532 nm variable power 300 mW laser, specifically characterizing how the % strain is affected by PS-DR1 film thickness and temperature. With future work, this

photomechanically labeled polymer has the potential to be used as a localized internal strain generator, where a thin film of PS-DR1 could be inserted at variable positions within a bulk PS film from interfaces including polymer-air, polymer-polymer, and polymer-substrates in PS films.

6.2 INTRODUCTION

6.2.1 Modulus of Polymer Films in Confined Thin Film Geometries

An equally important material property of glass formers affected by perturbative interfaces and confined geometries is the material's dynamical response, or modulus. Modulus characterizes the material's response to external tensile, compression, shear, static or dynamical forces and typically depends on strain rates, stain amplitudes, and operating temperature. Unlike granular materials or colloidal suspensions, the modulus of polymers with molecular weights above the entanglement density possesses three distinct regimes. The glassy modulus or the low temperature/high frequency limit transitions into the rubbery plateau by increasing the temperature or decreasing the frequency through the dynamic T_g or transition zone of the modulus curve. As discussed in Chapter 1, the modulus decreases by three orders of magnitude when transitioning between the glassy GPa to the rubbery MPa response, where flow only occurs at much higher temperatures or lower frequencies depending on the molecular weight of the polymer.[16,17] Experimentally, modulus bulk properties of many materials have been extensively studied with values tabulated in handbooks,[18] but little is understood of how glass forming materials respond to forces on confined, local length scales.

In recent years, there have been a number of experiments that attempted to quantify how modulus is affected by confinement in supported and free-standing polymer films upon decreasing film thickness. What has been observed is that confinement effects are not only dependent on the perturbative interfaces, but that the distinct regimes of the modulus curve seem to show starkly different behavior. In particular, the research literature does not seem to agree if the glassy response (low temperature or high frequency) increases,[1-3] decreases,[4-7] or shows no change[8] upon decreasing film thickness. For example, picosecond acoustic experiments measured the longitudinal wave velocities in supported poly(methyl methacrylate) (PMMA) films and found that the longitudinal p-wave glassy modulus increases by almost an order of magnitude in 20 nm thick films,[1] while acoustic Brillouin Light Scattering (BLS) measurements seem to show no change in the glassy response for free standing PS films.[8] Though there is an ongoing debate in the research literature regarding directly comparing time of flight techniques such as the picosecond acoustic measurements to other acoustic techniques such as BLS.[8] In addition, other groups have expressed concern over the sensitivity of BLS measurements, which are difficult due to sample preparation, handling issues, and substrate interactions, leading to ever increasing experimental uncertainty in polymer thin film measurements.[5]

Direct mechanical contact load experiments and measurements of surface wrinkling mechanics also find contradictory glassy elastic modulus behavior. Nano-indentation techniques report that the glassy elastic modulus slightly increases upon confinement, but like BLS experiments, the sensitivity of the technique has been criticized in the literature.[2,3] It has been suggested that nano-indentation measurements might unintentionally introduce substrate perturbative effects upon contact of the atomic force

microscope (AFM) tip to the polymer film,[3] and that the precision of nano-indentation measurement depends on the precise contact area of the AFM tip, which can easily be deformed by the hard glassy polymer surface.[2] Contrary to other techniques, surface wrinkling measurements originally developed by the Stafford group[4,5,7] find that the glassy Young's modulus decreases upon decreasing film thickness and find that modulus correlates well with T_g for supported PS films,[5] but does not seem to show similar correlations between the glassy Young's modulus and confined T_g in poly(n-propyl methacrylate) (PnPMA) films.[6] The analysis of surface wrinkling follows the treatment of surface instabilities under applied axial compression loads, which requires a material with two moduli, or a polymer film on a substrate.[7] For a film on a more compliant substrate, the wavelength of the surface wrinkles depends on both the thickness and moduli of both the film and substrate by the following relation,[7]

$$\lambda = 2\pi \left(\frac{\bar{E}_f}{3\bar{E}_s}\right)^{1/3},$$

where λ is the ripple wavelength, and $\bar{E}_f$ and $\bar{E}_s$ are the Young's moduli of the film and substrate, respectively. The surface wrinkling measurements were all done with glassy polymer films atop thick rubbery crosslinked polydimethylsiloxane (PDMS) substrates, which inherently introduces a dissimilar polymer-polymer interface in the system. Though I have not measured the effects of a crosslinked rubbery component in glassy-rubbery semi-infinite bilayers, current efforts in the Roth lab include varying the crosslink density and thereby the modulus of PDMS in PS/PDMS bilayers.

Though thin film confinement effects in the glassy response regime are inconclusive and even contradictory, modulus measurements in the rubbery plateau show an even more unusual behavior in free-standing films. The McKenna group introduced a

thin film bubble creep compliance measurement technique, where confined poly(vinyl acetate) (PVAc), PS, and polycarbonate (PC) films were placed onto substrates with a regular array of pores.[9-11] The substrate and films were then positioned inside a temperature controlled pressure cell. Static stresses were induced by applying pressurized air to one side of the porous substrate while simultaneously measuring the creep compliance of the resulting nano-bubbles in the polymer film with an AFM. The work surprisingly finds rubbery stiffening upon confinement, and suggests that the glassy modulus of PS might be increasing relative to bulk PS glassy modulus for PS films thinner than 17.1 nm.[10] In typical nano-bubble inflation measurements of films in the glassy state, the high stiffness of the glassy film combined with a relatively thick film requires inflation pressures high enough to detach the film from the substrate in order for the inflated nano-bubble to stay in the membrane creep compliance regime.[10] Therefore, the nano-bubble inflation technique is generally limited to temperatures above polymer T_g or temperatures slightly below T_g for very thin films, making bulk glassy and even bulk rubbery modulus measurements experimentally difficult.

Measurements of a modulus curve with both the glassy and rubbery modulus obtained from one experimental technique that includes the transition zone are experimentally very challenging, especially for confined thin film. The closest such work is by Karim and McKenna that determined the surface compliance at the polymer-air interface of supported 15 – 110 micron thick poly(α-methylstyrene) (PαMS), linear PS, 3-arm star PS, and 8-arm star PS films by spontaneous particle embedding experiments.[19,20] Karim and McKenna observed that the PαMS surface softens (lower modulus) from room temperature to bulk PαMS T_g – 21 K and then begins to stiffen (higher modulus) at

temperatures bulk PαMS T_g – 18 K to bulk PαMS T_g + 21 K relative to the mechanical macroscopic compliance of PαMS.[19] In effect, the surface compliance transition zone of PαMS films shows a shift toward the glassy side of the modulus curve. In the case of linear PS and 3-arm star PS films, the transition zone shift shows opposing behavior relative PαMS.[20] PS surface compliance was observed to soften for temperatures up to bulk PS T_g + 6 K and then stiffens at higher temperatures.[20] 3-arm PS stars also showed surface softening at temperatures up to bulk 3-arm star PS T_g + 2 K and then surface stiffening for temperatures above bulk 3-arm star PS T_g + 4 K.[20] Interestingly, the surface compliance of 8-arm PS stars was observed to soften both below and above bulk 8-arm star PS T_g relative to mechanical macroscopic compliance of 8-arm PS stars.[20]

Though the temperature range in the spontaneous particle embedding experiments by Karim and McKenna includes the transition zone, it is not clear how the transition zone of the surface compliance shifts relative to the T_g difference between bulk T_g of the films and the T_g at the surface of the polymer-air interface. In Chapter 1, I showed that supported linear PS films exhibit strong average T_g reductions with decreasing PS film thickness. The average T_g of supported PαMS films shows a similar average T_g reduction with decreasing PαMS film thickness,[21] but in contrast to PS, PαMS lacks a high mobility liquid like layer at the polymer-air interface.[22] The average T_g of supported star PS films is more complicated because the average T_g depends on both the number of arms of the polymer and the molecular weight of the arms. For example, the average T_g of 8-arm star PS films with 42 kg/mol arms was observed to behave similarly to the average T_g reductions found in linear PS films, but when the molecular weight of the arms was reduced to 25 kg/mol, the magnitude of the average T_g reductions decreased.[23] Further decreasing the arm

molecular weight of the 8-arm PS stars to 10 kg/mol showed a strongly increasing average T_g upon decreasing film thickness.[23] This suggests that the surface T_g of 8-arm star PS films with 9.8 kg/mol arms in the Karim and McKenna spontaneous nanoparticle embedding experiments is most likely higher than bulk 8-arm star PS T_g, while that surface T_g of the linear PS and 3-arm star PS is likely reduced compared to bulk T_g. So far there is no conclusive correlation between the measured surface compliance and the T_g at the polymer-air interface.

A sketch of the full modulus curve summarizing the possible literature effects of confining polymer films in the different response regimes is shown in Figure 6.1. Though, the contradictory findings in the film average glassy response may possibly be explained if the transition zone, or the dynamic T_g, shifts analogous to the confined average film T_g, however there have been experiments demonstrating that elastic Young's modulus does not exactly track T_g for some polymers.[6] If the transition zone were to shift in temperature or frequency upon confinement, or maybe even broaden relative to bulk modulus, then those shifts may appear as an increase or decrease of the glassy modulus at certain temperatures or frequencies.

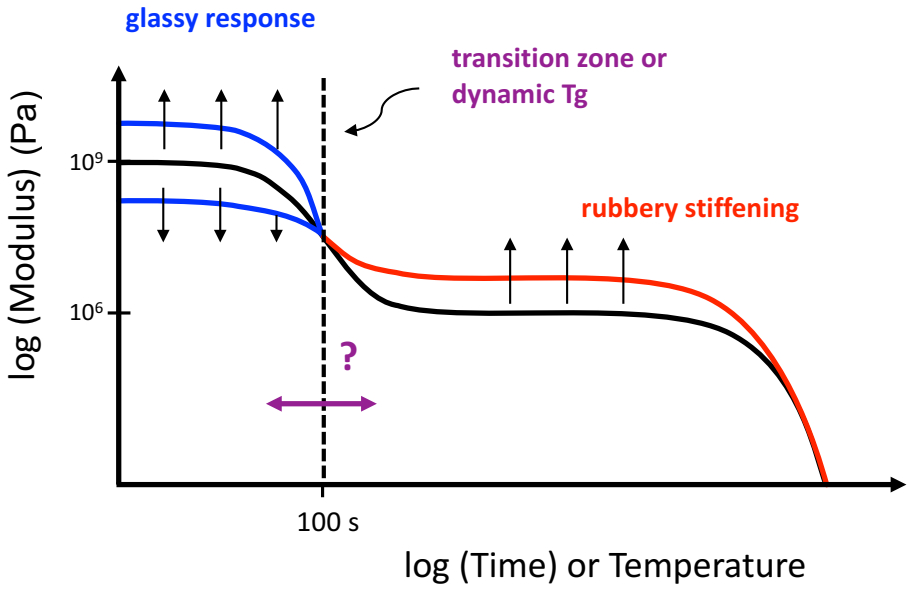

Figure 6.1: Schematic of modulus as a function of time or temperature summarizing shifts due to confinement effects reported in the literature for high molecular weight (above entanglement) supported and free-standing polymer films. The low temperature or high frequency glassy modulus regime (blue lines) has been contentiously observed to increase,[1] decrease,[4,6,7] or remain unaltered[8] relative to bulk modulus (black line) in confined polymer films. Surprisingly, the high temperature or low frequency rubbery modulus (red line) shows rubbery stiffening upon confinement of free standing polymer films in bubble inflation creep experiments.[9,10] However, how confinement affects the transition zone of the modulus curve is not yet understood.

6.2.2 Introduction to Photomechanical Azos and DR1

For the scope of this dissertation, here I provide a brief introduction to azobenzene type molecules and their photomechanical properties. In general, azos are a broad range of molecular compounds, classified by a double bonded nitrogen bridge between two functional groups. The most profound characteristic of aromatic azo type molecules is their ability to undergo photoisomerization when stimulated by light, shown in Figure 6.2. The change from *trans* to *cis* conformational states is energetically unfavorable and

statistically improbable without an external source kicking the system over the activation barrier.[12] Azobenzene molecules are able to cross back from the *cis* to *trans* state via a similar photomechanical process, either by heating or illuminating the sample with a different wavelength of light.[12] Though photoisomerization is possible on picosecond time scales for a single azo molecule,[24,25] statistically the time scales that induce photomechanical motion of the matrix material require a significant population of azo molecules to convert from *trans* to *cis* conformations, with ample amounts of *cis* conformational states populating the system only after hundreds of milliseconds post photoisomerization.[26]

Cis to *trans* non-stimulated relaxation rates (without the presence of a second light source or thermally activated recovery above ambient temperatures) are highly tunable and depend on the type of azobenzene. Non-stimulated decay rates for unsubstituted azobenzene, aminoazobenzene type, and pseudostilbene type molecules in solution phase are on the order of hours, minutes, and seconds respectively.[12] The wavelength of light for maximal photoisomerization is tunable by picking the correct azobenzene type, which will become important for modulus measurements. Notably, the photoisomerization process in azobenzene type molecules is free from all side reactions,[12] making azobenzene an excellent chemically stable probe or tracer for polymeric systems.

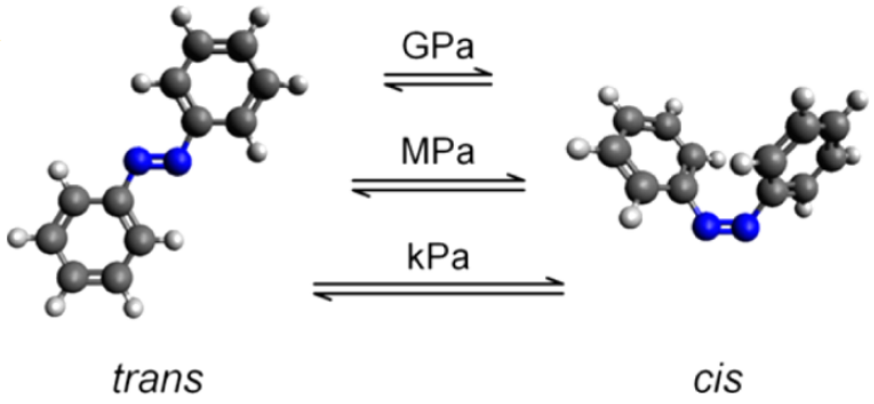

Figure 6.2: Example of an azobenzene molecule undergoing photoisomerization from *trans* to *cis* conformational states by photoisomerization. Azobenzene DR1 dye doped in and labeled to glassy PMMA (glassy modulus of the PMMA matrix is several GPa) is shown to still undergo photoisomerization under GPa of external pressures in a diamond anvil spectroscopic cell. (Figure reproduced from ref.[26] with permission from American Chemical Society Publications.)

Photomechanically, the photoreaction from *trans* to *cis* conformational states induces a .12 – .38 nm^3 free volume change, with forces reaching up to several nano Newtons.[12,13,15] Those forces acting on such small volumes induce exceptionally high internal pressures in the system on the order of GPa. Singleton *et al.*[26] demonstrated that the photoisomerization of DR1 is even possible under extreme external pressures of up to 1.5 GPa inside a diamond anvil spectroscopic cell. DR1 chemically labeled to glassy poly(methyl methacrylate) (PMMA) (glassy modulus of PMMA is several GPa) was still able to achieve about 20 % *cis* content within the PMMA matrix.

Because the free volume change associated with photoisomerization induces such large internal pressures even within a glassy polymer matrix, azo molecules have been coined as “molecular muscles” in the photomechanics literature. For example, Eisenbach crosslinked poly(ethyl acetate) (PEA) films with 2 mol % of 4,4'-

di(methacryloylaminoazobenzene) (DMAAB).[27] The crosslinked PEA film was then elongated above T_g, which microscopically stretched portions of the entangled PEA film and formed aligned pseudo nematic networks. After exposing the film to a 365 nm source, the PEA film contracted, achieving strain cycles of about .25 %. This study most importantly showed that the photoisomerization of an azobenzene crosslinker on the nano scale can generate enough force microscopically to induce macroscopic motion in liquid crystal elastomers or liquid crystal networks (LCNs).

Recent studies of LCN photo actuators crosslinked with azos show strong strain-power dependence on the amplitude of the oscillations upon increasing the excitation power from 1 W/cm^2 to 1.6 W/cm^2, resulting in an approximately 80 % increase to the strain cycle. Surprisingly, the power of the source shows no effect on the oscillation frequency of the actuator,[28] suggesting that photoisomerization time scales are independent of power. Additionally, recent experiments induced vortex-type deformations on the surface of acrylic polymer films absent of any crosslinker or nematic networks, but had polymer that contained azobenzene type side groups. The vortices revealed the formation of basins up to 200 nm in depth,[29,30] showing that just the presence of azobenzene in the side group of the polymer is enough to generate substantial strain. Most notably, the Ikeda group was able to achieve completely reversible, macroscopically visible strain cycles in LCNs crosslinked with azobenzene and in polymer liquid crystals containing azobenzene side groups. The group later showed that photo induced mechanical motion[31-33] and photomechanical information and energy storage is possible with azo molecules.[34,35]

6.3 CHARACTERIZATION OF PS LABELED WITH DR1

6.3.1 Polymerization and Characterization of PS labeled with DR1 and PS-DR1 Thin Film Sample Preparation

PS labeled with .45 mol % DR1 (PS-DR1) was synthesized via free radical polymerization with azobisisobutyronitrile (AIBN) as initiator as follows. 0.297 grams of *N*-ethyl-*N*-(2-hydroxyethyl)-4-(4-nitrophenylazo) aniline methacrylate (DR1-MMA) monomer purchased from Polymer Source was copolymerized at 50 ^{o}C with 12.5 mL of deinhibited styrene and 0.0021 grams of AIBN for 24 h under a nitrogen environment. The initial test trial ratios of AIBN to DR1-MMA monomer and styrene were taken from polymerization of PS-pyrene used in Chapters 2, 3 and 4. The resulting polymerization conditions did not produce visual particulates of polymer when the solution was precipitated in a methanol bath. As a result, the initiator content, temperature and polymerization time were raised to increase yield of material. 0.304 grams of DR1-MMA monomer was then copolymerized at 60 ^{o}C with 12.5 mL of deinhibited styrene and 0.0669 grams of AIBN for 42 h under a nitrogen environment. A secondary batch of PS-DR1 was polymerized with the same ratios of AIBN initiator and DR1 monomer to styrene content at 60 ^{o}C for 2 weeks under nitrogen to further increase yield of PS-DR1 polymer.

The resulting PS-DR1 polymer that was polymerized for 42 h was dissolved in tetrahydrofuran (THF) and subsequently re-precipitated in methanol to remove any unreacted monomer and chromophores. Great care was taken when re-precipitating PS-DR1 due to its low molecular weight compared to PS-pyrene and PnBMA-pyrene polymer synthesized in Chapters 2 and 3. THF volumes of 10 mL or less were used to dissolve the polymerized PS-DR1, with methanol volumes exceeding 1 liter in each re-precipitation

step. The solution of PS-DR1 in THF was poured very slowly into the methanol to not break up the polymer and cloud the methanol with small precipitates of PS-DR1, which would become stuck between the fibers of the filter paper used to remove the polymer from the methanol and thereby reduce the material yield. If the methanol bath clouded with PS-DR1 precipitates, the methanol PS-DR1 solution was left uncovered in the fume hood until the methanol completely evaporated from the beaker. The remaining PS-DR1 polymer was carefully removed from the walls of the beaker and dissolved again in small volumes (10 mL or less) of THF before repeating the re-precipitation step. After the washing procedure was completed 7 times, PS-DR1 was annealed overnight under vacuum at room temperature to remove any residual THF and methanol present in the polymer. PS-DR1 polymer polymerized for 2 weeks was washed once because the yield did not seem to dramatically increase after increasing the polymerization time. Because the washing procedure is laborious, the author has left the 2-week polymerized PS-DR1 for the next students who embarks on tackling this project. This dissertation uses the washed PS-DR1 that was polymerized for 42 h.

The .45 mol % label content of DR1 in PS-DR1 was determined from the extinction coefficient, ϵ_{475}, of DR1-MMA monomer measured at 475 nm (99,545 M^{-1} cm^{-1}). The extinction coefficient was characterized by measuring absorbance of trace amounts of pure DR1-MMA monomer (in accordance with Beer's Law) in spectroscopic grade THF using ultraviolet-visible spectroscopy, where the slope of Figure 6.2a is the extinction coefficient at 475 nm. Figure 6.3b plots the absorption spectra of DR1-MMA monomer (black circles) and PS labeled with DR1 (red upside-down triangles) in spectroscopic grade THF normalized by the 475 nm peak of DR1-MMA. The absorption spectrum of PD-DR1 is

slightly blue shifted relative to neat DR1 at wavelengths below 425 nm but remains unaltered at higher wavelengths. By comparing the absorption spectra of pure DR1-MMA monomer to PS-DR1 polymer, we can see that the polymerization of DR1 with styrene does not significantly alter the absorption of the DR1 chromophore when attached to a PS backbone. The absorption spectra indicate that there is no preferential positioning of DR1 along the PS backbone that would result in the aggregation of the DR1 chromophore. Additionally, absorption spectra show that the photoisomerization absorption spectrum of pure DR1-MMA does not change with polymerization of DR1 with styrene.

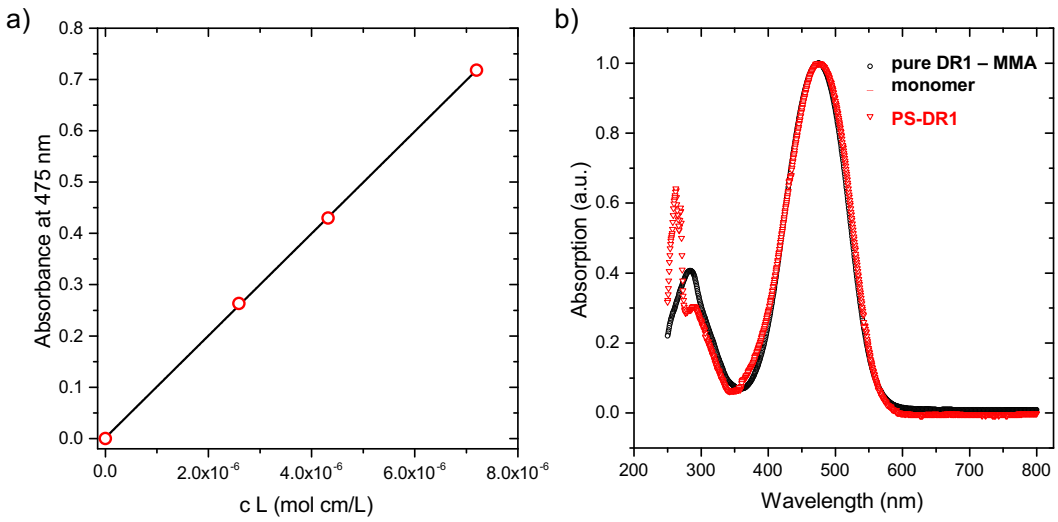

Figure 6.3: (a) Absorbance of trace amounts of pure DR1-MMA monomer measured at 475 nm by ultraviolet-visible spectroscopy in spectroscopic grade THF. The extinction coefficient of pure DR1-MMA used to determine the .45 mol % label content of DR1 in PS-DR1 polymer is given by the slope of the line (99,545 M^{-1} cm^{-1}). (b) Normalized pure DR1-MMA monomer and PS labeled with DR1 (PS-DR1) absorption spectra in spectroscopic grade THF. Polymerization of DR1-MMA monomer with styrene does not significantly alter the absorption spectrum of DR1 dye, indicating that the DR1 chromophore is not aggregating on the PS backbone nor changing the photoisomerization absorption wavelength.

Samples containing trace amounts of washed PS-DR1 dissolved in filtered spectroscopic grade toluene were inserted into a room temperature (25 ^{o}C) toluene bath of an ALV-CGS3 compact dynamic light scattering (DLS) system to measure the weight average molecular weight (M_w) of PS-DR1. Any dust still present in the toluene bath was left to settle over the course of a week prior to making any measurements. DLS measures the dynamic (Brownian motion) changes to the light intensity of scattered light or the diffusion coefficient, where the scattering volume is less than the wavelength of the beam in dilute solutions of effective point scatterers. The hydrodynamic radius, R_h, is then determined from the Stokes-Einstein equation given by equation 6.1,

$$R_h = \frac{k_B T}{6\eta D_t} \tag{6.1}$$

that depends on the temperature, *T*, and viscosity, η, of the solvent. The ALV-CGS3 DLS system determines the appropriate viscosity in equation 6.1 after the solvent (toluene) and temperature is provided as input into the system. DLS first measures the tracer diffusion coefficient, D_t, from which the internal software calculates R_h. The linear scaling factor, *X*, between R_h and the radius of gyration, R_g, of the polymer (and therefore the M_w) is determined by equation 6.2 from ref.[36],

$$R_h = X\, R_g \tag{6.2}$$

where the solvent dependent conversion *X* values can be calculated from R_h and M_w or looked up in tables.[36,37] R_g of PS in room temperature toluene solutions scales with M_w by $R_g/\mathrm{nm} = 0.01234 \times \left(M_w/\frac{\mathrm{g}}{\mathrm{mol}}\right)^{.5936}$, where this relation between R_g and M_w comes from curve fitting data from light scattering experiments.[37,38] Using this experimentally determined relation between R_g and M_w, I calculated that $R_g = 10.21$ nm

of 84,000 g/mol PS in toluene from ref.[37] that has a measured R_h = 7.16 nm value for 84,000 g/mol PS in toluene. I then determined the scaling factor $X = .701$ between R_g and R_h for PS in room temperature toluene using $R_g = 10.21$ nm and R_h = 7.16 nm for 84,000 g/mol PS in toluene. The R_h^{PS-DR1} = 6 – 7 nm of PS-DR1 as measured by our DLS system was then converted to $R_g^{PS-DR1} = 9 – 10$ nm of PS-DR1 with the scaling factor $X = .701$ calculated from R_g and R_h from ref.[37] The now converted $R_g^{PS-DR1} = 9 – 10$ nm was then used to estimate the ~ 70,000 g/mol M_w of PS-DR1 in room temperature toluene, again from the experimentally determined scaling relation between R_g and M_w given by refs.[37,38]

PS-DR1 films were spin coated from toluene solution onto freshly cleaved mica, varying the spin speed and solution concentration to achieve desired film thicknesses. The films spin coated onto mica substrates were subsequently annealed at 120 ^oC for over 18 h to remove any residual solvent and stresses imparted by spin coating. The annealed PS-DR1 films were then transferred from mica onto silicon substrates via a standard water transfer procedure and let thoroughly dry prior to ellipsometry measurements. No further annealing steps were taken to reset the thermal history of the films post transferring the films from mica onto silicon.

6.3.2 Calibration of the Laser System

In initial trials, photomechanical *trans* to *cis* isomerization of PS-DR1 films was excited by a 532 nm 50 mW continuous wave laser (CrystaLaser), a solid-state laser borrowed from the Prof. Laura Finzi lab. The laser was circularly polarized by a quarter wave plate from Edmund Optics using 2 polarizers. Measurements of PS-DR1 films done

prior to circularly polarizing the laser induced a non-uniform photoisomerization of DR1 that introduces optical anisotropy.[26,39] The Woollam M-2000 ellipsometer used throughout this dissertation was not able to deconvolve the optical anisotropy induced by DR1 with standard models, where artifacts became apparent in the parameters. For example, prior to circularly polarizing the laser, the PS-DR1 film thickness would increase upon photoisomerization of DR1, while the fitted index of refraction would simultaneously and unphysically appear to increase as well, indicating a breakdown somewhere in the ellipsometry model. Between the laser aperture and the quarter waveplate, I used a defocusing lens (Edmund Optics) to expand the beam. The diameter of the laser beam was increased to approximately 8.5 mm, ensuring that the laser beam exciting DR1 was larger than the ellipsometry measurement beam. Increasing the laser beam diameter alleviated complications in the ellipsometry model that would have had to account for only a portion of the measured sample undergoing photoisomerization and any associated edge effects or lateral film distortions.

A high power 532 nm, 300 mW continuous wave, solid state laser with a power supply capable of varying the laser power output was purchased from LaserGlow to characterize the photomechanical response of PS-DR1 films at different power densities. The LaserGlow laser was interfaced with an Arduino that ran on MatLab code built by Benjamin Kasavan to control the laser on, off, wait, and repeat sequences at various laser power levels. The laser power was calibrated by first measuring the laser power as a function of the analog power dial setting on the laser power supply with a S121C silicon power meter and PM100 control box (borrowed from the Prof. Hayk Harutyunyan lab). The MatLab code takes the desired laser power setting and preforms a linear fit around the

4 closest points in the calibration curve for a given power level input, and then outputs the analog dial setting for the desired power. At the intersection of the two power regimes of the power supply (2 linear regions), the code estimates the dial setting of the power supply for a given desired power input with a forth order polynomial fit around the data. Figure 6.4 graphs the measured laser power (black circles) as a function of the analog dial reading of the power supply and simultaneously plots the computer estimated analog dial setting for a given desired laser power input (red triangles).

Though all other setting of the high power LaserGlow laser including the quarter waveplate and beam diameter follow the same protocol established with the 50 mW CrytaLaser, the incidence angle of the laser beam to the sample could not be reproduced for both systems. The 50 mW data collected with the CrystaLaser was originally intended to collect preliminary data to fund the PS-DR1 project when we lacked equipment to permanently attach a laser to the ellipsometer. Because the LaserGlow laser introduced more parameters into the system such as power and incident angle, my dissertation will present DR1 photoisomerization data excited by the 532 nm 50 mW CrystaLaser and the 532 nm variable power laser from LaserGlow in two different sections.

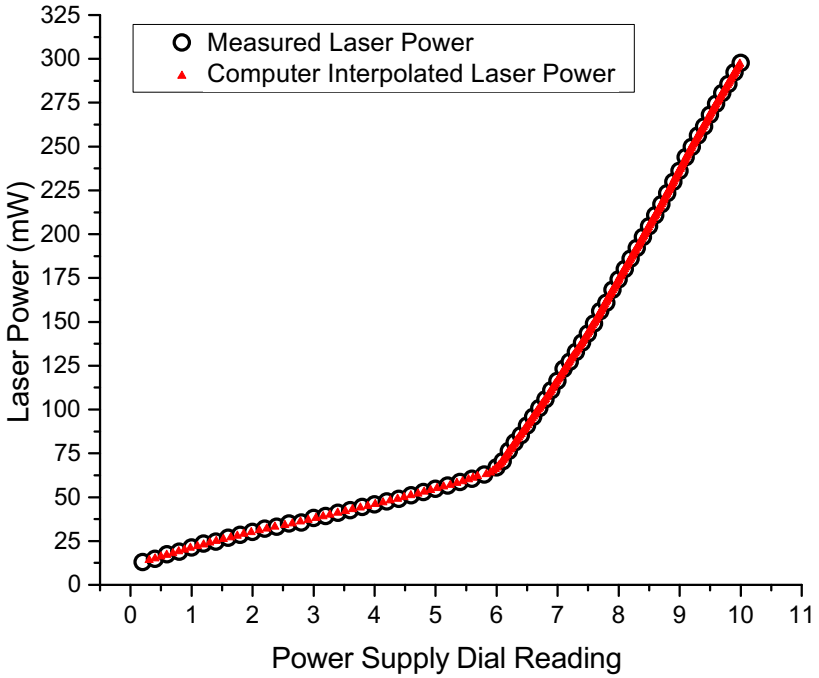

Figure 6.4: Laser power of the high power 525 nm 300 mW LaserGlow laser as a function of the analog dial reading on the variable power supply (black circles), combined with computer laser power input with the analog dial setting output (red triangles) from the MatLab code written by Benjamin Kasavan.

6.3.3 Ellipsometry Film Thickness Measurements of PS Labeled with Photomechanical DR1 Excited by a 532 nm 50 mW Laser

A Woollam M-2000 multiangle and wavelength ellipsometer, equipped with a 20 Hz compensator and a relative film thickness resolution of less than .02 %[40] was used to characterize PS-DR1 film thickness and % strain during the photoisomerization cycles of the DR1 dye. The ellipsometer layer model was restricted to only fit the 600 to 1000 nm wavelength range, avoiding DR1 absorption wavelengths (see Figure 6.3) and thereby simplifying model fitting. All ellipsometry data were collected at a fixed 65^{o} angle of incidence with the excitation laser mounted at an angle such that the reflected beam pointed away from the ellipsometer detector. Prior to collecting data, the excitation laser beam was

expanded to 8.5 mm (diameter) to completely cover the ellipsometer measurement beam. Expanding the laser beam ensured that the ellipsometer averaged over a region of the film that is entirely illuminated by the laser, thereby avoiding non-uniform excitations of the DR1 dye.

PS-DR1 film thickness (black circles) and PS-DR1 index of refraction at 633 nm (blue triangles) of an 83.5 nm thick PS-DR1 film excited with the 532 nm 50 mW laser (CrystaLaser) at 80 ^{o}C is plotted it Figure 6.5. The black horizontal bars indicate when the excitation laser was toggled on and off via a mechanical shutter covering the laser beam, and directly shows where the photoisomerization of DR1 was induced in the PS-DR1 film. In this set of experiments, the shutter of the excitation laser was held open for a duration of 420 s in each period, demonstrating the robustness of PS-DR1 films. Exciting PS-DR1 films (laser on) induces multiple rapid switching of DR1 from the ground *trans* state to the excited *cis* state that elevates the percentage of DR1 dyes in the *cis* state. When the DR1 dye is photomechanically excited by the laser, the PS-DR1 film thickness data in Figure 6.5 shows that continuously switching DR1 dye between *trans* and *cis* conformational states with a higher percentage of *cis* states relative to the unexcited PS-DR1 film induces a volume change within the PS-DR1 film and effectively expands the PS matrix internally. As expected, the index of refraction decreases as the film thickness of the PS-DR1 film increases. Upon turning off the laser, the elevated percentage of DR1 dye in the *cis* state relaxes back to the *trans* state, which is likely too fast for us to detect, thereby allowing the polymer matrix to relax. The relaxation of PS-DR1 shown in Figure 6.5 will be discussed in further sections. From this data, I demonstrate that .45 mol % DR1 labeled to PS is

powerful enough to expand bulk PS-DR1 films at temperatures below T_g even with a relatively low label content of the chromophore.

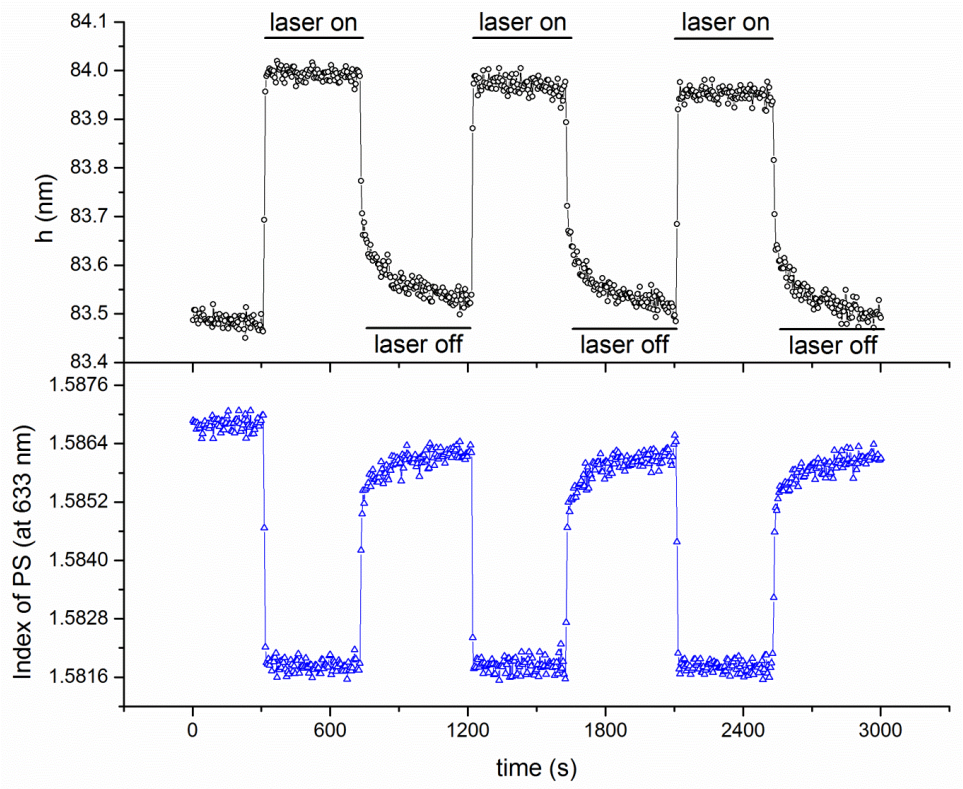

Figure 6.5: Raw PS-DR1 film thickness *h* (black circles) and PS-DR1 index of refraction at 633 nm (blue triangles) collected while photomechanically exciting DR1 with a 532 nm 50 mW laser at 80 ^{o}C. Black horizontal bars indicate when the laser was toggled on and off via a mechanical shudder to excite DR1 photoisomerization.

Figure 6.6a plots PS-DR1 film thickness and % strain for an 83.5 nm thick film excited at three different temperatures normalized by the initial film thickness prior to exciting the DR1 dye. The temperature window was chosen to lie far below, close to, and above the ~100 ^{o}C glass transition temperature of neat bulk PS where the DR1 photomechanical excitations are cycled at constant temperatures of 25 (blue triangles), 80

(black circles) and 110 (red squares) ^{o}C, respectively. The photoisomerization of PS-DR1 films at these temperatures shows that DR1 is capable of inducing a significant and measurable volume change in PS-DR1 films on a broad temperature range that is typically employed in T_g experiments.

The % strains observed in Figure 6.6a show a distinct PS-DR1 photomechanical temperature dependence. For example, in Figure 6.6a the induced % strain due to the photomechanical expansion of DR1 in an 83.5 nm thick PS-DR1 film shows a decreasing temperature dependence above bulk PS T_g with the total % strain ranging from approximately .2 % at 110 ^{o}C to .7 % at 25 ^{o}C. Here I define the recoverable % strain as the ratio between the recoverable film thickness during the off period of the laser after the first laser excitation and the film thickness after subsequent excitations of PS-DR1 film when the laser is turned on. From this definition, the recoverable % at temperatures of 25, 80, and 110 ^{o}C was measured to be 0.34, 0.55, and 0.24 % respectively. Figure 6.6b plots the relaxation (laser off) of the 83.5 nm thick PS-DR1 film measured at 25 ^{o}C (blue symbols, top) and 80 ^{o}C (black symbols, bottom) after the excitation laser was blocked by a mechanical shutter. Each of the relaxation decay curves was fit to a simple exponential decay function starting after the initial fast drop in film thickness of the PS-DR1 film with the following fitting equation in equation 6.3,

$$h(t) = \Delta h \exp\left(-\frac{t}{\tau}\right) + h_o^*, \tag{6.3}$$

where h_o^* is the recoverable PS-DR1 film thickness, Δh is the PS-DR1 film thickness difference between film thickness h after initial fast film thickness decrease and h_o^*, and relaxation time τ. The initial fast drop in film thickness that occurs a few seconds after the laser was turned off suggests that the PS matrix was possibly undergoing elastic recovery,

which will also be discussed further in the next section. Figure 6.6c plots the PS-DR1 film relaxation curves from Figure 6.6b on a semi-log scale. To first approximation, Figure 6.6c suggests that a single exponential decay is a good fit to the relaxation of the PS-DR1 film, but there are still some features in the data that need to be further looked into in the future. Currently I am not certain where the curvature during the initial 30 seconds of the data originates from. Possibly I am still capturing a small portion of the elastic recovery from the PS matrix before the film stabilizes and continues into the linear (on the ln axis of Figure 6.6c) relaxation regime. Plotting the full relaxation regime (nonlinear elastic and linear) in such a way might be a good method in the future to identify the onset of the nonlinear elastic recovery, though one would have to find a means of extracting h_o^* without fitting the exponential decay to the PS-DR1 film relaxation curves shown in Figure 6.6b.

All three parameters in the fitting function defined in equation 6.3 were fit to each relaxation curve in Figure 6.6b with relaxation times τ of 2.4 ± .1 min measured at 25 ^{o}C and 1.9 ± .2 min measured at 80 ^{o}C. At 110 ^{o}C, the PS-DR1 film relaxation was too fast to measure after closing the mechanical shutter of the excitation laser (the off period of the laser cycle). Most notable, PS-DR1 film relaxation time scales range from minutes at 80 ^{o}C to seconds at 110 ^{o}C. If PS-DR1 relaxation time scales measured by photomechanically exciting DR1 dyes can be linked to the relaxation timescales of the polymer matrix, then a labeled photomechanical dye such as DR1 can possibly be used to preform mechanical deformation experiments in polymer thin films.

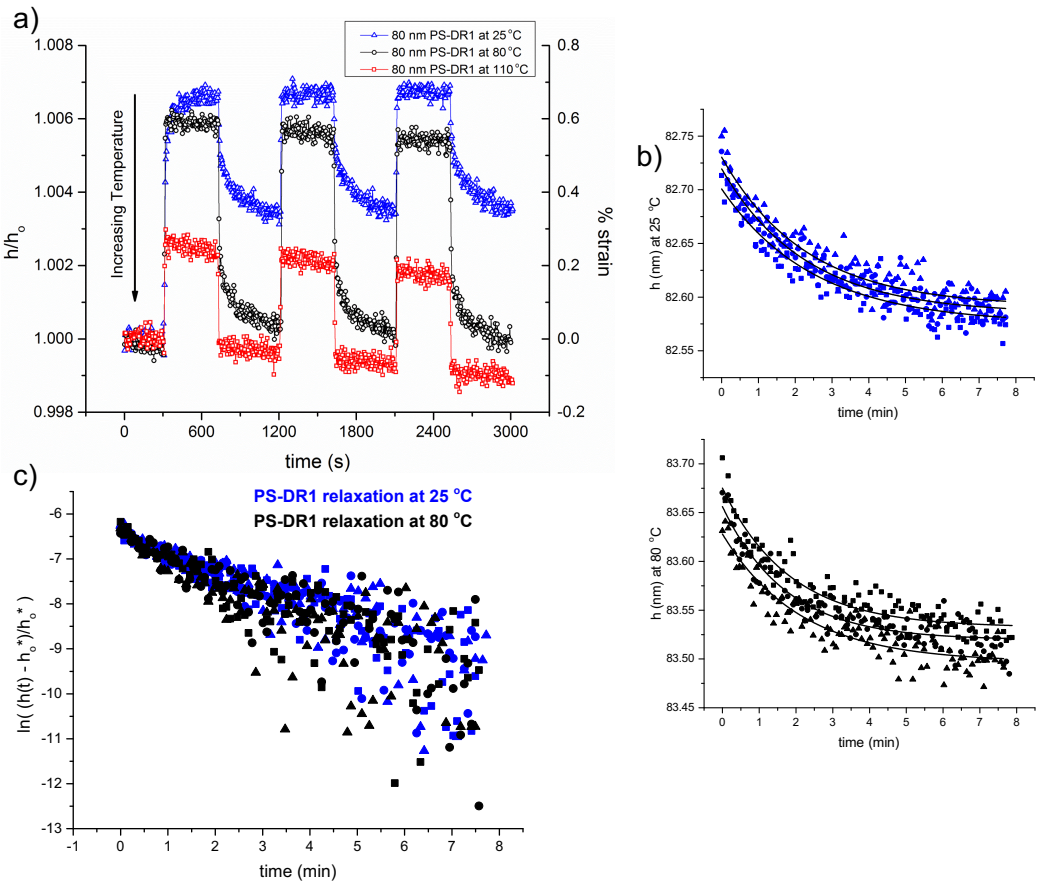

Figure 6.6: (a) Film thickness and % strain of the 83.5 nm thick PS-DR1 film with photoisomerization of the DR1 dye at temperatures far below (blue triangle at 25 °C), above (red squares at 110 °C), and close to (black circles at 80 °C) ~100 °C neat bulk PS T_g. The PS-DR1 film shows a decreasing total % strain with increasing temperature, where the total non-recoverable % strain ranges from approximately .2 % at 110 °C to .7 % at 25 °C. PS-DR1 film thickness h was normalized by the initial PS-DR1 film thickness h_o prior to exciting the film with the laser. (b) Relaxation of the 83.5 nm thick PS-DR1 film during the off period of the excitation laser cycle. Each of the three relaxation curves measured at 25 °C (blue symbols, top) and 80 °C (black symbols, bottom) are independently fit to the exponential decay in equation 6.3 with relaxation times τ of 2.4 ± .1 min at 25 °C and 1.9 ± .2 min at 80 °C. (c) Semi-log plot of PS-DR1 film relaxation curves at 25 °C (blue symbols) and 80 °C (black symbols).

Normalized PS-DR1 film thickness and % strain are plotted in Figure 6.7 for 30 nm thick (red squares) and 83.5 nm thick (black circles) films photomechanically excited by the laser at 80 ^{o}C. Interestingly, the observed recoverable % strain of 30 nm and 83.5 nm thick films at constant temperature collapses to approximately .6 %, indicating that there is no film thickness dependence on the recoverable % strain at 80 ^{o}C. The similarity in % strain for different PS-DR1 film thicknesses suggests that the DR1 photoinduced % strain may depend on the concentration of DR1 or the mol % of DR1 in a PS film, which can possibly be tuned in the future by varying DR1 monomer and styrene content during polymerization of PS-DR1 polymer. In addition, a neat (no DR1 dye) 80 nm thick PS film (blue triangles) is shown as a control excited by the 532 nm 50 mW laser as indicated by the black horizontal bars. No change to thickness or index of the 80 nm thick PS film was observed within the ellipsometer noise threshold, demonstrating that residual heating is not responsible for the film thickness increases observed in PS-DR1 films.

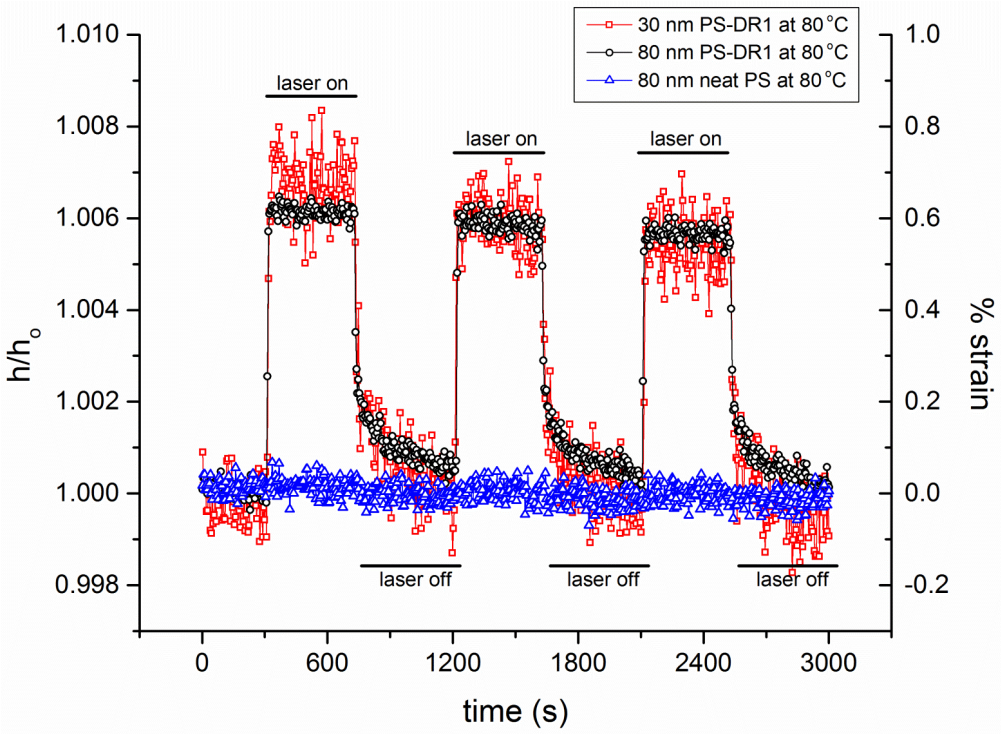

Figure 6.7: Film thickness and % strain of normalized PS-DR1 30 nm thick (red squares) and 83.5 nm thick (black circles) films excited at 80 °C. A neat 80 nm thick PS film (blue triangles) was also irradiated with the 532 nm 50 mW laser, which showed no observable film thickness dependence within noise. The % strain of the 30 nm thick and 83.5 nm thick PS-DR1 films collapses to approximately .6 % strain.

6.3.4 Ellipsometry Film Thickness Measurements of PS Labeled with Photomechanical DR1 Excited by a 532 nm Variable Power Laser

As in the previous section, the ellipsometer was fixed at a 65° angle of incidence and restricted to fit the 600 to 1000 nm wavelength range to avoid absorption wavelengths associated with DR1 and the 532 nm variable power laser. The excitation laser beam was expanded to 8 – 9 mm (diameter) to completely cover the ellipsometer measurement beam and mounted at an approximately 30 – 40° angle of incidence such that the reflected beam pointed away from the ellipsometer detector, though the exact angle at which the 532 nm 50 mW laser was mounted could not be reproduced. Our initial measurements to date

suggest the angle of incidence of the DR1 excitation laser relative to the ellipsometer plane of incidence may be an important factor to control that future measurements should address.

Figure 6.8 plots normalized film thickness of a 58 nm thick PS-DR1 film excited at room temperature by a 532 nm variable power laser as a function of power density (mW/cm^2) demonstrating the expansion of the film with increasing laser power. Power density error bars account for the uncertainty in the size of the laser spot area, with the variation in power density calculated for a laser spot with an 8 mm (upper bound) and 9 mm (lower bound) diameter, based on the total power of the beam measured by the power meter shown in Figure 6.4. Though a power density plateau was not reached, the largest % strain for an experimentally reasonable 125 mW/ cm^2 power range is observed between 75 to 200 mW/cm^2.

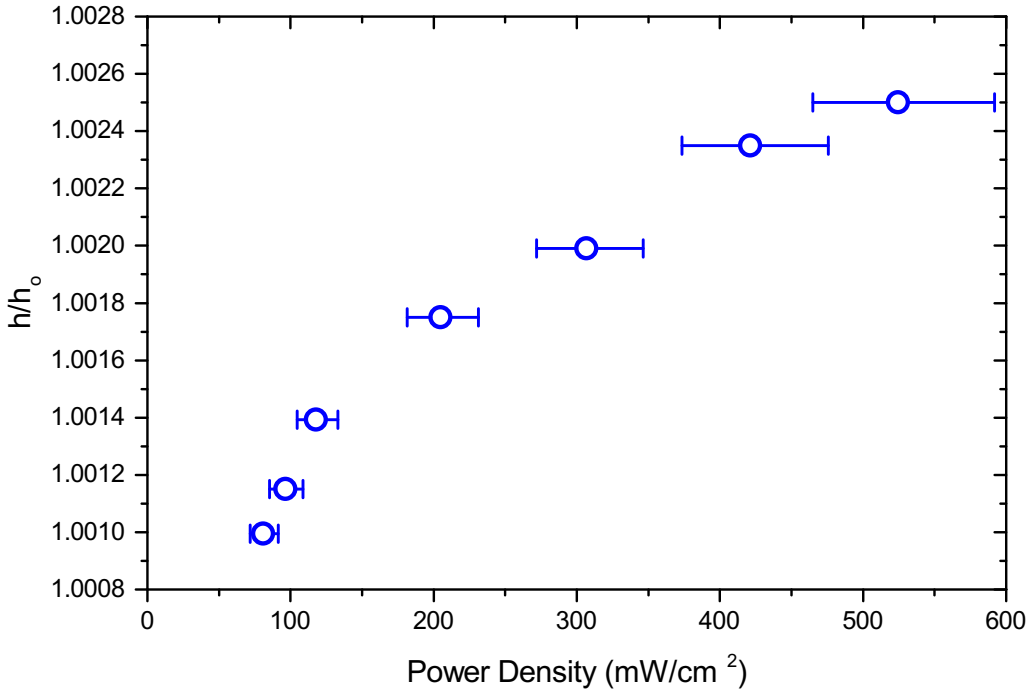

Figure 6.8: Normalized film thickness of a 58 nm thick PS-DR1 film excited at room temperature by a 532 nm variable power laser plotted as a function of laser power density. Power densities between 75 to 200 mW/cm^2 show the largest increase in % strain with increasing power density.

Figure 6.9a plots temperature profiles collected from 40 ^{o}C to 110 ^{o}C in 10 K steps for multiple photoisomerization periods when the laser is turned on for an 80 nm thick PS-DR1 film. The PS-DR1 film underwent two laser on-off cycles before measuring a final 20 min thermal relaxation of the PS-DR1 film. The power density of the excitation laser was set to 524 mW/cm^2 to maximize the photomechanical response of the PS-DR1 film. Because the laser excitation beam is at an angle from the detector, the heater cover that provides added thermal stability, especially for temperatures above 80 ^{o}C, had to be removed since the cover blocks a portion of the excitation laser. A persistent film thickness decrease with time is observed at temperatures above 80 ^{o}C, likely due to photobleaching of the dye from the oxygen exposure at high temperatures. This will be improved upon

after a new heater cover is machined and the thermal stability of the heater is subsequently retested. Each PS-DR1 temperature profile was then renormalized by its initial temperature dependent film thickness h_o and plotted in Figure 6.9b. The renormalized photomechanical response of the PS-DR1 film shows that % strain is still measurable at temperatures above 80 ^{o}C, even though there is a significant time-dependent thickness decrease above 80 ^{o}C.

Relaxation curves of the 80 nm thick PS-DR1 film measured over 20 min at the end of each temperature run for temperatures below 80 ^{o}C are plotted in Figure 6.9c and fit to the exponential decay function defined in equation 6.3. The relaxation curves above 80 ^{o}C are not fit to avoid the time-temperature thickness decrease that would affect the fit and the relaxation time constant, τ. Equation 6.3 was only fit to the relaxation curves after the initial fast drop in film thickness of the PS-DR1 film present in the first few seconds after the laser was turned off. Figure 6.9d plots the magnitude of the initial fast drop in film thickness of the PS-DR1 film occurring during the first 6 – 8 seconds (3 – 4 data points) after the laser was turned off. The magnitude of the initial film thickness drop increases with increasing temperature, which would be expected if the PS matrix was undergoing elastic recovery in the initial stages of the relaxation curves.

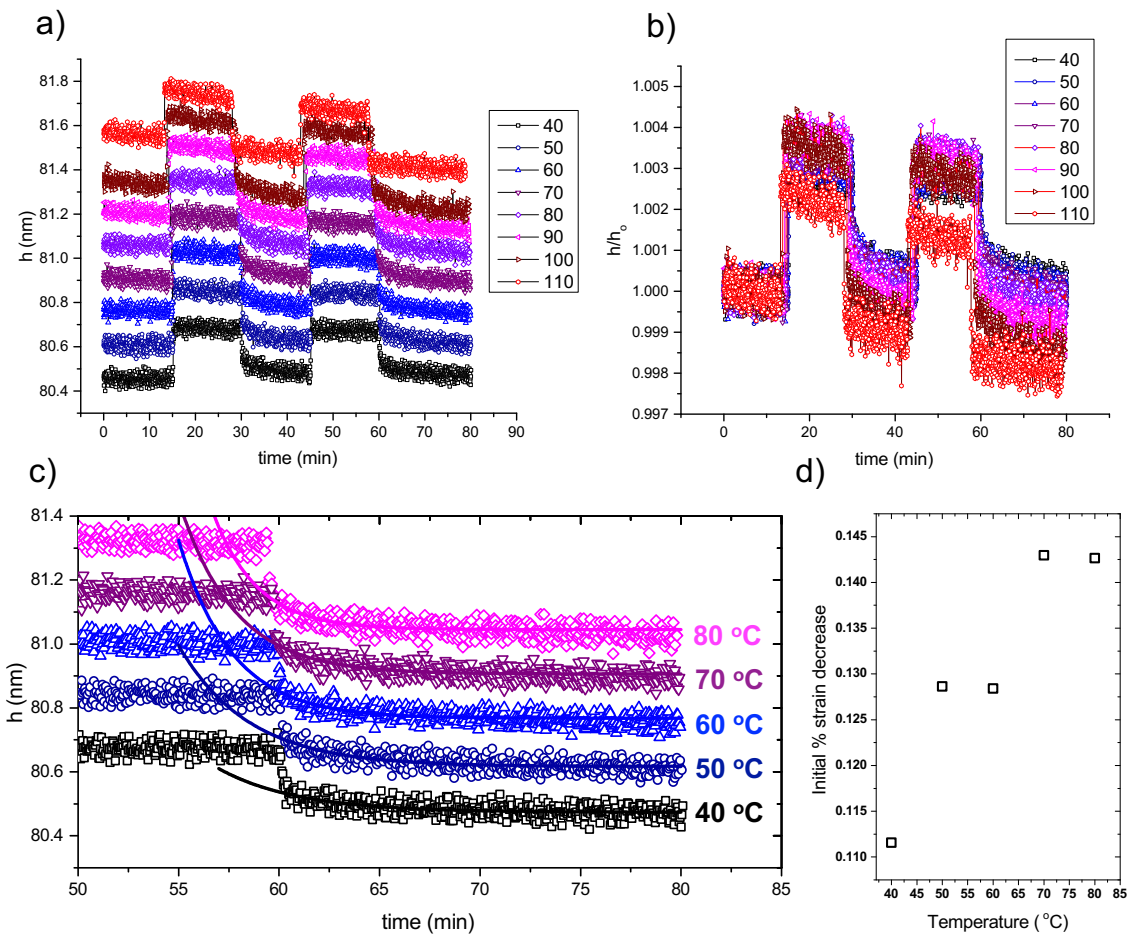

Figure 6.9: (a) Temperature profiles of an 80 nm thick PS-DR1 film excited with a 524 mW/cm^2 power density over multiple photoisomerization periods when the laser was turned on for temperatures ranging from 40 °C to 110 °C in 10 K steps. (b) The temperature profiles renormalized by the initial film thickness h_o at each temperature (40 °C to 110 °C). h/h_o persistently decreases with time at temperatures above 80 °C, likely due to photobleaching of the DR1 dye. (c) 20 min PS-DR1 film relaxation curves measured at the end of each run for temperatures below 80 °C are fit to an exponential decay defined in equation 6.3 from which I determine a temperature dependent relaxation decay constant, τ. The fit does not include the initial fast drop in film thickness of the PS-DR1 film. (d) The initial fast drop in film thickness of the PS-DR1 film occurring during the first 6 – 8 seconds (3 – 4 data points) after the laser was turned off for temperatures below 80 °C. The initial fast drop in film thickness could correspond to the elastic recovery of the PS matrix.

Figure 6.10 plots the recoverable % strain in terms of h/h_o (solid blue circles) for the 80 nm thick PS-DR1 film photomechanically excited with a 524 mW/cm^2 power density for temperatures ranging from 40 ^{o}C to 110 ^{o}C in 10 K steps, from data fit in Figure 6.9. Relaxation time constant, τ, (red triangles) was determined from fitting the 20 min relaxation at the end of each temperature profile to equation 6.3 for temperatures below 80 ^{o}C. The error bars in τ are calculated by the fit. The recoverable % strain increases as the temperature increases to about 90 ^{o}C, and then rapidly starts to decrease as the temperature is raised above ~100 ^{o}C bulk PS T_g. In addition, I plot the recoverable % strain in terms of h/h_o (open blue circles) of the 83.5 nm thick PS-DR1 film from section *6.3.3*, demonstrating that the shape of both curves is consistent, where both curves show a decrease in the recoverable % strain above 100 ^{o}C. The relaxation time τ in section *6.3.3* and τ observed in Figure 6.10 both decrease with increasing temperature as expected, although there is still work necessary to deconvolve how the measured decay relates to the response of the PS matrix.

Comparing the results in section *6.3.3* to the results shown here, both sets of data show that the total film thickness of an ~80 nm thick PS-DR1 film increases upon exciting the DR1 dye with a 532 nm laser, with recoverable % strains reaching .55 % at 80 ^{o}C in section *6.3.3* and .36 % at 90 ^{o}C in section *6.3.4*. Interestingly the % strain measured in section *6.3.3* is overall larger than the % strain measured with the current laser setup. The initial non-recoverable region in the data presented in section *6.3.4* seems to be an absence in the data in section *6.3.3*, which will further have to be investigated in future experiments. These quantitative differences between data in sections *6.3.3* and *6.3.4* could be associated with the different laser used, or differences in angle of incidence. Though in both cases

the recoverable % strain of PS-DR1 films increases with increasing temperature but then begins to dramatically decrease at temperatures above ~100 ^{o}C bulk PS T_g. Additionally, the relaxation times τ in section *6.3.3* (τ = 2.4 ± .1 min at 25 ^{o}C and 1.9 ± .2 min at 80 ^{o}C) are smaller than the relaxation times observed in this section (τ = 3.9 ± .8 min at 40 ^{o}C and 2.2 ± .3 min at 80 ^{o}C), but the overall temperature dependence of τ is in agreement between both data sets. The set of experiments in this section shows that even though the photoisomerization data of PS-DR1 excited by the 532 nm 50 mW laser was collected under different incidence angles of the laser and with different power densities, along with the data in section *6.3.3* taken 3 years apart from the photoisomerization data presented in this section, the overall photomechanical behavior of PS-DR1 excited by a 532 nm laser is reproducible.

Currently there are a number of open questions about the PS-DR1 film excitation measurements presented in this Chapter. How are we dynamically forcing the PS matrix and subsequently, what are we measuring? By exciting DR1 dye in the PS-DR1 films, are we applying continuous stresses from the DR1 dye within the PS matrix that would result in a creep experiment? Or are we applying a strain where we are measuring the stress relaxation of the PS matrix? This seemingly simple question does not yet have a trivial solution. Exciting DR1 dye creates a dynamic two-level system where the % population of *cis* states is elevated by the excitation laser. One can imagine that the continuous *trans*/*cis* switching induces local stresses in the PS matrix or possibly a continuous material strain. Can we then infer that we are measuring some kind of fast elastic recovery of the PS matrix if we are inducing continuous local stresses? Are PS-DR1 film relaxation times, τ, related to the PS matrix, and if so, how do we relate the relaxation times to the modulus

of PS-DR1 films? Identifying the molecular and dynamic role of the DR1 dye is important for analyzing the measurements presented in this Chapter and designing future works.

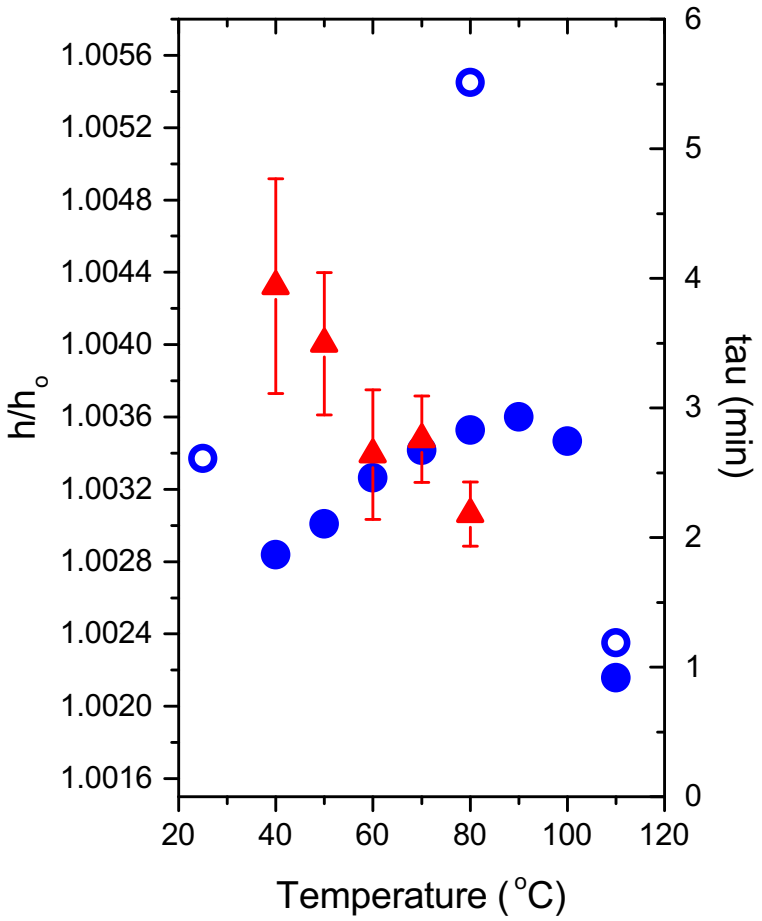

Figure 6.10: Recoverable % strain in terms of h/h_o (solid blue circles) and relaxation time constant τ (red triangles) for the 80 nm thick PS-DR1 film excited with a 524 mW/cm^2 laser power density as a function of temperature. The recoverable % strain decreases at temperatures close to and above bulk PS T_g. I also plot the recoverable % strain (open blue circles) for the 83.5 nm thick PS-DR1 film from section *6.3.3* that shows qualitatively similar behavior both above and below bulk PS T_g. Note that τ is decreasing with increasing temperature as expected.

6.4 REFERENCES

[1] Y.C. Lee, K.C. Bretz, F.W. Wise, and W. Sachse, Appl. Phys. Lett. **69**, 1692 (1996).

[2] B.J. Briscoe, L. Florl, and E. Pelillo, J. Phys. D: Appl. Phys. **31**, 2395 (1998).

[3] C.A. Tweedie, G. Constantinides, K.E. Lehman, D.J. Brill, G.S. Blackman, and K.J. Van Vliet, Adv. Mater. **19**, 2540 (2007).

[4] C.M. Stafford, C. Harrison, K.L. Beers, A. Karim, E.J. Amis, M.R. VanLandingham, H.-C. Kim, W. Volksen, R.D. Miller, and E.E. Simonyi, Nat Mater **3**, 545 (2004).

[5] C.M. Stafford, B.D. Vogt, C. Harrison, D. Julthongpiput, and R. Huang, Macromolecules **39**, 5095 (2006).

[6] J.M. Torres, C.M. Stafford, and B.D. Vogt, ACS Nano **3**, 2677 (2009).

[7] J.Y. Chung, A.J. Nolte, and C.M. Stafford, Adv. Mater. **23**, 349 (2010).

[8] J.A. Forrest, K. Dalnoki-Veress, and J.R. Dutcher, Phys. Rev. E **58**, 6109 (1998).

[9] P.A. O'Connell and G.B. McKenna, Science **307**, 1760 (2005).

[10] P.A. O'Connell, S.A. Hutcheson, and G.B. McKenna, J Polym Sci, Part B: Polym Phys **46**, 1952 (2008).

[11] P.A. O'Connell, J. Wang, T.A. Ishola, and G.B. McKenna, Macromolecules **45**, 2453 (2012).

[12] Z. Mahimwalla, K.G. Yager, J.-I. Mamiya, A. Shishido, A. Priimagi, and C.J. Barrett, Polym. Bull. **69**, 967 (2012).

[13] T. Naito, K. Horie, and I. Mita, Macromolecules **24**, 2907 (1991).

[14] C.S. Paik and H. Morawetz, Macromolecules **5**, 171 (1972).

[15] L. Lamarre and C.S.P. Sung, Macromolecules **16**, 1729 (1983).

[16] P.C. Hiemenz and T.P. Lodge, *Polymer Chemistry*, 2nd ed. (CRC Press, Boca Raton, 2007).

[17] G.R. Strobl, *The Physics of Polymers*, 3rd ed. (Springer, Verlag Berlin Heidelberg, 2007).

[18] Y. Du, Y. Xue, and H.L. Frisch, *Physical Properties of Polymers* (AIP Press, New York, 1996), pp. 227–239.

[19] T.B. Karim and G.B. McKenna, Macromolecules **45**, 9697 (2012).

[20] T.B. Karim and G.B. McKenna, Polymer **54**, 5928 (2013).

[21] J.H. Kim, J. Jang, and W.-C. Zin, Langmuir **16**, 4064 (2000).

[22] K. Paeng and M.D. Ediger, Macromolecules **44**, 7034 (2011).

[23] E. Glynos, B. Frieberg, H. Oh, M. Liu, D.W. Gidley, and P.F. Green, Phys. Rev. Lett. **106**, 128301 (2011).

[24] T. Kobayashi, E.O. Degenkolb, and P.M. Rentzepis, J. Phys. Chem. **83**, 2431 (1979).

[25] I.K. Lednev, T.-Q. Ye, R.E. Hester, and J.N. Moore, J. Phys. Chem. **100**, 13338 (1996).

[26] T.A. Singleton, K.S. Ramsay, M.M. Barsan, I.S. Butler, and C.J. Barrett, J. Phys. Chem. B **116**, 9860 (2012).

[27] C.D. Eisenbach, Polymer **21**, 1175 (1980).

[28] K.M. Lee, M.L. Smith, H. Koerner, N. Tabiryan, R.A. Vaia, T.J. Bunning, and T.J. White, Adv. Funct. Mater. **21**, 2913 (2011).

[29] A. Ambrosio, L. Marrucci, F. Borbone, A. Roviello, and P. Maddalena, Nat Commun **3**, 989 (2012).

[30] A. Ambrosio, P. Maddalena, and L. Marrucci, Phys. Rev. Lett. **110**, 146102 (2013).

[31] T. Ikeda, M. Nakano, Y. Yu, O. Tsutsumi, and A. Kanazawa, Adv. Mater. **15**, 201 (2003).

[32] C.J. Barrett, J.-I. Mamiya, K.G. Yager, and T. Ikeda, Soft Matter **3**, 1249 (2007).

[33] M. Yamada, M. Kondo, J.-I. Mamiya, Y. Yu, M. Kinoshita, C.J. Barrett, and T. Ikeda, Angew. Chem. Int. Ed. **47**, 4986 (2008).

[34] S. Yoneyama, T. Yamamoto, O. Tsutsumi, A. Kanazawa, T. Shiono, and T. Ikeda, Macromolecules **35**, 8751 (2002).

[35] H. Yu, K. Okano, A. Shishido, T. Ikeda, K. Kamata, M. Komura, and T. Iyoda, Adv. Mater. **17**, 2184 (2005).

[36] C.M. Kok and A. Rudin, Macromol. Rapid Commun. **2**, 655 (1981).

[37] L.J. Fetters, N. Hadjichristidis, J.S. Lindner, and J.W. Mays, J. Chem. Phys. Ref. Data **23**, 619 (1994).

[38] I. Teraoka, *Polymer Solutions: an Introduction to Physical Properties.* (John Wiley & Sons, Inc., New York, 2002), pp. 1–349.

[39] Z. Sekkat, G. Kleideiter, and W. Knoll, J. Opt. Soc. Am. B **18**, 1854 (2001).

[40] E.A. Baker, P. Rittigstein, J.M. Torkelson, and C.B. Roth, J Polym Sci, Part B: Polym Phys **47**, 2509 (2009).

Chapter 7

Summary and Conclusions

In this dissertation, I used a modified version of a fluorescence technique originally developed by the Torkleson group[1] to measure how dissimilar polymer-polymer interfaces perturb the glass transition temperature *locally* in nanostructured polymer films. Local T_g measurements were achieved by chemically labeling a 10 – 15 nm thick polymer layer with a fluorescent T_g sensitive pyrene dye. The fluorescently labeled layer was then inserted at distances z from dissimilar polymer-polymer interfaces, thereby mapping local $T_g(z)$ profiles for a variety of dissimilar polymer pairs.

One of the most interesting puzzles in the confinement literature is to understand the mechanisms by which interfaces such as polymer-air, polymer-substrate, polymer-liquid and dissimilar polymer-polymer interfaces affect local properties of the material. Are there any intrinsic material length scales that are somehow coupled to the observed perturbative effects due to interfaces? What are the similarities and differences between different interfaces that seem to cause diverse T_g perturbations in thin films?

Prior to my work published as a 2015 Communication in the *Journal of Chemical Physics*[2] and a later follow-up article in 2017 *Journal of Chemical Physics*,[3] theory on miscible polymer blends[4] would have suggested that T_g is a local property associated with the local composition within a small region the size of a Kuhn length (few nanometers) beyond which the rest of the material does not contribute to the mean field approximation. Literature on phase separated polymer blends would have similarly assumed that each

domain would have a T_g equivalent to the bulk T_g value for each component a few nanometers away from the interface.[5,6] If we apply this thinking to the types of samples studied in this dissertation, then the prevailing paradigm would have predicted that local $T_g(z)$ profiles across dissimilar polymer-polymer bilayers should simply follow the sharp composition profile, $\phi(z) \approx \tanh(2z/w)$, across the polymer interface, where w is the interfacial width.[4,5,7-9] In contrast, confinement literature has shown that interfaces such as polymer-air and polymer-substrate can perturb local dynamics tens of nanometers deep into the material.[1,10-14] Before my contributions to the field, the confinement literature was only starting to look at the effects of dissimilar polymer-polymer interfaces in experiments,[15-17] computer simulations,[18] and theory.[19]

My most significant contribution to the research literature is demonstrating that local $T_g(z)$ profiles emanating from dissimilar polymer-polymer interfaces are much more long ranged than previously expected and that the $T_g(z)$ profiles are asymmetric, biased towards the high T_g component of the semi-infinite polymer-polymer bilayer. For example, the local $T_g(z)$ profile of a polystyrene (PS) / poly(n-butyl methacrylate) (PnBMA) semi-infinite bilayer with a static and equilibrated 7 nm PS/PnBMA interface and an 80 K T_g difference between the bulk T_gs of glassy, high T_g PS ($T_g^{\text{bulk, PS}} = 101\ ^{\circ}\text{C}$) and rubbery, low T_g PnBMA ($T_g^{\text{bulk, PnBMA}} = 21\ ^{\circ}\text{C}$) components, extends 350 – 400 nm.[2] Confinement studies would not predict such a long 350 – 400 nm length scale being required before bulk T_gs of each component were recovered across a dissimilar polymer-polymer interface. Although, a then very recent kinetically facilitated Limited Mobility model by the Lipson and Milner groups did predict an asymmetrical mobility profile that extends deeper into the low mobility component.[19,20]

Expanding the semi-infinite bilayer to a series of polymer pairs, my results suggest a universality in the observed length scales, which does not depend on the T_g difference across the dissimilar polymer-polymer interface, the interaction parameter between dissimilar polymers, chemical structure, or fragility.[3] Instead, I found that the local $T_g(z)$ profiles are grouped by if the measured polymer component is the high T_g component, where the local T_g is perturbed for 225 – 250 nm from the interface before bulk T_g is recovered, or low T_g component, where the local T_g is perturbed for 100 – 125 nm before bulk T_g is recovered in the semi-infinite polymer-polymer bilayer. The published results in Chapters 3 and 4 suggest that the perturbations to T_g are primarily controlled by whether the measured polymer is confined by a hard or soft equilibrated polymer-polymer interface.[2,3] Most recently, the results in Chapters 3 and 4 have motivated Benjamin L. Kasavan's recent experiments that measured the effect of small molecule additives present in unwashed polybutadiene (PB) as a stabilizer to the $T_g(z)$ profile in PS/PB semi-infinite bilayers. Kasavan's results are published as B.L. Kasavan, R.R. Baglay, and C.B. Roth, *Molecular Chemistry and Physics*, 2017.[21]

In Chapter 4, I further showed that the extent to which two dissimilar polymers are allowed to interdiffuse at the polymer-polymer interface is an important factor that affects the dynamical coupling across the interface. By restricting the amount of annealing done at a PS/polysulfone (PSF) interface in PS/PSF semi-infinite bilayers, I showed that the $T_g(z)$ profile was sharper for short annealing times and continued to evolve until the PS/PSF interface reached equilibrium, where I finally observed no further measurable evolution of the $T_g(z)$ profile with additional annealing. This suggests that perhaps the distinctiveness of dissimilar polymer-polymer interfaces may be attributed to the extensive 5 to 7 nm

interfacial width of the polymer-polymer interfaces that develops during annealing of the polymer pairs, compared to the ~0.5 nm[22] breadth of polymer-air interfaces.

Currently there are a number of groups working on modeling systems similar to the semi-infinite bilayers discussed in my dissertation. At the beginning of my Ph.D. research, a kinetically facilitated Limited Mobility (LM) model was being developed by the Lipson and Milner groups.[20] The LM model was extended to simulate local mobility across interfaces between slabs of material with different bulk mobilities.[19] This work[19] predicted an asymmetric mobility profile that extends further into the lower mobility component of the material,[19] a prediction which has now been supported by my data.[2] More recently, the Lipson and Milner groups have extended this LM model to try and make qualitative comparisons with the fluorescence measurements of the Torkelson group,[1,23] where T_g is measured with simulated "reporting layers" in free standing and supported films.[24] The Lipson and Milner groups suggest that in future work they will potentially employ the LM model to simulate a material that would mimic a system composed of a high mobility and low mobility component, akin to the semi-infinite bilayer films in this dissertation.[24]

A glass transition theory proposed by Mirigian and Schweizer has successfully modeled the air interface in free-standing thin film geometries.[25-28] In their theory, a local modulus term adds a long-range elastic component to the probability of α-relaxation events that accurately captures key features of molecular glasses over 14 decades in time without fit parameters.[25] Mirigian and Schweizer have recently predicted that if the interfacial width of the free-surface vapor layer is slightly increased, the T_g reductions due to the air interface are much longer and greater.[28] Mirigian and Schweizer speculate that the large polymer-polymer interfacial width might be relevant for the extended length scales found

in my results.[28] My work on PS/PSF semi-infinite bilayers demonstrated that restrictive annealing of the PS/PSF interfaces before equilibrium is reached diminishes the $T_g(z)$ profile,[3] supporting these ideas of Mirigian and Schweizer.[3] These results from our group[3] (Chapter 4) and the Schweizer group[28] were published in the same special issue of the *Journal of Chemical Physics* on "Dynamics of Polymer Materials in Thin Films and Related Geometries" edited by Mark Ediger and Ken Schweizer.

In Chapter 5 that was recently published in *ACS Macro Letters*,[29] I measured how T_g is locally affected by the presence of two dissimilar PS/PnBMA interfaces in a fixed 300 nm thick PS domain sandwiched between two PnBMA layers. The experimental conditions in Chapter 5 were motivated by simulations from the Simmons group[30] that employed commonly used periodic boundary conditions in simulations[31] to model the T_g of nanolayered films made by coextrusion.[32,33] The Simmons group demonstrated that in addition to the glassy high T_g and rubbery low T_g components both exhibiting T_g perturbations close to the interface, that the magnitude of the T_g perturbation of the rubbery low T_g component depends on the interfacial energy at the interface.[30] Note that in their simulations, varying the interfacial energy also varies the amount of interdiffusion at the interface, an important parameter that I address in Chapter 4. In my set of experiments, I showed that T_g perturbations from two dissimilar polymer-polymer interfaces are not simply cumulative, with bulk PS T_g never recovering at any position within the entire 300 nm PS domain. I also showed that when the $T_g(z,y)$ profile of the 300 nm PS domain is measured at higher cooling rates (faster timescales), the $T_g(z,y)$ profile diminishes and truncates, consistent with previous works on supported PS films.[34,35] Our results provide an interesting comparison to computer simulations that might be relevant to why computer

simulations such as the ones from the Simmons group[30] do not directly observe long range length scales in their simulated nanolayers when compared to our experiments.

Recently a collaboration between the Priestley and Register groups has polymerized PS-co-PnBMA diblock copolymers where the fluorescent T_g sensitive pyrene dye is chemically labeled at known positions along the PS or PnBMA backbone of the copolymer.[36] This diblock copolymer system self-assembles into lamellae structures with alternating PS/PnBMA domains of ~20 nm in size. In 2017 and 2016 American Physical Society March Meeting presentations, [36,37] graduate student Dane Christie showed that the local T_g measured as a function of distance from the PS/PnBMA interface in the lamella structures also contains an asymmetric bias toward the glassy high T_g PS component of the copolymer. In addition, molecular dynamics simulations of block copolymers by the Ganesan group that were motivated by the Priestley and Register work on labeled block copolymer lamella structures, simulated lamella di-block copolymers with tagged locations along the copolymer backbone to study the relationship between local segmental dynamics and single monomer dynamics.[38] Though the experiments on lamella block copolymers[39] do not show the extensive length scales observed in our work,[2,3,29] my work in Chapter 5 would suggest that the geometry of semi-infinite PS/PnBMA bilayers and PS/PnBMA lamella copolymers are fundamentally different. The block copolymer lamella geometry severely limits the domain size of each component and introduces additional interfaces in the system.

The results of my Ph.D. work have left a number of open questions regarding the mechanisms behind the long-ranged length scales and asymmetry of $T_g(z)$ profiles emanating from dissimilar polymer-polymer interfaces. Why do we observe such extended

perturbative length scales in systems with dissimilar polymer-polymer interfaces compared to polymer films with polymer-air, polymer-liquid, and polymer-substrate interfaces? My work suggests that chain connectivity may play an integral role in coupling dynamics across a polymer-polymer interface, where the length scale can be diminished if the interface is not allowed to form to equilibrium. Though the mechanism by which mobility is transferred across a polymer-polymer interface still remains unclear. Once the interface is formed to equilibrium, how does a hard vs. soft polymer-polymer interface so dramatically change the magnitude of the $T_g(z)$ profiles? David Simmons originally proposed that maybe an elastic component coupled at the interface of two dissimilar polymers might be responsible for the long-range length scales demonstrated in this dissertation. Would then a long-range component such as the elastic modulus present in the theory of Mirigian and Schweitzer provide predictive power in systems containing polymer-polymer interfaces?

Finally, in Chapter 6 I introduced a photomechanical azobenzene dye that has been billed as a molecular "artificial muscle."[40] I polymerized *N*-ethyl-*N*-(2-hydroxyethyl)-4-(4-nitrophenylazo) aniline methacrylate (DR1-MMA) monomer with styrene, creating a .45 mol % DR1 label in PS-DR1 polymer capable of photomechanical motion via excitation of the polymer with a 532 nm laser. I showed that the film thickness of PS-DR1 films increases by exciting the DR1 dye between the *trans*-to-*cis* conformational states, resulting in a recoverable % strain of the PS-DR1 film increasing as a function of temperature before decreasing at temperatures above ~100 ^{o}C PS bulk T_g. The relaxation of the PS-DR1 films after the excitation laser was turned off showed a fast relaxation regime, suggestive of an elastic response from the PS matrix, and a slower relaxation

timescale τ that decreases with increasing temperature. Since the PS-DR1 project is still in its relative infancy, the project is now handed over to a younger graduate student to tackle.

REFERENCES

[1] C.J. Ellison and J.M. Torkelson, Nat Mater **2**, 695 (2003).

[2] R.R. Baglay and C.B. Roth, J Chem Phys **143**, 111101 (2015).

[3] R.R. Baglay and C.B. Roth, J Chem Phys **146**, 203307 (2017).

[4] T.P. Lodge and T.C.B. McLeish, Macromolecules **33**, 5278 (2000).

[5] E. Hempel, G. Hempel, A. Hensel, C. Schick, and E. Donth, J. Phys. Chem. B **104**, 2460 (2000).

[6] P.C. Hiemenz and T.P. Lodge, *Polymer Chemistry*, 2nd ed. (CRC Press, Boca Raton, 2007).

[7] Y. He, T.R. Lutz, and M.D. Ediger, J Chem Phys **119**, 9956 (2003).

[8] S.K. Kumar, S. Shenogin, and R.H. Colby, Macromolecules **40**, 5759 (2007).

[9] P.R. Couchman, Macromolecules **11**, 1156 (1978).

[10] J.L. Keddie, R.A.L. Jones, and R.A. Cory, Europhys. Lett. **27**, 59 (1994).

[11] C.J. Ellison, S.D. Kim, D.B. Hall, and J.M. Torkelson, Eur. Phys. J. E **8**, 155 (2002).

[12] C.J. Ellison, M.K. Mundra, and J.M. Torkelson, Macromolecules **38**, 1767 (2005).

[13] C.B. Roth and J.R. Dutcher, Journal of Electroanalytical Chemistry **584**, 13 (2005).

[14] M.D. Ediger and J.A. Forrest, Macromolecules **47**, 471 (2014).

[15] C.B. Roth, K.L. McNerny, W.F. Jager, and J.M. Torkelson, Macromolecules **40**, 2568 (2007).

[16] C.B. Roth and J.M. Torkelson, Macromolecules **40**, 3328 (2007).

[17] C.M. Evans, S. Narayanan, Z. Jiang, and J.M. Torkelson, Phys. Rev. Lett. **109**, 038302 (2012).

[18] R.J. Lang and D.S. Simmons, Macromolecules **46**, 9818 (2013).

[19] N.B. Tito, J.E.G. Lipson, and S.T. Milner, Soft Matter **9**, 9403 (2013).

[20] N.B. Tito, J.E.G. Lipson, and S.T. Milner, Soft Matter **9**, 3173 (2013).

[21] B.L. Kasavan, R.R. Baglay, and C.B. Roth, Macromol. Chem. Phys. (2017) DOI: 10.1002/macp.201700328.

[22] H.J. Butt, K. Graf, and M. Kappl, *Physics and Chemistry of Interfaces*, 3rd ed. (Wiley-VCH Verlag GmbH, Weinheim, Germany, 2013).

[23] S. Kim and J.M. Torkelson, Macromolecules **44**, 4546 (2011).

[24] J. DeFelice, S.T. Milner, and J.E.G. Lipson, Macromolecules **49**, 1822 (2016).

[25] S. Mirigian and K.S. Schweizer, J. Phys. Chem. Lett. **4**, 3648 (2013).

[26] S. Mirigian and K.S. Schweizer, J Chem Phys **140**, 194507 (2014).

[27] S. Mirigian and K.S. Schweizer, J Chem Phys **141**, 161103 (2014).

[28] S. Mirigian and K.S. Schweizer, J Chem Phys **146**, 203301 (2017).

[29] R.R. Baglay and C.B. Roth, ACS Macro Lett. 887 (2017).

[30] R.J. Lang, W.L. Merling, and D.S. Simmons, ACS Macro Lett. **3**, 758 (2014).

[31] J. Baschnagel and F. Varnik, J Phys: Condens Matter **17**, R851 (2005).

[32] R.Y.F. Liu, Y. Jin, A. Hiltner, and E. Baer, Macromol. Rapid Commun. **24**, 943 (2003).

[33] R.Y.F. Liu, T.E. Bernal-Lara, A. Hiltner, and E. Baer, Macromolecules **38**, 4819 (2005).

[34] Z. Fakhraai and J.A. Forrest, Phys. Rev. Lett. **95**, 025701 (2005).

[35] E.C. Glor and Z. Fakhraai, J Chem Phys **141**, 194505 (2014).

[36] D. Christie, R. Register, and R.D. Priestley, in *APS March Meeting* (New Orleans, 2017).

[37] D. Christie, R. Register, and R.D. Priestley, in *APS March Meeting* (Baltimore, 2016).

[38] V. Sethuraman and V. Ganesan, J Chem Phys **147**, 104901 (2017).

[39] D. Christie, C. Zhang, J. Fu, B. Koel, and R.D. Priestley, J Polym Sci, Part B: Polym Phys **54**, 1776 (2016).

[40] Z. Mahimwalla, K.G. Yager, J.-I. Mamiya, A. Shishido, A. Priimagi, and C.J. Barrett, Polym. Bull. **69**, 967 (2012).